

University of New Hampshire University of New Hampshire Scholars' Repository

Master's Theses and Capstones

Student Scholarship

Fall 2009

Detecting bedform migration from high-resolution multibeam bathymetry in Portsmouth Harbor, New Hampshire, USA

Janice A. Felzenberg

University of New Hampshire, Durham

Follow this and additional works at: <https://scholars.unh.edu/thesis>

Recommended Citation

Felzenberg, Janice A., "Detecting bedform migration from high-resolution multibeam bathymetry in Portsmouth Harbor, New Hampshire, USA" (2009). *Master's Theses and Capstones*. 475.

<https://scholars.unh.edu/thesis/475>

This Thesis is brought to you for free and open access by the Student Scholarship at University of New Hampshire Scholars' Repository. It has been accepted for inclusion in Master's Theses and Capstones by an authorized administrator of University of New Hampshire Scholars' Repository. For more information, please contact nicole.hentz@unh.edu.

**DETECTING BEDFORM MIGRATION FROM HIGH-
RESOLUTION MULTIBEAM BATHYMETRY IN
PORTSMOUTH HARBOR, NEW HAMPSHIRE, USA**

BY

JANICE A. FELZENBERG

B.A., Wesleyan University, 2005

THESIS

Submitted to the University of New Hampshire

In Partial Fulfillment of

The Requirements for the Degree of

Master of Science

in

Earth Sciences – Ocean Mapping

September, 2009

UMI Number: 1472060

INFORMATION TO USERS

The quality of this reproduction is dependent upon the quality of the copy submitted. Broken or indistinct print, colored or poor quality illustrations and photographs, print bleed-through, substandard margins, and improper alignment can adversely affect reproduction.

In the unlikely event that the author did not send a complete manuscript and there are missing pages, these will be noted. Also, if unauthorized copyright material had to be removed, a note will indicate the deletion.

UMI[®]

UMI Microform 1472060
Copyright 2009 by ProQuest LLC
All rights reserved. This microform edition is protected against
unauthorized copying under Title 17, United States Code.

ProQuest LLC
789 East Eisenhower Parkway
P.O. Box 1346
Ann Arbor, MI 48106-1346

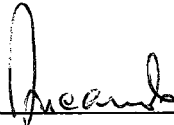
This thesis has been examined and approved.



Thesis Director, Larry G. Ward,
Research Associate Professor of Earth Sciences



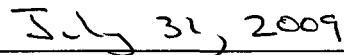
Larry A. Mayer,
Professor of Ocean Engineering and Earth Sciences



Yuri Rzhanov,
Research Associate Professor of Ocean Engineering



James V. Gardner,
Research Professor of Ocean Engineering and Affiliate
Professor of Earth Sciences



Date

DEDICATION

This thesis is dedicated to my family and to my teachers, and to my fiancé, Yiftach Eisenberg, whose encouragement and support have made this work possible.

ACKNOWLEDGEMENTS

I wish to thank the faculty and staff of the University of New Hampshire Center for Coastal and Ocean Mapping and Joint Hydrographic Center (UNH CCOM/JHC) for their assistance and support. I especially wish to thank my thesis advisor, Dr. Larry Ward, for his guidance and insight throughout my M.S. studies. I gratefully acknowledge Dr. Yuri Rzhakov, Dr. Larry Mayer, Dr. James Gardner, Dr. Brian Calder, Dr. Christopher Sherwood and Dr. Diane Foster for their knowledge and wisdom, and for their many ideas and suggestions. I would like to thank Dr. James Irish for his ingenuity and hard work with regard to planning and executing the current-meter deployments. Many thanks to Dr. Semme Dijkstra, Capt. Andrew Armstrong, Dr. Shachak Pe'eri, Paul Lavoie, Carl Kammerer, Elizabeth Kintzing and Glenn McGillicuddy for their assistance with conducting fieldwork. My gratitude is to Capt. Ben Smith of R/V *Coastal Surveyor* and to Capt. Paul Pelletier, Capt. Brian Soares and Debra Brewitt of R/V *Gulf Challenger* for their hard work. Many thanks to the current and former members of the UNH CCOM/JHC community who have given me their advice, their encouragement, and their friendship at all stages of my research: Michelle Weirathmueller, Nicholas Forfinski, Mashkoor Malik, Val Schmidt, Kurt Schwehr, Monica Wolfson, Brian O'Donnell, Lynnette Morgan, Nathan Wardwell, Marc Moser, Robert Bogucki, Gretchen Imahori, Luis Rosa, Rochelle Wigley, Donya Frank, Rachel Soraruf and Nicole Kuenzel.

This research was supported by the National Oceanic and Atmospheric Administration (NOAA) under grant number NA05NOS4001153.

TABLE OF CONTENTS

Dedication.....	iii
Acknowledgements.....	iv
List of Tables	vii
List of Figures.....	viii
Abstract.....	x
CHAPTER	
1 INTRODUCTION	1
2 PHYSICAL SETTING	6
3 DATA AND METHODS	10
3.1 Sediment Samples.....	10
3.2 Underwater Videography.....	11
3.3 Multibeam Echosounder Surveys	12
3.4 Multibeam Data Post-Processing.....	14
3.5 Current Observations	15
3.6 Bed Shear Stress	17
3.6.1 Critical Bed Shear Stress	17
3.6.2 Total Bed Shear Stress.....	20
3.6.2 Partitioning Bed Shear Stress.....	22
4 DETECTING BEDFORM MIGRATION.....	24
4.1 BISHNU: A New Technique for Ridge Detection	24

4.2	Spatial Cross-Correlation.....	30
5	RESULTS	37
5.1	Sediment Samples and Underwater Videography	37
5.2	Bathymetry and Dune Morphology	42
5.3	Ridge Maps and Dune Migration.....	50
5.3.1	BISHNU Results.....	50
5.3.2	Spatial Cross-Correlation Results	53
5.4	Current Observations	63
5.5	Bed Shear Stress	66
6	DISCUSSION.....	71
6.1	Bedform Migration in Portsmouth Harbor	71
7	CONCLUSIONS.....	87
8	List of References	91

LIST OF TABLES

Table 4-1. Preliminary classificaiton of a pixel during BISHNU first pass	29
Table 5-1. Grain-size statistics from Portsmouth Harbor sediment samples.....	38
Table 5-2. Timing of multibeam echosounder surveys	42

LIST OF FIGURES

Figure 1-1.	Location of study area.....	3
Figure 2-1.	Map of sediment classes in Portsmouth Harbor.....	7
Figure 3-1.	Location of data sets in Portsmouth Harbor.....	11
Figure 3-2.	Threshold of sediment motion from Shields (1936)	19
Figure 4-1.	Preliminary classification of a pixel during BISHNU first pass	28
Figure 4-2.	Final classification of pixel during BISHNU second pass.....	31
Figure 4-3.	Comparison of candidate input surfaces to cross-correlation algorithm.....	32
Figure 4-4.	Cross-correlation spatial variables	34
Figure 4-5.	Weighted centroid method for defining bedform migration vector	36
Figure 5-1.	Location of sediment samples from Portsmouth Harbor	39
Figure 5-2.	Ternary diagram of Portsmouth Harbor sediment samples.....	40
Figure 5-3.	Seafloor video imagery from Portsmouth Harbor.....	41
Figure 5-4.	Bathymetry from 2007 multibeam echosounder surveys.....	44
Figure 5-5.	Bathymetry from 2008 multibeam echosounder surveys.....	45
Figure 5-6.	Histograms of horizontal total propagated uncertainty	46
Figure 5-7.	Bed elevation profiles from 2007 bathymetry.	47
Figure 5-8.	Bed elevation profiles from 2008 bathymetry.	48
Figure 5-9.	Close-up views of complex bedform morphology.....	49
Figure 5-10.	BISHNU ridge map from 8 June 2007 (1400 UTC).....	51
Figure 5-11.	BISHNU ridge map from 3 July 2008 (1420 UTC).....	52

Figure 5-12. Dune migration vector field from cross-correlation algorithm	56
Figure 5-13. Spatially averaged migration vectors, 8 June 2007 (1400 - 2000 UTC)....	57
Figure 5-14. Spatially averaged migration vectors, 14 June 2007 (1330 - 1930 UTC)...	58
Figure 5-15. Spatially averaged migration vectors, 14-15 June 2007	59
Figure 5-16. Spatially averaged migration vectors, 8-15 June 2007	60
Figure 5-17. Spatially averaged migration vectors, 3-9 July 2008	61
Figure 5-18. Histograms of dune migration direction and magnitude.....	62
Figure 5-19. Time-series of ADCP and MAVS current speed and direction.	64
Figure 5-20. Time-series of ADCP current speed and direction (full water column)	65
Figure 5-21. Plot of ADCP residual velocities	67
Figure 5-22. Log-fit method estimates of bed shear stress at ADCP site.....	69
Figure 5-23. Plot of partitioned bed shear stress at ADCP and MAVS sites.....	70
Figure 6-1. Reson 8101 bathymetry (November 2000).....	73
Figure 6-2. Kongsberg EM3000D bathymetry (June 2001)	74
Figure 6-3. Reson 8125 bathymetry (November 2001).....	75
Figure 6-4. Kongsberg EM3002 bathymetry (June 2004).....	76
Figure 6-5. Kongsberg EM3002D bathymetry (June 2007)	77
Figure 6-6. Kongsberg EM3002D bathymetry (July 2008).....	78
Figure 6-7. Cross-sections from Portsmouth Harbor bathymetry (2000-2008).....	79
Figure 6-8. Location of bed elevation profiles from 2007 bathymetry.....	81
Figure 6-9. Bed elevation profiles from 2007 bathymetry	82
Figure 6-10. Time-series of atmospheric and wave data from GoMOOS Buoy B01.....	85
Figure 6-11. Residual water level from NOAA/NOS/CO-OPS Gauge 8423898.....	86

ABSTRACT

DETECTING BEDFORM MIGRATION FROM HIGH-RESOLUTION MULTIBEAM BATHYMETRY IN PORTSMOUTH HARBOR, NEW HAMPSHIRE, USA

by

Janice A. Felzenberg

University of New Hampshire, September, 2009

A study was undertaken to quantify dune migration in Portsmouth Harbor, New Hampshire, USA from repeat high-resolution multibeam echosounder (MBES) surveys. Repeat MBES surveys were conducted in June 2007 and July 2008 over periods ranging from 6 hours to 7 days in order to capture the response of dune morphology to ebb-flood and spring-neap tidal cycles. A new technique was developed for detecting bedform migration. This approach utilizes a fingerprint-detection algorithm (Bishnu et al., 2002) to convert the bathymetric surface to a binary map of bedform crests, which are subsequently tracked using a spatial cross-correlation technique (Duffy and Hughes-Clarke, 2005). Acoustic current-meter observations from July 2008 provided context for the observed bedform-migration patterns, and were subsequently used to compute bed shear stress. Results indicate that dune migration occurred over periods as short as 6 hours. Dune migration distances in excess of 2 m were observed over 6- and 7-day periods.

CHAPTER 1

INTRODUCTION

Bedforms of varying scales are widespread features in sand-dominated shallow marine and estuarine environments. Small to large subaqueous dunes with wavelengths of several meters to several tens of meters (Ashley, 1990), are both ubiquitous and highly dynamic under strong tidal conditions, and can migrate with speeds of up to tens of meters per year (van Dijk and Kleinhans, 2005; Buijsman and Ridderinkhof, 2008). Consequently, the presence of dunes often evokes questions regarding the spatial and temporal stability of the seafloor. Understanding seafloor stability is particularly important in the estuarine and coastal environment, where migrating bedforms have the ability to impact cable and pipeline routes (Morelissen et al., 2003), marine habitats (Daniell et al., 2008), and maintenance of navigable channels (Lindenbergh et al., 2007), and to influence target-detection capabilities (Mayer et al., 2007; Wolfson et al., 2007).

In recent years numerous laboratory studies have examined mechanisms of bedform generation and evolution (Hulscher, 1996; Nemeth et al., 2002; Besio et al., 2003; Besio et al., 2004), and other papers have presented methods for predicting bedform morphology and migration (Lesser et al., 2004; Lindenbergh et al., 2007). To determine actual dune migration rates, however, it is necessary to perform repeated surveys of the same area of the seabed. Studies continue to utilize repeated single-beam sonar surveys (Terwindt, 1971; Bokuniewicz et al., 1977; FitzGerald et al., 2000;

Kostaschuk and Best, 2005), although major drawbacks of this method are the lack of spatial resolution and difficulty of ensuring that profiles are taken normal to dune crests. The use of repeat multibeam echosounder (MBES) surveys has surged in popularity in recent years (Ernstsen et al., 2005; Ernstsen et al., 2006b; Nittrouer et al., 2008) due to the high resolution and precision of many MBES systems, as well as the ability of MBES to produce bathymetry with full swath coverage. Though use of repeat MBES surveys presents a significant advantage over other techniques, the ability to successfully detect bedform migration from MBES bathymetry depends on the survey resolution and knowledge of positioning uncertainty (Ernstsen et al., 2006a), as well as the survey-repetition rate. Many bedform-migration studies utilizing MBES rely upon differential GPS (DGPS) for positioning, which is capable of achieving a horizontal positioning uncertainty of several decimeters at the DGPS receiver (Nittrouer et al., 2008).

This study presents a novel approach that improves upon existing methods for detecting bedform migration from high-resolution MBES bathymetry, and applies this approach to assess dune migration in a bedform field located near the entrance to Portsmouth Harbor, New Hampshire, USA (Fig. 1-1). Recent bedform-migration studies have focused on the comparison of sequential bed elevation profiles from MBES bathymetry (Ernstsen et al., 2005; Ernstsen et al., 2006b; Nittrouer et al., 2008); manual definition of minimum-perpendicular-distance between crest positions identified on a bathymetric digital terrain model (DTM) (Knaapen et al., 2005; Daniell et al., 2008); and spatial cross-correlation of a series of DTMs (Duffy and Hughes-Clarke, 2005; Buijsman and Ridderinkhof, 2008; van Dijk and Egberts, 2008). A significant disadvantage of the first method is that it lacks the full spatial resolution inherent in the MBES bathymetry, as

migration vectors are defined only along transects. The second method yields better spatial resolution, but is problematic in that bedform migration does not always occur along a direction strictly perpendicular to the dune crests. The third method fully exploits the spatial resolution of the underlying MBES bathymetry and has the added advantage of measuring dune migration over the region in a DTM in which the dune morphology is most highly correlated (Duffy and Hughes-Clarke, 2005).

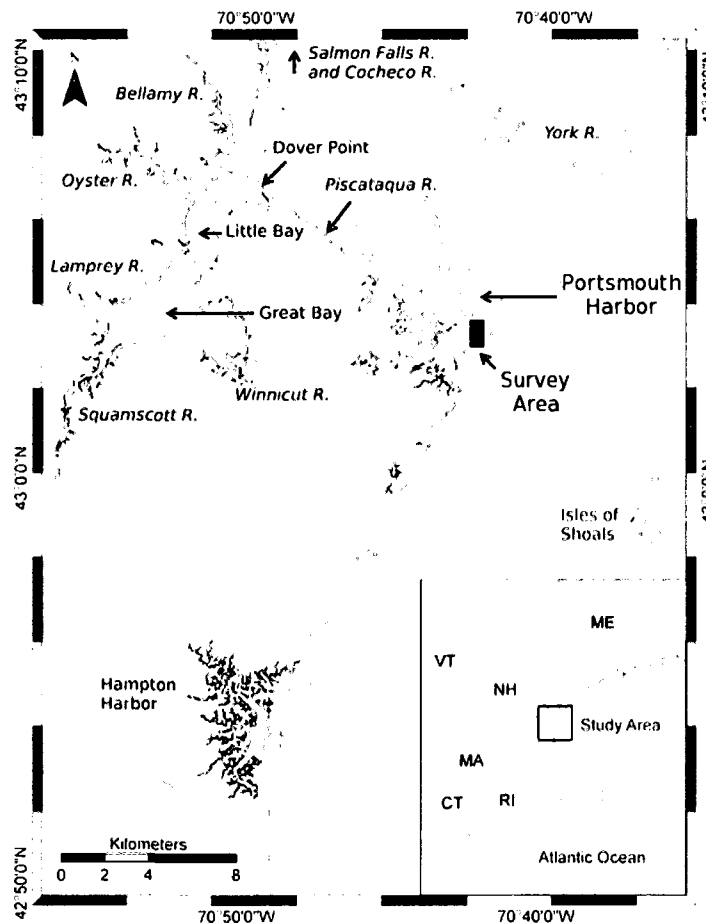


Figure 1-1. Location map of study area in Portsmouth Harbor, New Hampshire, USA.

The spatial cross-correlation method of Duffy and Hughes-Clarke (2005) is applied here to binary images (“ridge maps”) of dune crest locations defined from the MBES bathymetry. Ridge maps are created from the bathymetry using a novel algorithm (BISHNU) inspired by fingerprint detection techniques (Bishnu et al., 2002). The ridge map is a more suitable surface for cross-correlation than the bathymetry or maximum-slope surface because it more adequately emphasizes the dune crest, which is the morphologic feature that is principally used in tracking dune migration. Indeed, many studies of bedform migration have focused only on the dune crests rather than the entire bathymetric surface (Knaapen et al., 2005; Daniell et al., 2008; Whitmeyer and FitzGerald, 2008).

Repeat MBES surveys utilized for detecting bedform migration in this study were conducted over periods ranging from 6 hours to 7 days, with the intention of capturing the seafloor response to ebb-flood and spring-neap tidal cycles. Other studies have examined bedform dynamics on time-scales of hours to days (Kostaschuk and Best, 2005; Ernstsens et al., 2006b; Nittrouer et al., 2008), although many of these studies are qualitative in nature and few have published bedform-migration rates. With the goal of successfully detecting bedform migrations in the range of several decimeters, this study has implemented positioning from real-time kinematic (RTK) GPS, which is capable of achieving a horizontal positioning uncertainty of several centimeters at the GPS receiver. To provide further context for the observed bedform migration rates and patterns, acoustic current-meter observations were made concurrently with several of the MBES surveys. Bed shear stress was subsequently calculated from the current-meter data to

determine whether threshold conditions for initiation of bedload sediment transport were exceeded during the observation period.

CHAPTER 2

PHYSICAL SETTING

Portsmouth Harbor is located in the lower reaches of the Piscataqua River, which connects Great Bay Estuary of southeastern New Hampshire and southwestern Maine, USA to the Gulf of Maine (Fig. 1-1). Great Bay Estuary is a bedrock-controlled estuary eroded into a complex assemblage of metasedimentary, metavolcanic and plutonic bedrock ranging in age from 300 to 600 Ma (Ward, 1992). The sedimentary framework of the estuary is heavily influenced by the Quaternary glacial history and associated isostatic and eustatic sea-level change within the Gulf of Maine, and is dominated by glacial tills, stratified ice-contact deposits, glacial-marine muds and sands, and marsh deposits (Belknap et al., 1987; Ward, 1995; Barnhardt et al., 1997; Belknap et al., 2002).

The distribution of surficial sediments within the lower estuary has been mapped by Ward (1995; 2008). Major surficial-sediment classes include gravel, sandy gravel, gravelly sand, sand, muddy sand and sandy mud (Fig. 2-1). Gravels and sandy gravels dominate tidal channels within the lower estuary, whereas the shallower areas are dominated by sands, muddy sands and sandy muds (Ward, 1995; 2008). Intertidal bedrock is also present along the shallower areas, particularly along the eastern shoreline of New Castle Island and the southern shoreline of Gerrish Island.

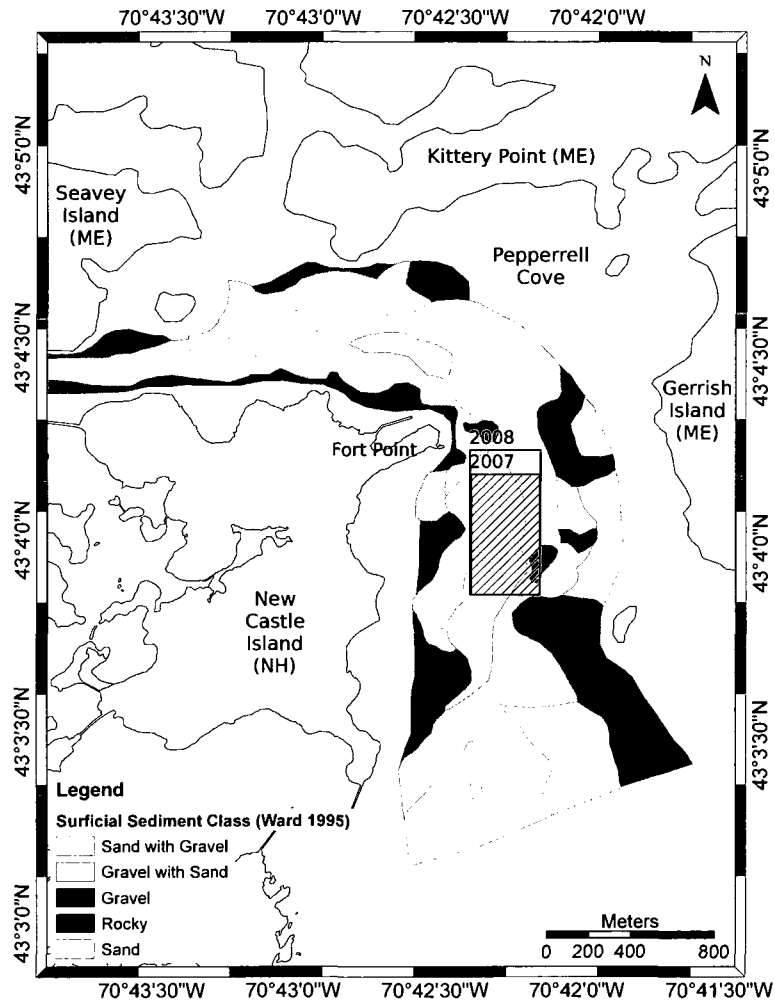


Figure 2-1. Map of surficial sediment classes within the main tidal channel of the Piscataqua River, Portsmouth Harbor, New Hampshire, USA. Modified from Ward (2008). Sediment classes along shoreline (not mapped here) are muds and sandy muds along Seavey Island, and sand, gravelly sand, and sandy gravel within Pepperrell Cove (Ward, 1995). Rectangles indicate extents of 2007 and 2008 multibeam surveys.

Great Bay Estuary is a complex hydrodynamic system that can be divided into lower and upper reaches. The lower estuary is comprised of Portsmouth Harbor and the lower Piscataqua River. The lower estuary extends northward from the Portsmouth Harbor mouth to Dover Point, where the system bifurcates into the upper Piscataqua River and Great and Little Bays (Fig. 1-1). The upper Piscataqua reach intersects the Cocheco and Salmon Falls Rivers. Great Bay and Little Bay are intersected by the

Squamscott, Lamprey, Oyster, Bellamy and Winnicut Rivers, which, along with the Cocheco and Salmon Falls Rivers, are the major freshwater tributaries to the estuary. Lower Great Bay Estuary is a marine-dominated system with bedrock-incised channels up to 25 m in depth. The upper reaches of Great Bay Estuary are comprised of shallow tidal channels up to 13 m in depth flanked by extensive intertidal mud flats (Short, 1992). Great Bay Estuary comprises a total area of 2409 km², whereas the tidal waters of the estuary cover approximately 44 km² with nearly 160 km of shoreline (Reichard and Celikkol, 1978).

The lower estuary at Portsmouth Harbor is mesotidal and varies from stratified to moderately well-mixed, depending on freshwater-discharge conditions and the phase of tide (Ward and Bub, 2005). Freshwater discharge into the estuary varies seasonally and is typically 1% or less of the total tidal prism (Bilgili et al., 1996). The range of tide within Great Bay Estuary is greatest at Portsmouth Harbor. The tidal range decreases from Portsmouth Harbor toward Dover Point, and from Dover Point increases slightly toward the mouth of the Squamscott River (Reichard and Celikkol, 1978). The tidal range at Portsmouth Harbor is 3.5 m (\pm 0.5 m) under spring tidal conditions and 2 m (\pm 0.5 m) under neap tidal conditions (NOAA, 2009). Field programs conducted in 1977 and 2007 have observed flood and ebb tidal currents of up to 1.2 m/s in the vicinity of Fort Point (Swenson et al., 1977; NOAA, 2007).

The focus of this study is a bedform field located near the entrance to Portsmouth Harbor (Fig. 1-1, Fig. 3-1). The bedform field is located on a shallow (12 m deep), sandy bank between the main tidal channel and western shoreline. The bedform field is an elongate feature (900 m by 200 m) with its major axis oriented parallel to the north-south

main channel axis of the lowermost Piscataqua River. The bedform field is a persistent feature within Portsmouth Harbor and has been documented by numerous hydrographic surveys since 1992 (Ward, 1995; Huff, 2001; Cutter, 2005; Gostnell, 2005).

CHAPTER 3

DATA AND METHODS

New data sets were acquired in order to evaluate bedform migration and bed shear stress within Portsmouth Harbor during 2007 and 2008. The data sets included sediment samples, underwater videography, multibeam-echosounder bathymetry, and acoustic current-meter observations. This section provides an overview of the methods of data acquisition and of post-processing techniques applied to the data.

3.1 Sediment Samples

Sediment samples were acquired from 19 locations within the study area to provide ground-truth for bathymetric surveys and to obtain grain-size data for calculation of bed shear stress (Fig. 3-1). Samples were retrieved on 25 and 26 February 2008 using a Shipek grab sampler deployed from the University of New Hampshire (UNH) R/V *Gulf Challenger*, with the exception of samples ADCP and MAVS, which were obtained by research divers on 2 July 2008. Sample positioning was provided by Wide Area Augmentation System (WAAS) enabled GPS, which has an uncertainty of ± 5 m. Grain-size analysis was performed using standard sieve and pipette procedures (resolution of 0.5ϕ) described by Folk (1980). Sample statistics for the grain-size distribution data from these methods were calculated using logarithmic Folk and Ward (1957) graphical measures as implemented by the GRADISTAT grain-size analysis package (Blott and Pye, 2001).

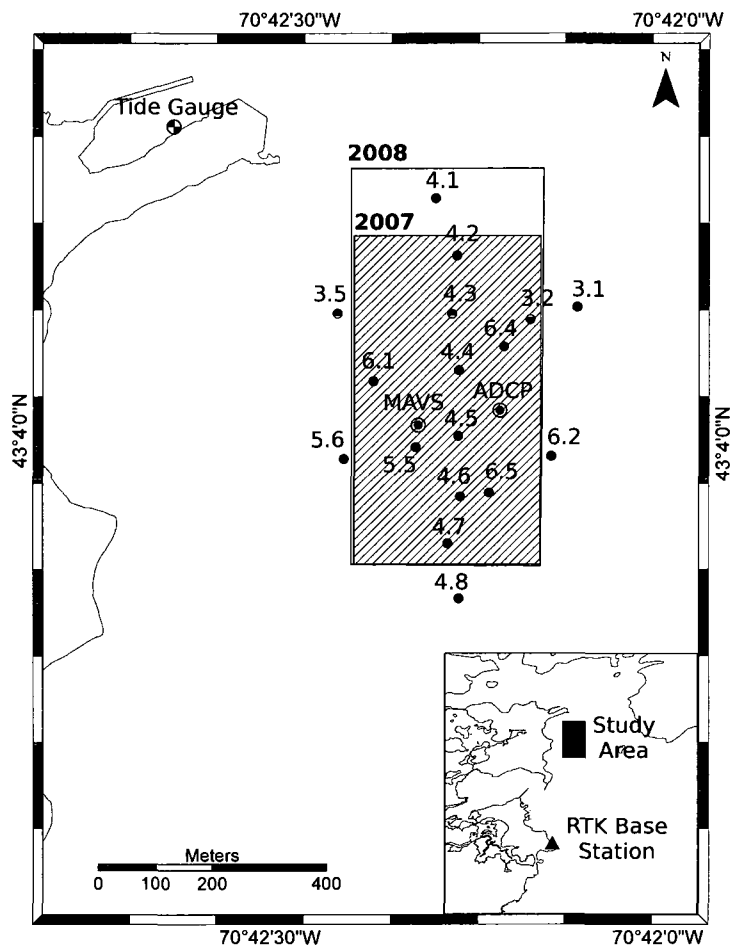


Figure 3-1. Location of sediment samples, underwater video observations, multibeam echosounder (MBES) surveys, and current meter stations in Portsmouth Harbor. Black circles indicate combined sediment sample and underwater video observation stations. Outlined black circles (i.e., MAVS and ADCP) indicate combined sediment sample and current meter stations. Polygons indicate extents of MBES surveys conducted in 2007 and 2008. Note positions of NOAA Tide Gauge 8423898 and RTK base station.

3.2 Underwater Videography

Underwater video was obtained from 17 locations within the study area in order to provide further *in situ* textural context for the sediment samples (Fig. 3-1). Observations were made on 25 and 26 February 2008 from a towed camera system with integrated WAAS-enabled GPS positioning deployed from the UNH R/V *Gulf Challenger*. The GPS receiver from which positioning data were obtained was mounted

on a stanchion on the starboard side of the vessel approximately 1 m before the A-frame. Video footage with superimposed digital overlay containing time-stamp and positioning data was recorded at a rate of 30 frames/s. Footage was subsequently sub-sampled to 1 frame/s in post-processing and frames that provided representative images of the seafloor were converted to JPG format.

3.3 Multibeam Echosounder Surveys

Seven multibeam echosounder surveys were acquired from June 2007 to July 2008. Surveys were conducted twice-daily (~ 6 hours apart) on 8 June 2007 and 14 June 2007 in order to capture the seafloor response to the flood-ebb tidal cycle under neap and spring conditions, respectively. An additional survey was conducted on 15 June 2007 with the intention of recording the seafloor response over a 24-hour period (e.g., from 14 June to 15 June 2007), as well as the seafloor response to the ~7-day duration neap-spring tidal cycle (e.g., from 8 June to 15 June 2007). Multibeam surveys were conducted again on 3 and 9 July 2008 in order to capture a second neap-spring tidal cycle, as well as to enable the determination of gross morphological change of the seafloor over a period of approximately one year. Each MBES survey was conducted within a one-hour window surrounding predicted slack water in order to record the seafloor in a state of “rest” with respect to time-dependent oscillating tidal currents.

Multibeam data were acquired with a dual-head Kongsberg EM3002D MBES system installed on the UNH vessel R/V *Coastal Surveyor*. The dual-head EM3002D operates in the 300-kHz frequency band and contains 320 dynamically focused beams (1.5° beamwidth at broadside). Multibeam data were acquired in equiangular beam-spacing mode with a user-specified total angular coverage of 120°. Position, heading,

vessel speed and attitude data were acquired with an Applanix POS/MV system with integrated real-time kinematic (RTK) GPS. RTK correctors were broadcast continuously to the R/V *Coastal Surveyor* receiver from a base station at the Seacoast Science Center, Rye, New Hampshire, located approximately 2 km line-of-sight from the survey area (Fig. 3-1). The multibeam data were logged using a Kongsberg SIS acquisition platform. Angular and level-arm offset measurements (made prior to each of the 2007 and 2008 survey seasons) were applied to the data in the Kongsberg SIS software, as were correctors for static draft, sound speed through the water column, and sound speed at the transducer face (required for beam steering). The application of a single sound-speed profile for each survey was deemed sufficient due to the short survey time (~1 hr) and small size of the survey area. The sound speed profile for each survey was obtained from the center of the study area (approximately 43.0672° N, 70.7046° W) prior to acquiring the multibeam echosounder data. The water depth was approximately 12.2 m at the site from which the sound speed profiles were obtained. Sound speed profiles were obtained from an Applied Microsystems *SV Plus* sound speed profiler, which measures the time-of-flight of an acoustic signal along a fixed axis and has a measurement uncertainty of +/- 0.03 m/s.

All MBES surveys consisted of 16 main-scheme lines oriented parallel to the major axis of the dune field, with two additional survey cross-lines oriented perpendicular to the main-scheme lines. Main-scheme lines were run at a line spacing of 19 m, yielding a swath overlap of 20.8 m (109% overlap) at a nominal water depth of 12 m. Main-scheme lines in 2007 were limited to 480 m in length in order to minimize total survey time to one hour (i.e., in case bedforms have a detectable migration response over

time periods much shorter than an ebb-flood tidal cycle), whereas main-scheme lines in 2008 were extended to 650 m in length. Surveys were conducted at a vessel speed of 5 knts at the maximum ping rate of 40 Hz, yielding a mean sampling density of approximately 18.5 pings per grid node (0.25 m grid resolution) at a nominal water depth of 12 m. The total areal extents of the 2007 and 2008 survey regions are 0.106 km² and 0.195 km², respectively.

3.4 Multibeam Data Post-Processing

All multibeam surveys were post-processed using CARIS HIPS 6.1 software. Survey data were reduced to mean lower low water (MLLW) chart datum using tide observations from NOAA Tidal Station 8423898 (Fort Point, New Castle, New Hampshire) (Fig. 3-1). Tidal amplitude and range correctors were deemed unnecessary due to the proximity of the tidal station to the survey area (~500 m). Corrections for dynamic draft were applied to the data in HIPS using an empirically derived dynamic draft table for R/V *Coastal Surveyor*.

Because bathymetric data uncertainty is a critical factor in quantifying bedform migration, total propagated uncertainty (TPU) was calculated for the MBES data using CARIS HIPS. TPU was calculated by applying real-time uncertainty data acquired by the POS/MV controller software during survey acquisition (in *.SBET format), yielding a more precise estimate of TPU than would be provided by using static error values in the HIPS vessel configuration file. Subsequent to TPU calculation, all survey data were filtered in HIPS to remove soundings with horizontal TPU values in excess of 0.5 m and vertical TPU values in excess of those specified by the International Hydrographic Organization (IHO) S-44 Special Order standard:

$$\text{Maximum Allowable Vertical TPU} = \pm\sqrt{a^2 + (b \times d)^2} \quad (3.1)$$

where $a = 0.25$ m, $b = 0.0075$ m, and $d =$ water depth (in meters) (IHO, 2008).

Each multibeam survey was gridded at a resolution of 0.25 m using the HIPS BASE surface generator. All survey grids were created from a common HIPS Field Sheet to ensure that grid node locations remained the same between surveys. The gridded data were exported (in *.BASE format) to IVS3D Fledermaus 6.4.1 software, where they were compiled into bathymetric digital terrain models (DTMs). Finally, the DTMs were exported from Fledermaus in *.XYZ format for further post-processing (e.g., detecting bedform migration) in MATLAB. While exporting the data from Fledermaus, data bounds were specified (to 0.001 m in precision) to ensure a common data extent for the 2007 and 2008 surveys.

No major data quality issues were encountered in post-processing; however, the 2008 multibeam data contain a static +0.30 m vertical offset with respect to the 2007 data. This offset is the result of an error in calculating the IMU-to-transducer vertical offset prior to the 3 July 2008 survey. The vertical offset was not considered to have any implications for the bedform-migration experiment, as it only affects the vertical inter-comparability of the 2007 and 2008 data. As such, no correction was applied to the 2008 data.

3.5 Current Observations

Acoustic current meters were deployed at two locations within the study area during the 2008 multibeam survey to provide simultaneous observations of near-bottom currents (Fig. 3-1). The current meters were positioned near the eastern and western margins of the bedform field to compare current regimes during spring tidal conditions

and to determine whether near-bottom currents were capable of initiating bedload sediment transport.

Instrumented frames bearing the current meters were deployed from the UNH R/V *Gulf Challenger* on 2 July 2009 and retrieved on 16 July 2009. Divers were utilized during the deployment to ensure proper positioning of the frames and to take *in situ* bottom photographs and sediment samples. An instrumented frame containing an ADCP (1200-kHz RDI Workhorse Sentinel) was deployed on the eastern margin of the bedform field at 43.06713°N, 70.70360°W. The ADCP frame additionally housed a Sea-Bird Electronics SBE-16*Plus* conductivity, temperature and depth (CTD) probe. A second frame containing a Nobska MAVS-3 acoustic current meter, which computes vector-averaged velocities from differential time-travel measurements across four acoustic axes, was deployed on the western margin of the bedform field at 43.06687°N, 70.70535°W. Each station was equipped with a Benthos pinger coupled with an EdgeTech CART acoustic release for purposes of retrieving the instrumentation at the end of the observation period.

The ADCP observed a time-series of current profiles from 1.03 to 8.83 m above bottom (0.20 m bin size). The record for each ADCP bin is comprised of 6-min averaged ensembles of 750 pings each, yielding a measurement uncertainty of 0.007 m/s. The MAVS current-meter observed current velocities at a height of 1.00 m above bottom with a measurement uncertainty of 0.003 m/s. The MAVS record is comprised of 2-min averaged ensembles (“bursts”) of 120 pings each, recorded every 6 min. CTD observations were made at a height of 0.40 m above bottom and were recorded at a variable rate (every 10-15 s) due to latency in the CTD software.

ADCP and MAVS observations were recorded as northgoing, eastgoing, and vertical current velocities, and were converted to vector-averaged current speed and direction in post-processing using MATLAB software. Correctors for magnetic declination (-15.6° in Portsmouth Harbor) were applied to the ADCP data at the time of acquisition, and to the MAVS data in post-processing. An additional corrector was applied to the MAVS data in post-processing to compensate for an inverted compass in the MAVS instrumentation at the time of acquisition, which caused northgoing velocities to be registered as negative rather than positive. A subsequent tank test determined that the switch had no effect on the measurement of eastgoing velocity.

3.6 Bed Shear Stress

Bed shear stress was calculated to determine whether the critical threshold for initiation of sediment motion was exceeded during the current observation period, thus validating bedform migration observed from the multibeam bathymetry. Bed shear stress was evaluated from the ADCP current observations using the log-profile method described by Sherwood et al. (2006) and others (Dyer, 1980; Middleton and Southard, 1984; Huntley, 1988). Additionally, bed shear stress was evaluated from the ADCP and MAVS data using a quadratic shear-stress equation. Results from both methods were compared against the critical bed-shear stress to determine whether the threshold of motion was exceeded during the observation period (3 to 5 July 2008) of near-bottom currents in Portsmouth Harbor.

3.6.1 Critical Bed Shear Stress

The critical bed shear stress can be described theoretically as the balance of forces acting on a sediment grain. These forces include the force imparted on the sediment

grain by its submerged weight (which acts as a stabilizing force to keep the sediment grain immobilized), and the force imparted on the sediment grain by the shear stress of the surrounding flow (which acts as a destabilizing force to move the sediment grain along the bed).

The critical bed shear stress is commonly given in terms of the Shields parameter, which is defined theoretically as:

$$\theta_{cr} = \frac{\tau_{cr}}{g(\rho_s - \rho)d} \quad (3.2)$$

where τ_{cr} is the threshold bed shear stress, g is the acceleration due to gravity, ρ_s is the grain density, ρ is water density, and d is the median grain diameter. In the theoretical evaluation of θ_{cr} presented in Equation (3.2), τ_{cr} is the shear stress imparted on the grain by the surrounding flow and $g(\rho_s - \rho)d$ is the submerged weight of the sediment grain.

In the time that has elapsed since Shields (1936) first evaluated the empirical relationship between grain size and the critical bed shear stress (yielding the ubiquitous Shields curve depicted in Figure 3-2), it has become commonplace to evaluate θ_{cr} as a function of the dimensionless grain size D_* :

$$D_* = \left[\frac{g(s-1)}{\nu^2} \right]^{1/3} d \quad (3.3)$$

where $s = \rho_s/\rho$ and ν is the kinematic viscosity of water. Soulsby (1997) provides an algebraic expression that yields a close fit to the original Shields curve for coarser grain sizes (Fig. 3-2):

$$\theta_{cr} = \frac{0.30}{1 + 1.2D_*} + 0.055(1 - e^{-0.020D_*}) \quad (3.4)$$

The critical value of the Shields parameter can subsequently be converted to bed shear stress using Equation (3.2).

Several field measurements are required in order to calculate θ_{cr} from Equations (3.3) and (3.4). Measurements of water temperature and salinity are necessary to evaluate the density and kinematic viscosity of water in Equation (3.3). Median grain size is also required as an input to Equation (3.3). Water temperature and salinity values for this study were taken from CTD observations made in July 2008. Median grain size was derived from grain-size analyses of sediment samples obtained at the ADCP and MAVS stations.

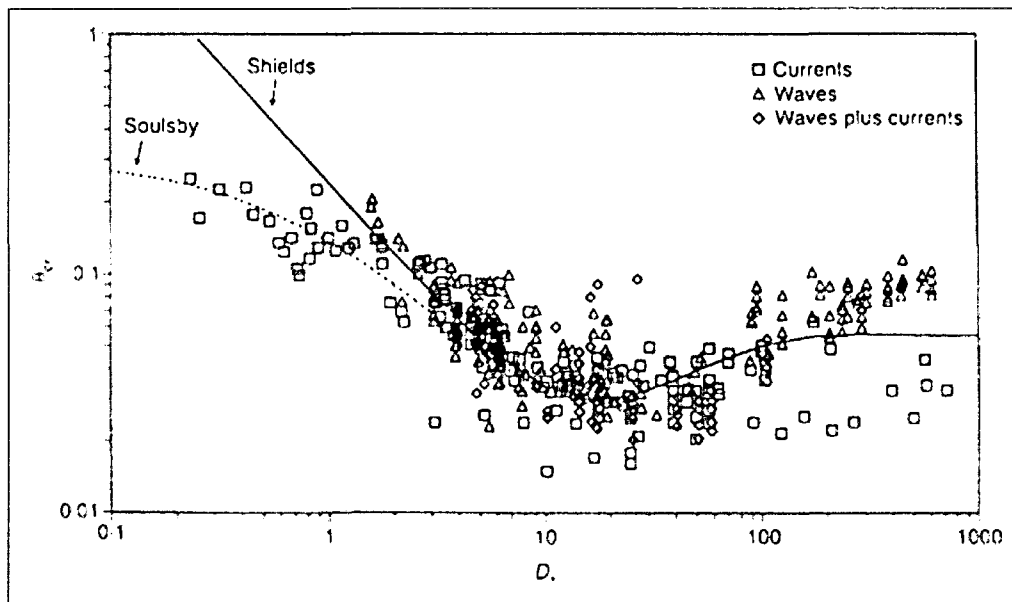


Figure 3-2. Shields (1936) empirical curve for threshold of sediment motion. The Shields parameter (θ_{cr}) and D^* are dimensionless values characterizing bottom shear stress and grain size, respectively. Parameterization of original Shields (1936) curve given by Equation (3.4) is depicted here as dotted curve. Data points indicate empirical observations of threshold bed shear-stress under conditions of currents, waves, and waves plus currents. Figure from Soulsby (1997).

3.6.2 Total Bed Shear Stress

Total bed shear stress (τ_b) was evaluated using two methods. The first estimate of τ_b was given by the log-profile (LP) method described by Sherwood et al. (2006) and others (Dyer, 1980; Middleton and Southard, 1984; Huntley, 1988). The second estimate of τ_b was obtained using the quadratic shear stress equation, which requires an empirical drag coefficient describing the bottom roughness. The second method is referred to here as the drag coefficient (DC) method.

The log-profile method of estimating bed shear stress requires observations of the vertical profile of current speed within the current bottom-boundary layer. The von Kármán-Prandtl equation, known as the logarithmic law of the wall, states that velocity in this layer varies as a function of shear velocity (u_*) and height above the bottom (z):

$$U(z) = \frac{u_*}{\kappa} \ln \left[\frac{z}{z_0} \right] \quad (3.5)$$

where $U(z)$ is mean velocity at height z above bottom, $\kappa = 0.408$ is the von Kármán constant, and z_0 is the hydraulic roughness length. Studies have shown that the law of the wall holds true for velocity profiles near the bed even when the flow is not strictly steady or uniform (Dyer, 1980), which is often the case in marine and estuarine systems such as Portsmouth Harbor. The von Kármán-Prandtl equation can be re-arranged as:

$$U(z) = \frac{u_*}{\kappa} (\ln(z) - \ln(z_0)) \quad (3.6)$$

where $U(z)$ is the dependent variable, u_*/κ is the slope, $\ln(z)$ is the independent variable and $\ln(z_0)$ is the y-intercept, thus allowing u_* and z_0 to be estimated from a linear least-squares fit to a measured velocity profile plotted as $\ln(z)$ vs. $U(z)$ (Sherwood et al., 2006).

The shear velocity u_* can subsequently be converted to bed shear stress:

$$\tau_b = \rho u_*^2 \quad (3.7)$$

A significant advantage of using the log-profile method to estimate bed shear stress is that the measured velocity profiles can be tested for log-linearity, thus giving a statistical measure of the goodness-of-fit (Sherwood et al., 2006). However, because the log-profile method requires measurements of current speed at several elevations above the bottom, this method was only applied to the ADCP current-meter station.

A second estimate of bed shear stress was calculated from a quadratic shear stress equation, which only requires measurement of current speed at a single location within the logarithmic current bottom-boundary layer. This method has been demonstrated to give a reasonable estimate of the magnitude of bed shear stress for current observations made some distance above the bed (Horne and Patton, 1989; Sanford, 1991; 1994; Soulsby, 1997). The quadratic shear stress equation is given as:

$$\tau_b = \rho C_{100} U_{100}^2 \quad (3.8)$$

where C_{100} is an empirical drag coefficient and U_{100} is the mean velocity at a height of 1 m above the bed. The value of C_{100} is related to the roughness length z_0 according to the relationship:

$$C_{100} = \left[\frac{\kappa}{\ln(1/z_0)} \right]^2 \quad (3.9)$$

where κ is the von Kármán constant. A typical value of C_{100} for a rippled, sandy bed is in the range 0.005 to 0.008 (Wright, 1995). This study evaluated Equation (3.8) using two different estimates of C_{100} . The first run applied a C_{100} value of 0.006, which is the theoretical bottom roughness for a rippled, sandy bed without larger-scale bedforms (Soulsby, 1997). The second run applied a C_{100} value based on the mean z_0 value

estimated by the log-profile method. The C_{100} value based on the log-profile method expresses the actual bottom roughness of the seabed at the ADCP station, where small, asymmetrical dunes (wavelength of 7m and height of 0.35 m) are present. The quadratic shear stress method was applied to the ADCP and MAVS data, as this method only requires measurements of velocity at a single point (e.g., 1 m above bottom).

3.6.3 Partitioning Bed Shear Stress

The presence of bedforms on the seafloor is a major consideration in evaluating bed shear stress (Smith and McLean, 1977; Dyer, 1980; Bennett and Best, 1995; McLean et al., 1999; Best, 2005). The presence of a bedform causes a horizontal pressure gradient within the surrounding flow as a result of flow separation and re-attachment over the bedform wavelength, and the horizontal pressure gradient in turn induces a horizontal drag force (Smith and McLean, 1977; Best, 2005). This drag force increases the total bed shear stress in the region away from the bed (the outer flow), while decreasing the skin-friction component of the total bed shear stress (the dominant force in the internal boundary layer near the bed), thus decreasing the ability of the shear stress to impact sediment grains on the bed. Where bedforms are present, it is thus necessary to isolate the skin-friction component of the total bed shear stress in order to calculate the excess bed shear stress for initiation of sediment motion. The difference between the skin-friction shear stress and the total bed shear stress is given by:

$$\tau_b = \tau_{sf} + \tau_{fd} \quad (3.10)$$

where τ_b is the total bed shear stress, τ_{sf} is the skin-friction shear stress, and τ_{fd} is the form drag. Because the skin-friction shear stress cannot be measured directly, it is necessary to calculate this value indirectly through drag partitioning. Smith and McLean (1977)

accomplish this by evaluating the form drag with respect to the total shear stress and the shear stress felt near the bed (i.e., the skin-friction shear stress):

$$F_D = \rho(C_D/2)U_r^2\eta = (\tau_b - \tau_{sf})\lambda \quad (3.11)$$

where F_D is the form drag, C_D is a drag coefficient that depends on the bedform shape, U_r is the reference velocity associated with the internal boundary layer, η is the bedform height, and λ is the bedform wavelength. Substituting Equation (3.5) for U_r , Equation (3.11) becomes:

$$\tau_b - \tau_{sf} = \frac{\rho C_D}{2} \left[\frac{(u_*)_n}{\kappa} \ln \frac{z_*}{(z_0)_n} \right]^2 \frac{\eta}{\lambda} \quad (3.12)$$

where $(u_*)_n$ and $(z_0)_n$ are the shear velocity and roughness length associated with the internal boundary layer and z_* is the “matching height” where the outer flow meets the internal flow. Evaluating $z_*/(z_0)_n$ in terms of the average height of the internal boundary layer over the bedform wavelength and substituting into Equation (3.12) yields the partitioning ratio τ_b/τ_{sf} :

$$\frac{\tau_b}{\tau_{sf}} = 1 + \frac{C_D}{2\kappa^2} \frac{\eta}{\lambda} \left[\ln a_1 \left(\frac{\lambda}{z_0} \right)^{4/5} \right]^2 \quad (3.13)$$

which is then used to approximate τ_{sf} from a reasonable estimate of τ_b . The partitioning ratio given by Equation (3.13) is typically in the range 2 to 3 for many natural systems (Harris, 2003).

CHAPTER 4

DETECTING BEDFORM MIGRATION

This chapter presents a new technique for quantifying bedform migration from high-resolution bathymetry. This novel approach explores the use of a fingerprint-detection algorithm (Bishnu et al., 2002) to convert bathymetry to a binary map of bedform crests, which are subsequently tracked using a normalized two-dimensional spatial cross-correlation technique (Duffy and Hughes-Clarke, 2005). This new approach has advantages over techniques currently used to track bedform migration, which tend to focus on surfaces (e.g. depth and maximum slope) which may not adequately emphasize bedform morphology (Duffy and Hughes-Clarke, 2005; Buijsman and Ridderinkhof, 2008).

4.1 BISHNU: A New Technique for Ridge Detection

A new algorithm (BISHNU) has been applied to delineate dune crest (“ridge”) locations from bathymetric data. BISHNU applies a two-pass combinatorial classification scheme to extract ridge locations from a bathymetric DTM, and produces a binary image (“ridge map”) of ridge-classified grid cells. The ridge maps are subsequently used to determine dune-crest displacements using a spatial cross-correlation technique (Duffy and Hughes-Clarke, 2004; 2005). This section provides a detailed overview of how BISHNU has been implemented to produce binary ridge maps from bathymetric data.

A brief overview of the algorithm is presented here to provide context for the in-depth discussion that follows in this section. BISHNU is comprised of several subroutines, which are implemented in sequential order. The subroutines implemented by BISHNU proceed as follows:

- (1) Convert gridded bathymetry (“DTM”) from XYZ format to a binary format (*.DBL);
- (2) Apply two-dimensional Gaussian filter to the binary DTM to reduce influence of noise;
- (3) Implement a (two-pass) combinatorial algorithm for classifying ridges based on topographical relationships between neighboring grid cells (“pixels”) in the binary DTM. In the first pass each pixel is assigned a label that may be “unambiguous” (ridge, valley, or slope) or “ambiguous” (ridge/valley, ridge/slope, or unknown). Ambiguously-labeled pixels are passed to subroutine (4);
- (4) Resolve ambiguous preliminary labels by examining their relationship with neighboring unambiguous pixels. In this second pass, all pixels receive an unambiguous, final label (slope, valley, crest).
- (5) Compile a map of all crest-labeled pixels. This is the binary ridge map, and is output in *.BMP image format.

As stated above, prior to running BISHNU the bathymetry must be converted to binary format. A program, XYZ2DBL, has been developed to convert the gridded bathymetry from XYZ format to the requisite binary format (*.DBL). Subsequently, the first step undertaken by BISHNU is to remove high-frequency noise from the DTM by

applying a two-dimensional Gaussian filter. Optional arguments allow the user to specify the kernel size (in grid cells) of the Gaussian filter, as well as the number of times the filter is applied to the DTM.

After smoothing the DTM, BISHNU begins a two-pass combinatorial algorithm for classifying ridges within the DTM based on topographical relationships (i.e., slope) between neighboring grid cells. This aspect of the algorithm was originally developed for ridge extraction in grayscale fingerprint images for the purposes of automated fingerprint identification (Bishnu et al., 2002). Here, DTM grayscale is a function of the gridded depth.

The first pass applied by BISHNU examines the gradient along a path (“walk”) through a grid cell (P) with boundary grid cells $B = \{p_{i-1,j}, p_{i+1,j}, p_{i-1,j-1}, p_{i+1,j+1}, p_{i,j-1}, p_{i,j+1}, p_{i+1,j-1}, p_{i-1,j+1}\}$ corresponding to directions $\{N, S, NW, SE, W, E, SW, NE\}$ (Fig. 4-1). There are four possible directions (D) for a straight-line walk from each point in B to another point in B through P , and these directions D are defined as $(k,l) \in \{(N,S), (NW,SE), (W,E), (SW,NE)\}$, where (k,l) is a fixed direction of walk from k to l . Two categories of elementary walks (w_1 and w_2) can be defined, where w_1 is defined as a movement from any point in B to P , and w_2 is defined as a movement from P to any point in B (Fig. 4-1). A straight-line walk along any of the directions of D (e.g. from NW to SE) consists of a walk w_1 followed by another walk w_2 in the same direction.

The first pass of BISHNU examines the gradient along each elementary walk w_1 and w_2 , where gradient is defined as the difference in depth (L) between P and any point on B (or vice versa). Note that depth L is positive. For the example of a walk through P along $(k,l) = (N, S)$, the gradient is measured as $L'_{w_1} = L(i-1,j) - L(i,j)$ for w_1 and as $L'_{w_2} =$

$L(i,j)-L(i+1,j)$ for w_2 (Fig. 4-1). The gradient along any direction $(k,l) \in D$ is defined as the first difference pair $\Delta_{(k,l)} = \{L'_{w1,(k,l)}, L'_{w2,(k,l)}\}$, and $sign(\Delta_{(k,l)}) = \{sign(L'_{w1,(k,l)}), sign(L'_{w2,(k,l)})\}$ denotes the sign of this pair, where there are three possible signs:

- (i) $sign(L'_{w_x(k,l)}) = +, L'_{w_x(k,l)} > 0$ (Depth decreases)
- (ii) $sign(L'_{w_x(k,l)}) = -, L'_{w_x(k,l)} < 0$ (Depth increases)
- (iii) $sign(L'_{w_x(k,l)}) = 0, L'_{w_x(k,l)} = 0$ (Depth remains the same)

In order to remove additional uncertainty from the gradient calculation, the directional average is taken for a 5 by 5 neighborhood of pixels along each of the directions $(k,l) \in D$ for calculating L'_{w1} and L'_{w2} .

The pixel P is classified along a single direction $(k,l) \in D$ with respect to the change in gradient along that direction $\Delta_{(k,l)} = \{L'_{w1,(k,l)}, L'_{w2,(k,l)}\}$. Figure 4-1 identifies the nine possible combinatorial possibilities for the sign of the first difference pair $sign(\Delta_{(k,l)}) = \{sign(L'_{w1,(k,l)}), sign(L'_{w2,(k,l)})\}$, resulting in four possible labels for P : crest (CR), valley (VA), slope (SL) and unknown (UN). Note that the first three of these labels are unambiguous, while the fourth is ambiguous.

The preliminary label given to P during the first pass of BISHNU is determined by the combination of labels given to P along all four directions $(k,l) \in \{(N,S), (NW,SE), (W,E), (SW,NE)\}$. Bishnu et al. (2002) identify 35 possible combinatorial possibilities for the generation of this preliminary label, summarized in Table 4-1. This table is implemented by BISHNU as a look-up table (LUT). Depending on the labels assigned along the four directions, a grid cell is assigned to an unambiguous class CR , VA , or SL ; or to an ambiguous class CV (can be crest or valley), CS (can be crest or slope), VS (can

be valley or slope), or XX (can be crest, valley, or slope). All cases that cannot be unambiguously classified are processed further during the second pass of BISHNU.

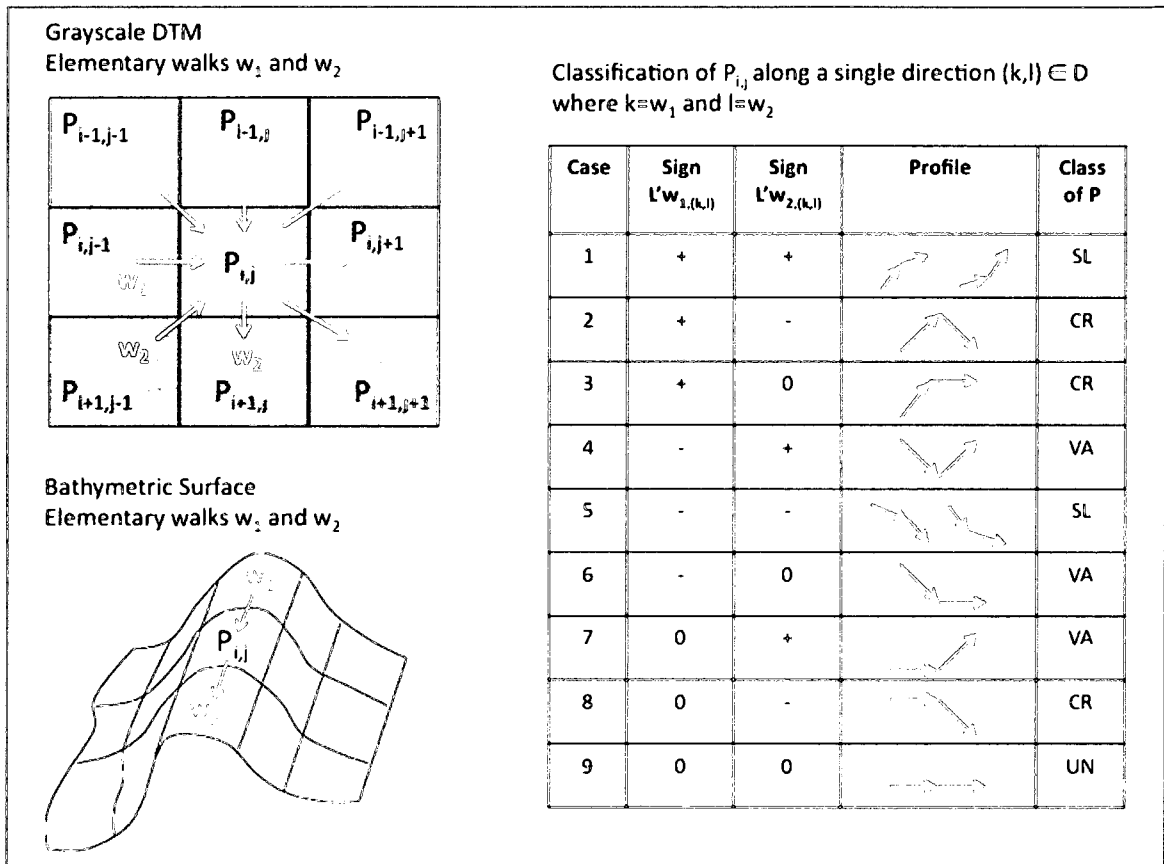


Figure 4-1. Left: bathymetric DTM with depiction of gradient along a straight-line walk $\{w_1, w_2\}$ through grid cell $P_{i,j}$. DTM grayscale values correspond to gridded depth. Right: preliminary classification of $P_{i,j}$ along a single straight-line walk $\{w_1, w_2\}$. The four possible labels $\{SL, CR, VA, UN\}$ assigned to grid cell $P_{i,j}$ correspond to slope, crest, valley and unknown, respectively. Figure adapted from Bishnu et al. (2002).

Table 4-1. Preliminary classification of P_{ij} during first pass of BISHNU (combinatorial approach). Table from Bishnu et al. (2002).

No. of Cases	No. of classes in preliminary set				Preliminary Label
	CR	VA	SL	UN	
1	0	0	0	4	XX
2	0	0	1	3	XX
3	0	0	2	2	XX
4	0	0	3	1	SL
5	0	0	4	0	SL
6	0	1	0	3	XX
7	0	1	1	2	XX
8	0	1	2	1	XX
9	0	1	3	0	VS
10	0	2	0	2	VA
11	0	2	1	1	VA
12	0	2	2	0	VS
13	0	3	0	1	VA
14	0	3	1	0	VA
15	0	4	0	0	VA
16	1	0	0	3	XX
17	1	0	1	2	XX
18	1	0	2	1	CS
19	1	0	3	0	CS
20	1	1	0	2	CV
21	1	1	1	1	CV
22	1	1	2	0	CV
23	1	2	0	1	CV
24	1	2	1	0	CV
25	1	3	0	0	VA
26	2	0	0	2	CR
27	2	0	1	1	CR
28	2	0	2	0	CR
29	2	1	0	1	CR
30	2	1	1	0	CR
31	2	2	0	0	CV
32	3	0	0	1	CR
33	3	0	1	0	CR
34	3	1	0	0	CR
35	4	0	0	0	CR

The second pass of BISHNU determines the final label for all ambiguously classified grid cells (CV , CS , VS , XX). These grid cells are finally classified by inspecting a square neighborhood $R(P)$ for the presence of unambiguously classified grid cells (CR , VA , SL) (Fig. 4-2). BISHNU calculates the mean grayscale value of the pixels within each class CR , VA and SL in $R(P)$ as $Mean(CR)$, $Mean(VA)$, and $Mean(SL)$, respectively, and classifies the grid cell $P \in (CV, VS, VS, XX)$ based on the closeness of the grayscale value $L_{(i,j)}$ of P to a class-averaged value $Mean(CR)$, $Mean(VA)$, and $Mean(SL)$. For example, $P \in CV$ is classified as either CR or VA based on the closeness of $L_{(i,j)}$ to $Mean(CR)$ or $Mean(VA)$. A grid cell $P \in XX$ is assigned to either CR , VA or SL (Fig. 4-2). BISHNU allows the user to specify the dimensions of $R(P)$ to be used in the second pass. Bishnu et al. (2002) recommend that the user select a region of size ($W \times W$) where $W=(r\lambda)/\sqrt{2}$ and r is the desirable number of crest lines (~ 3) located in $R(P)$. Following this method, the appropriate value of W for this study would be at least 10 m. We determined, however, that a much smaller value of $W = 0.5\lambda = 2.5$ m yielded a better result (e.g., smoother ridge lines), where λ is the minimum wavelength (5 m) within the DTM.

4.2 Spatial Cross-Correlation

Although many methods exist for quantifying bedform migration, it is often difficult to detect movements of very small magnitude (decimeters or less). Moreover, many methods, particularly profile-based methods, are unable to capture the full spatial resolution of bedform migration across a three-dimensional seafloor. In this study, a spatial cross-correlation method for detecting bedform migration (Duffy and Hughes-Clarke, 2005) has been adapted for analysis of binary ridge maps produced by BISHNU.

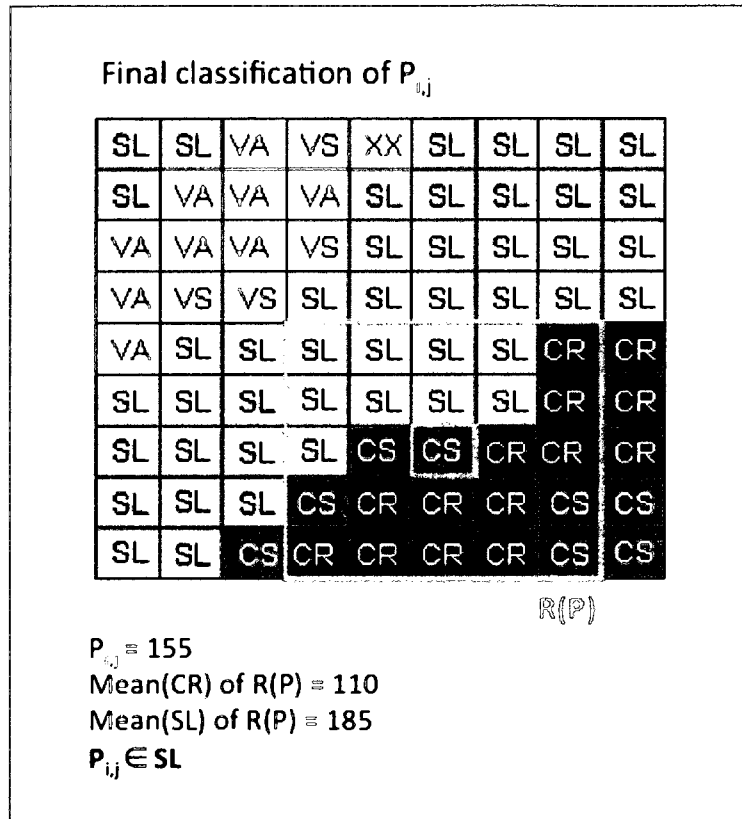


Figure 4-2. Second pass of BISHNU, where final label is assigned to grid cell P_{ij} at center of R(P). This step is repeated for all pixels with ambiguous labels {CV, CS, VS, XX}. Pixels assigned an ambiguous label {CV, CS, VS, XX} may be a crest or valley (CV); crest or slope (CS); valley or slope (VS), or a crest, valley, or slope (XX).

The technique of Duffy and Hughes-Clarke (2005) uses a simple, normalized two-dimensional cross-correlation routine to measure bedform migration by identifying the region over which two bathymetric datasets are most highly correlated (i.e., most similar). This technique has been implemented on a number of representations of the bathymetric surface, including bathymetric DTMs, grayscale images of maximum slope, and grids of variance around mean depth derived from ADCP profiles (Duffy and Hughes-Clarke, 2005; Buijsman and Ridderinkhof, 2008). As Duffy and Hughes-Clarke (2005) note, the cross-correlation method works best where bedforms dominate the input

imagery. Whereas the maximum slope surface more strongly emphasizes the dune morphology with respect to the bathymetric DTM, the slope surface is also prone to emphasizing any artifacts present in the underlying bathymetry (e.g., heave, tide, and/or offset artifacts) (Fig. 4-3). Conversely, binary ridge maps derived from the bathymetric surface provide maximum contrast between the dune crests and the surrounding seafloor, while excluding artifacts (that are smoothed by a Gaussian filter in BISHNU).

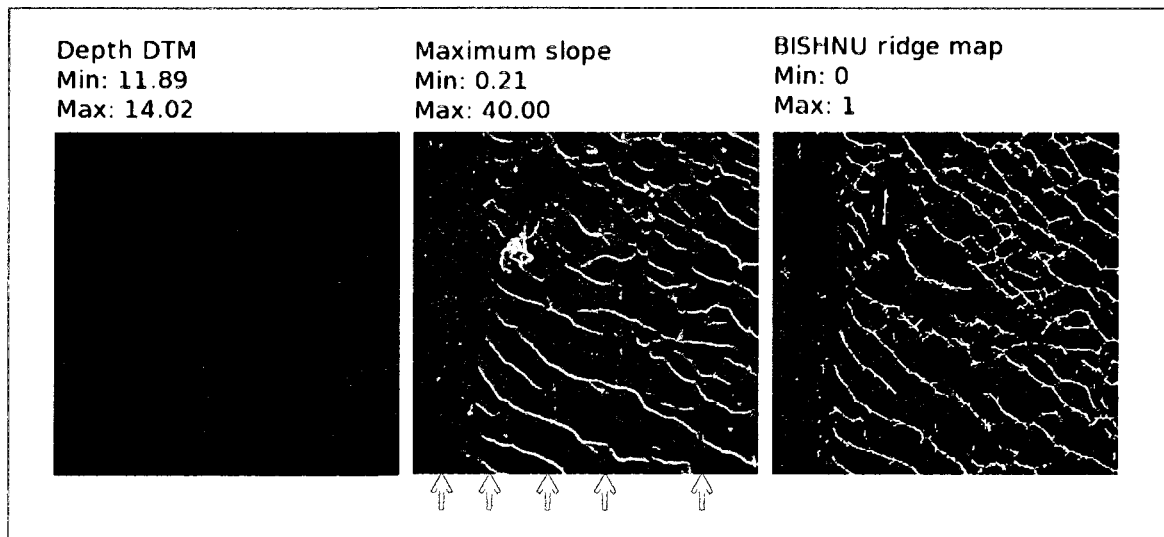


Figure 4-3. Comparison of candidate input surfaces to cross-correlation algorithm. From left to right: depth, slope, and ridge map (output from BISHNU). Dynamic range of each candidate surface is noted. Morphology is obscured in depth DTM because of the narrow dynamic range {11.89, 14.02} which appears as near-black in a grayscale image (0=black, 255=white). Maximum slope has a wider dynamic range {0.21 40.00} but emphasizes data artifacts, which are indicated by red arrows. BISHNU ridge map is a binary image with range {0, 1}, where ridge pixels are assigned a value of 1 and non-ridge pixels are assigned a value of 0. Ridge map most strongly emphasizes the dune morphology.

The cross-correlation (CC) method is used to examine spatial patterns from a series of two discrete data sets, which are defined here as two binary ridge maps, MAP₁ and MAP₂, acquired at time steps t_1 and t_2 . The cross-correlation coefficient quantifies the strength of correlation of MAP₁ and MAP₂, and is the sum of the products of overlapping pixels of windowed spatial variables $f(x,y)$ and $g(x,y)$, where $f(x,y)$ is a subset of MAP₁ and $g(x,y)$ is a subset of MAP₂ (Fig. 4-4). The calculation of the cross-correlation coefficient is iterated by incrementing and decrementing the relative displacement in the x and y directions by k and l , respectively. The cross-correlation coefficient is given by:

$$R_{k,l} = \frac{\sum_{x=0}^{w_x} \sum_{y=0}^{w_y} [f(x,y) - \bar{f}][g(x-k, y-l) - \bar{g}_{k,l}]}{\sqrt{\sum_{x=0}^{w_x} \sum_{y=0}^{w_y} [f(x,y) - \bar{f}]^2 \sum_{x=0}^{w_x} \sum_{y=0}^{w_y} [g(x-k, y-l) - \bar{g}_{k,l}]^2}} \quad (4.1)$$

$$-M \leq k \leq M, k \in Z, \quad -N \leq l \leq N, l \in Z,$$

$$R = \begin{bmatrix} R_{-M,N} & \cdots & \cdots & \cdots & R_{M,N} \\ \vdots & & & R_{k_{MAX},l_{MAX}} & \vdots \\ \vdots & & R_{0,0} & & \vdots \\ \vdots & & & & \vdots \\ R_{-M,-N} & \cdots & \cdots & \cdots & R_{M,-N} \end{bmatrix}$$

where the cross-correlation coefficient $R_{k,l}$ is normalized to $\{-1, 1\}$ by subtracting the mean of each spatial variable and dividing by the standard deviation. The position of the maximum $R_{k_{MAX},l_{MAX}}$ of the resulting $2M+1$ by $2N+1$ cross-correlation coefficient matrix R is the integer displacement of $g(x,y)$ relative to $f(x,y)$ where they are highest correlated. $R_{0,0}$ defines the zero lag position, i.e., where there is no displacement of $g(x,y)$ relative to $f(x,y)$. The cross-correlation coefficient matrix R is populated as $f(x,y)$ and $g(x,y)$ are displaced relative to one another; once R is fully populated, the windows $f(x,y)$ and $g(x,y)$ are advanced to the next position in the data set (Fig. 4-4).

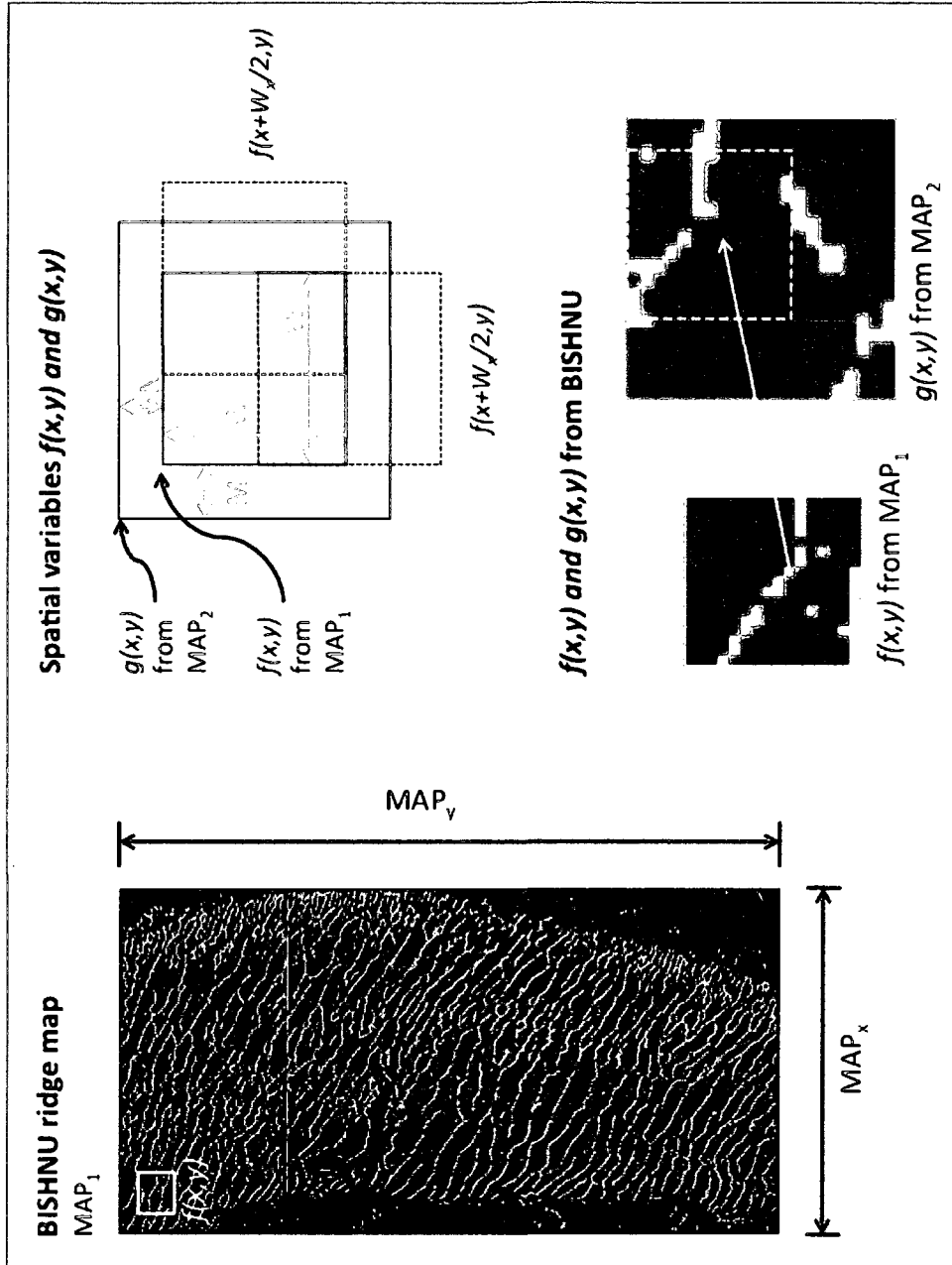


Figure 4-4. Relationship between BISHNU ridge map MAP₁ and the cross-correlation spatial variables $g(x,y)$ and $f(x,y)$. Figure modified from Duffy and Hughes-Clarke (2005).

Duffy and Hughes-Clarke (2005) present several methods for choosing the migration vector from the cross-correlation coefficient matrix R . This study uses the weighted centroid method, which draws the migration vector from the zero lag position to the weighted centroid of a threshold region around $R_{k_{MAX},l_{MAX}}$ (Fig. 4-5). This method, which takes into consideration the shape of the region of maximum correlation in R , is an improvement upon the often-erratic maximum correlation pick, where the migration vector extends from the zero lag position to $R_{k_{MAX},l_{MAX}}$. The threshold region is defined as the region around $R_{k_{MAX},l_{MAX}}$ where $R_{k,l}$ exceeds a threshold value of $R_{k_{MAX},l_{MAX}}/\sqrt{2}$ (Duffy and Hughes-Clarke, 2005). Although the weighted centroid method was used in this study, it was found to yield unreliable results where a weak correlation existed between the spatial variables $f(x,y)$ and $g(x,y)$. Thus, the cross-correlation routine was not performed when $R_{k_{MAX},l_{MAX}}$ fell below a critical value, which was chosen from a cumulative frequency curve of all $R_{k_{MAX},l_{MAX}}$. The critical value is defined here as 0.7, which is the value exceeded by 95% of all $R_{k_{MAX},l_{MAX}}$.

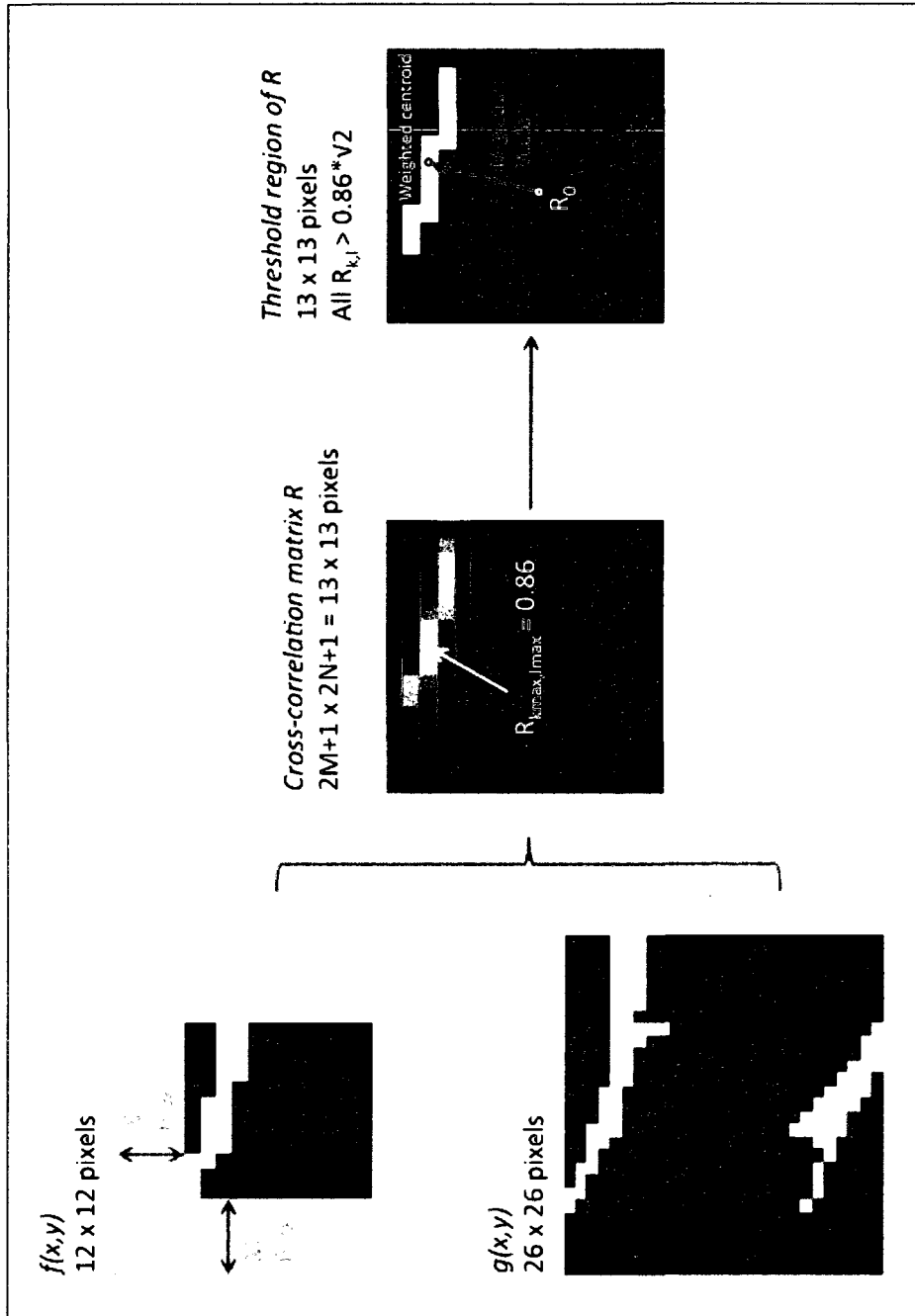


Figure 4-5. Weighted centroid method of Duffy and Hughes-Clarke (2005). At far right is a binary image of the threshold region of R , where all “threshold” pixels $> 0.86 \cdot \sqrt{2}$ are labeled. The migration vector is drawn from the zero lag position to the weighted centroid of this threshold region.

CHAPTER 5

RESULTS

This chapter presents results from field surveys undertaken to assess bedform migration and bed shear stress in Portsmouth Harbor. Results from sediment sampling and underwater videography surveys are presented in Section 5.1. Sections 5.2 and 5.3 present results from multibeam echosounder surveys conducted in June 2007 and July 2008, as well as an overview of bedform-migration results produced by spatial cross-correlation of the BISHNU ridge maps. Sections 5.4 and 5.5 present results from the July 2008 current-meter deployment in Portsmouth Harbor, as well as bed shear stress estimates using the log-profile (LP) and drag-coefficient (DC) techniques discussed in Chapter 3.

5.1 Sediment Samples and Underwater Videography

Results from grain-size analyses of 19 sediment samples from Portsmouth Harbor are presented in Table 5-1. Ten samples are located within the dune field, and four are located along the eastern periphery of the dune field, adjacent to the channel thalweg. Of the remaining five samples, two are located in the channel thalweg to the east of the dune field and three are located near the shoreline to the west of the dune field (Fig. 5-1). Grain-size distributions of the sediment samples are shown in Figure 5-1. A ternary plot showing the relative distributions of gravel, sand and mud for the sediment samples is presented in Figure 5-2.

The sediment samples retrieved from Portsmouth Harbor are predominantly sand and gravel and contain very little silt and clay; no sample contains more than 3.5%

combined silt and clay. Sediments within the dune field are predominantly medium sands; mean grain size ranges from 1.73 to 0.80 ϕ (0.30 to 0.57 mm) and median grain size ranges from 1.75 to 0.91 ϕ (0.30 to 0.53 mm). Sediments along the dune field periphery are predominantly coarse sands, with a mean grain size range of 1.05 to -0.69 ϕ (0.48 to 1.61 mm) and a median grain size range of 1.10 to -0.35 ϕ (0.47 to 1.27 mm). Sediments in the channel thalweg and along the shoreline range from medium and coarse sands to gravel. Mean grain size in these areas varies from 0.33 to -2.87 ϕ (0.80 to 7.31 mm), whereas median grain size varies from 1.70 to -4.18 ϕ (0.31 to 18.13 mm).

Table 5-1. Grain-size statistics from Portsmouth Harbor sediment samples, using Folk and Ward (1957) logarithmic method. Mean and median grain size and sorting are in units of ϕ , where $\phi = -\log_2(\text{mm})$. Skewness and kurtosis are dimensionless. See Figure 5-1 for station locations.

Station ID	Mean (ϕ)	Median (ϕ)	Sorting (ϕ)	Skewness	Kurtosis
ADCP	1.048	1.103	0.742	-0.191	1.213
MAVS	1.733	1.753	0.536	-0.189	1.739
3.1	-0.456	0.286	2.52	-0.319	0.553
3.2	-0.691	-0.349	2.309	-0.156	0.546
3.5	-2.87	-4.175	2.33	0.787	2.656
4.1	0.685	1.015	1.203	-0.46	1.074
4.2	1.158	1.22	0.742	-0.194	1.152
4.3	0.94	1.196	1.125	-0.355	1.032
4.4	1.066	1.18	0.824	-0.281	1.175
4.5	1.384	1.509	0.754	-0.339	1.444
4.6	0.8	0.912	0.897	-0.23	1.04
4.7	0.936	0.991	0.771	-0.15	1.111
4.8	0.072	0.234	1.667	-0.154	0.844
5.4	1.132	1.196	0.72	-0.21	1.071
5.5	1.464	1.65	0.9	-0.381	1.464
5.6	0.334	1.632	2.541	-0.597	0.529
6.1	0.33	1.695	2.437	-0.663	0.731
6.4	0.211	0.23	1.192	-0.044	0.825
6.5	-0.669	0.003	2.577	-0.306	0.82

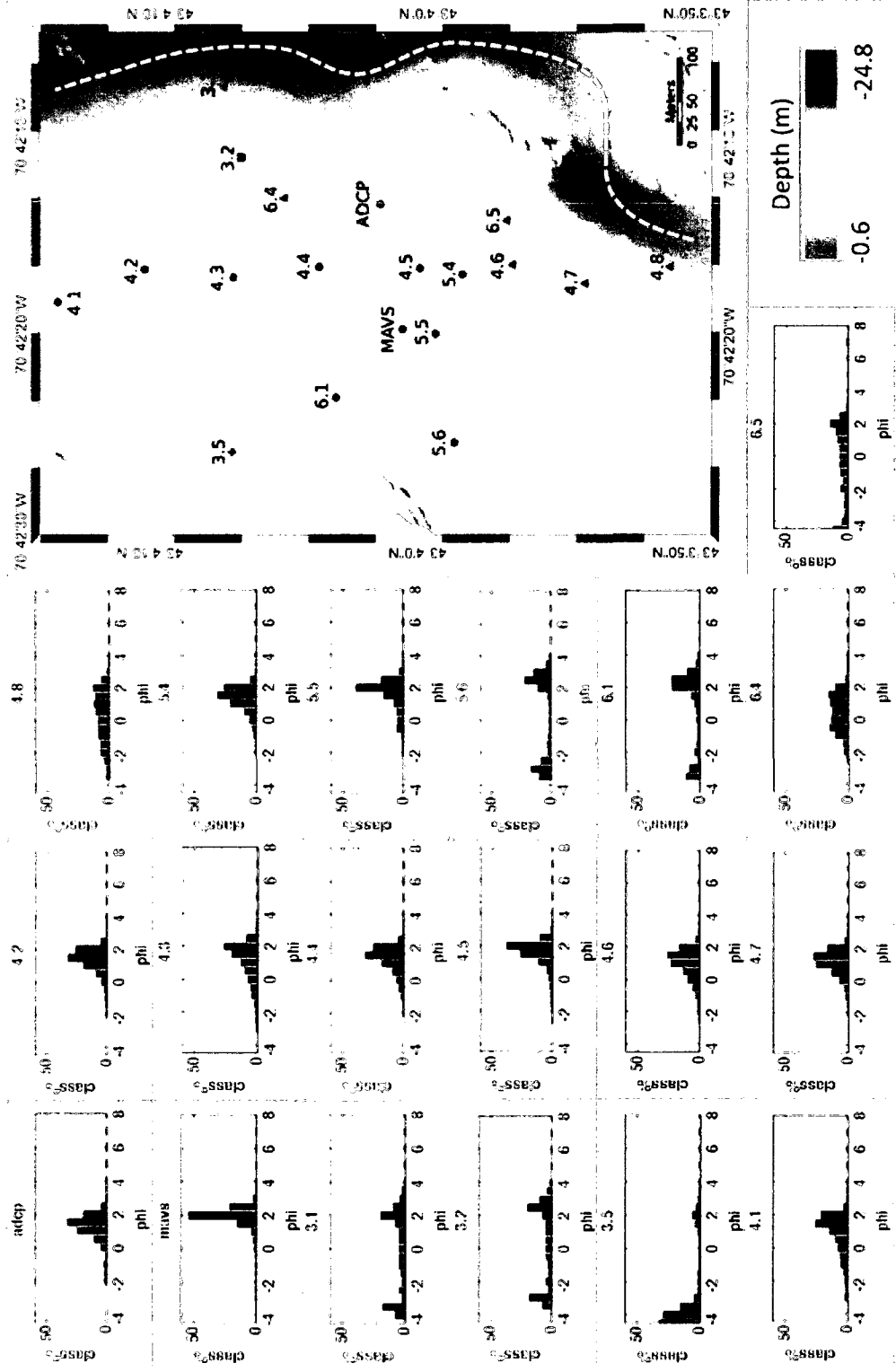


Figure 5-1. Location map of sediment samples in Portsmouth Harbor acquired on 25-26 February 2008 and on 2 July 2008. Histograms depict grain-size distribution for each sediment sample. White line on sample location map indicates approximate location of channel thalweg.

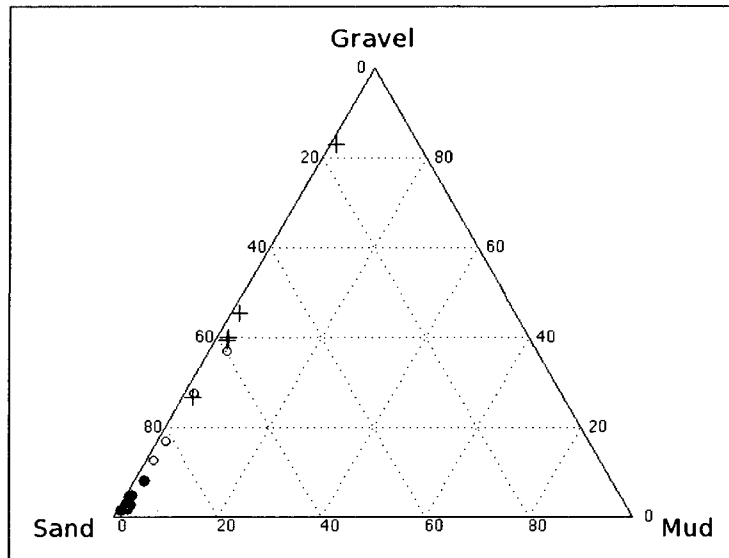


Figure 5-2. Ternary diagram showing percentages of gravel, sand and mud for Portsmouth Harbor sediment samples acquired on 25-26 February 2008. Filled circles represent samples taken from dune field; open circles represent samples taken from periphery of dune field; and crosses represent samples taken from locations outside of the dune field.

Selected images from the video survey are presented in Figure 5-3. Video imagery of the dune field reveals the presence of ripples (wavelength of ~0.20 m), which are superimposed on larger-scale sand dunes. The troughs of these ripples are delineated by the presence of shell hash (see Station 4.7 in Fig. 5-3). Several stations (e.g., Station 4.3 in Figure 5-3) within the sand wave field were populated by large colonies of sand dollars (*Echinarachnius parma* and/or *Mellita quinquesperforata*) (Dijkstra, Pers. Comm). Video observations from the periphery of the dune field reveal the presence of gravels and coarse shell hash just outside of the boundary of the dune field; observations from Station 4.8 capture the abrupt transition from sandy to gravelly sediments across this boundary (Fig. 5-3). Elsewhere, video imagery from the channel thalweg and shoreline indicate the presence of gravel pavement (Station 3.1) and cobbles with sand-and-gravel matrix (Station 6.1) (Fig. 5-3).

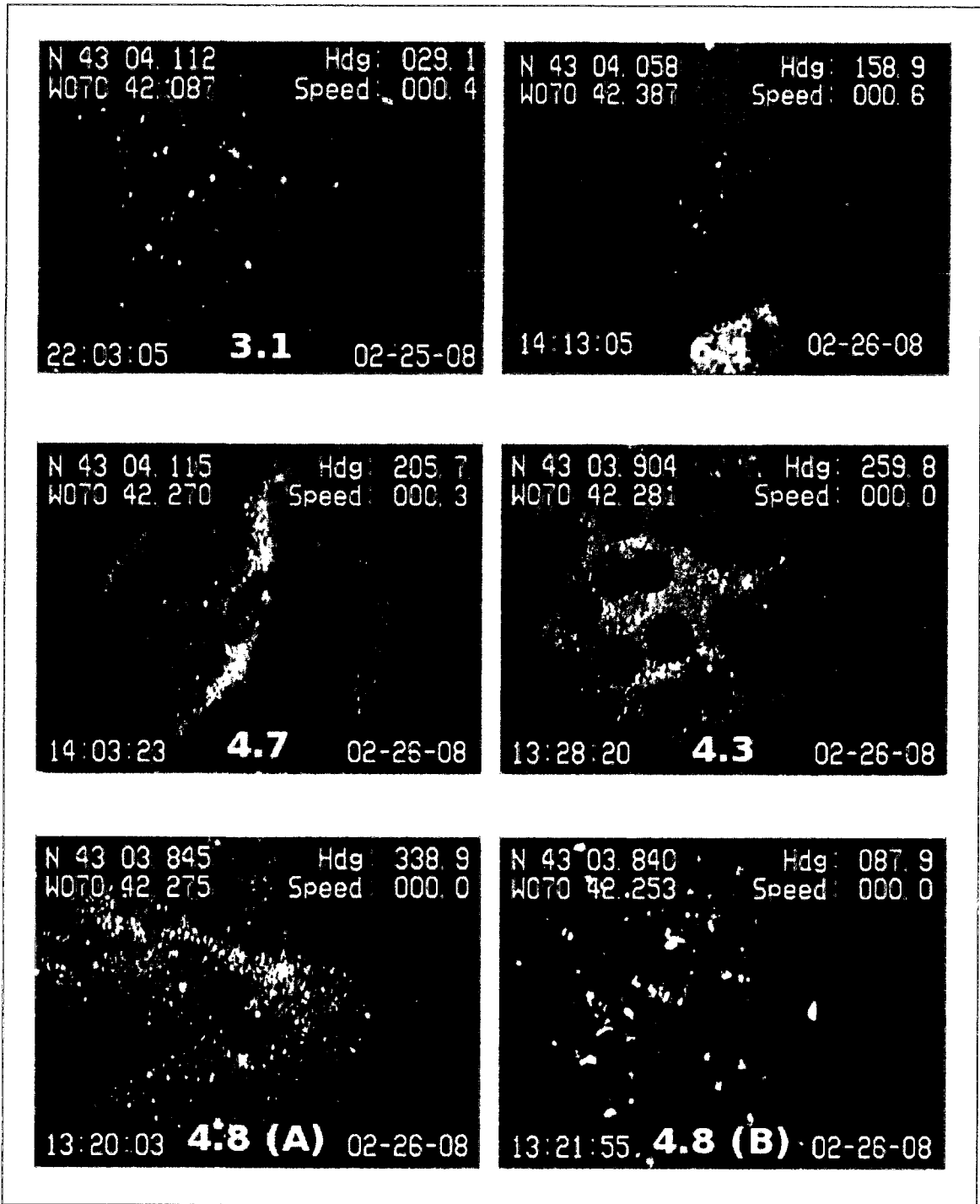


Figure 5-3. Still images from underwater video footage of sediment sampling stations in Portsmouth Harbor. Video survey was conducted on 25-26 February 2008. Distance between laser points in each image is 10 cm. Note the transition from sandy to gravelly sediments across the boundary of the dune field in images 4.8(A) and 4.8(B).

5.2 Bathymetry and Dune Morphology

Multibeam echosounder surveys were run on 9 June 2007 (1400 UTC), 9 June 2007 (2000 UTC), 14 June 2007 (1330 UTC), 14 June 2007 (1930 UTC), 15 June 2007 (1400 UTC), and on 3 July 2008 (1420 UTC) and 9 July 2008 (1630 UTC) (Table 5-2). Bathymetry from the 2007 MBES surveys is presented in Figure 5-4 and bathymetry from the 2008 MBES surveys is presented in Figure 5-5. The range of surveyed water depth within the survey area was 10 meters to 20.5 meters relative to mean lower low water (MLLW).

Table 5-2. Timing of multibeam echosounder surveys from 2007 and 2008.

Survey	Date	Start Time	End Time	Stage of Tide	Neap or Spring
1	8-Jun-07	1400 UTC	1530 UTC	Low Slack	Neap
2	8-Jun-07	2000 UTC	2130 UTC	High Slack	Neap
3	14-Jun-07	1330 UTC	1440 UTC	High Slack	Spring
4	14-Jun-07	1930 UTC	2050 UTC	Low Slack	Spring
5	15-Jun-07	1400 UTC	1530 UTC	High Slack	Spring
6	3-Jul-08	1420 UTC	1630 UTC	High Slack	Spring
7	9-Jul-08	1630 UTC	1810 UTC	Low Slack	Neap

Histograms of the horizontal total propagated uncertainty (HzTPU) of soundings from the seven completed MBES surveys are presented in Figure 5-6. HzTPU was calculated in CARIS HIPS using real-time *.SBET error data as described in Chapter 3. Typical HzTPU values for the MBES surveys (reported at 2DRMS) are in the range 0.15 to 0.25 m, which is just less than the resolution of the gridded data (0.25 m). The HzTPU values represent the absolute horizontal positioning uncertainty for each sounding. It is important to note, however, that bedform migration estimates are derived from the gridded data. The gridded data were processed using the CUBE algorithm implemented

in CARIS HIPS 6.1, and thus contain a separate vertical uncertainty estimate for each grid node that is a factor of the HzTPU and DpTPU (depth total propagated uncertainty) of the soundings contributed to each node. Moreover, the high-resolution MBES data yield a high concentration of soundings per grid node (approximately 18.5 soundings/node), which further decreases the uncertainty estimate associated with the gridded data. Because the HzTPU and DpTPU values from the seven completed MBES surveys are less than the resolution of the gridded data (0.25 m), and because of the high concentration of soundings contributing to each grid node, it is assumed that the horizontal positioning uncertainty of the gridded data is unlikely to be a source of significant error in determining the bedform-migration rates.

Gross morphology of the dune field did not appreciably change during periods observed in 2007 or in 2008, although the morphology changed dramatically during the roughly one-year period between the 2007 and 2008 surveys. Figure 5-7 presents detailed bathymetry from the 2007 field season, with cross sections to emphasize dune morphology. Figure 5-8 presents bathymetry from the 2008 field season. In 2007 and 2008, the interior of the dune field is populated by medium to large, two-dimensional, predominantly asymmetric subaqueous dunes (Ashley, 1990) with wavelengths of 8 to 12 m and heights of 0.4 to 0.8 m. The eastern periphery of the dune field is populated by small, two-dimensional, symmetric and asymmetric dunes with wavelengths of 3 to 5 m and heights of 0.1 to 0.5 m (e.g., cross sections C and H in Figure 5-7 and cross sections D and H in Figure 5-8). Dune-crest bifurcations are abundant, particularly in the interior of the dune field in both survey years. Complex bedforms including ladderbacks and cusped bedforms are dominant in the northwest quadrant of the dune field in both years.

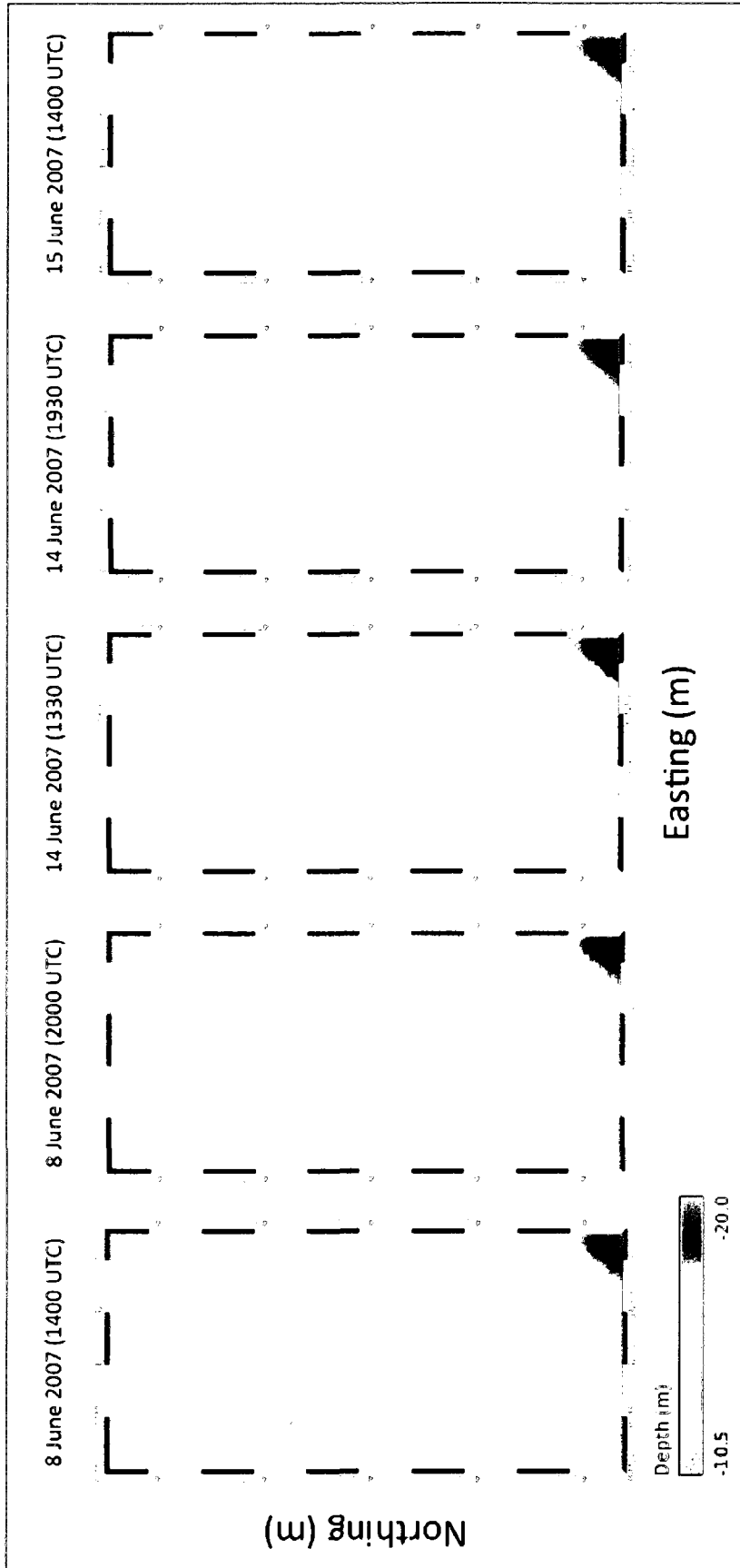


Figure 5-4. Multibeam echosounder (MBES) surveys of Portsmouth Harbor study area conducted from 8 June 2007 to 15 June 2007. Positioning is given in UTM coordinates (in meters, UTM Zone 19 N) to provide scale for the bathymetry. Map dimensions are 480 meters by 210 m.

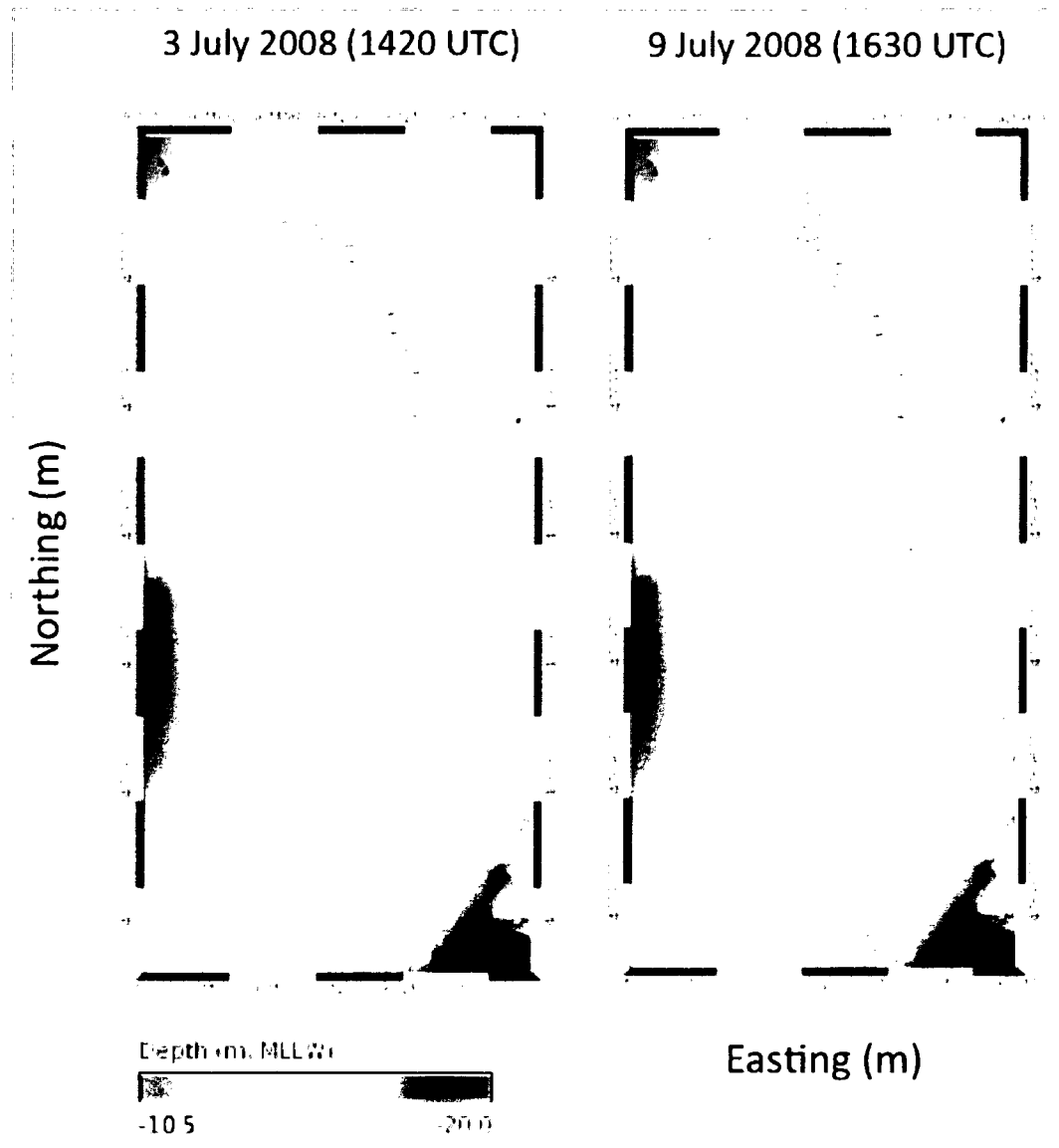


Figure 5-5. Multibeam echosounder (MBES) surveys of Portsmouth Harbor study area conducted on 3 July 2008 and 9 July 2008. Positioning is given in UTM coordinates (in meters, UTM Zone 19 N) to provide scale for the bathymetry. Black spots (in both images) on the shoal to the west of the dune field indicate areas with depths less than 10.5 m. Note that 2008 MBES survey area is larger than that of 2007. Map dimensions are 650 m by 300 m.

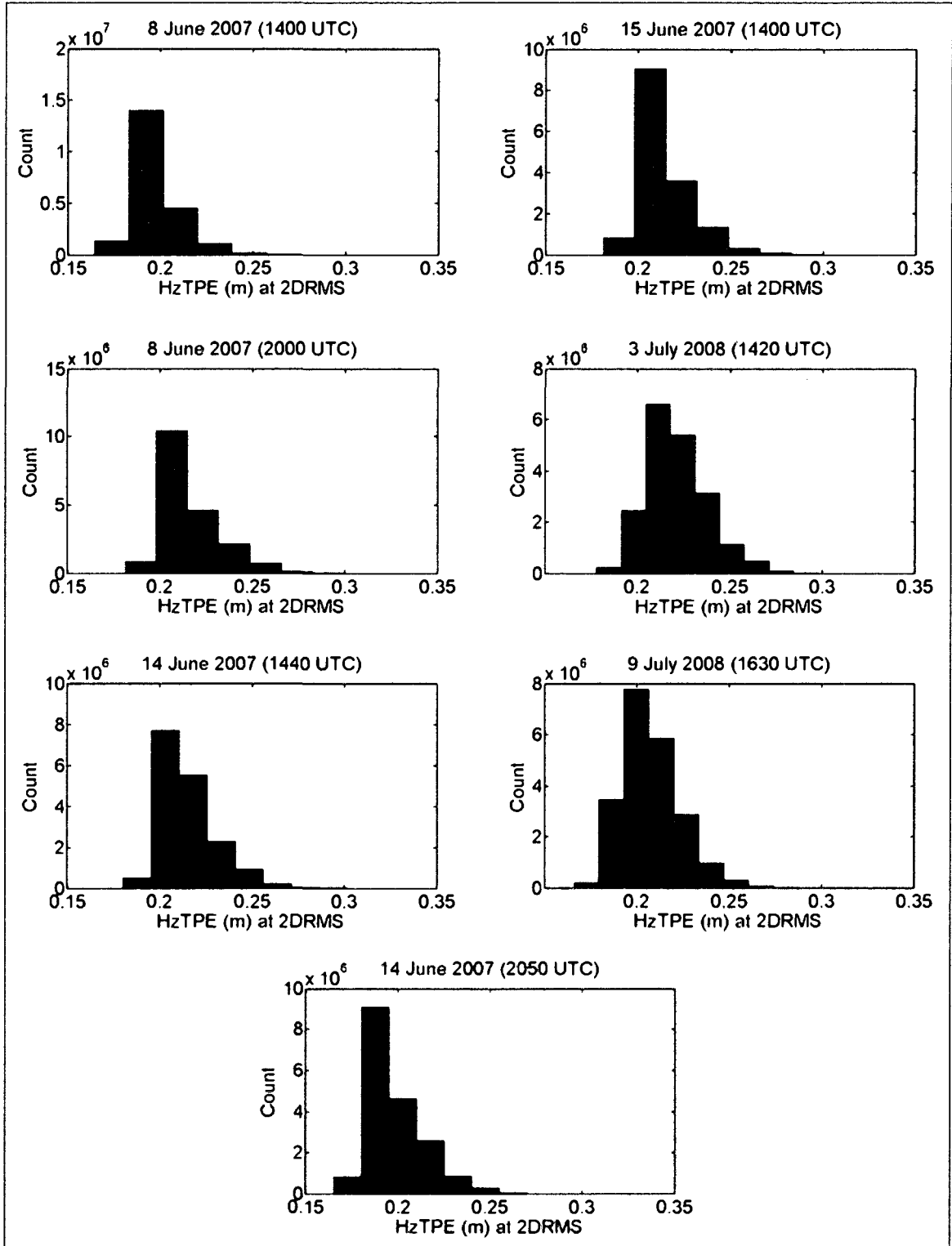


Figure 5-6. Histograms of horizontal total propagated uncertainty (HzTPE) of soundings from the seven multibeam echosounder surveys. HzTPE is reported at 2DRMS.

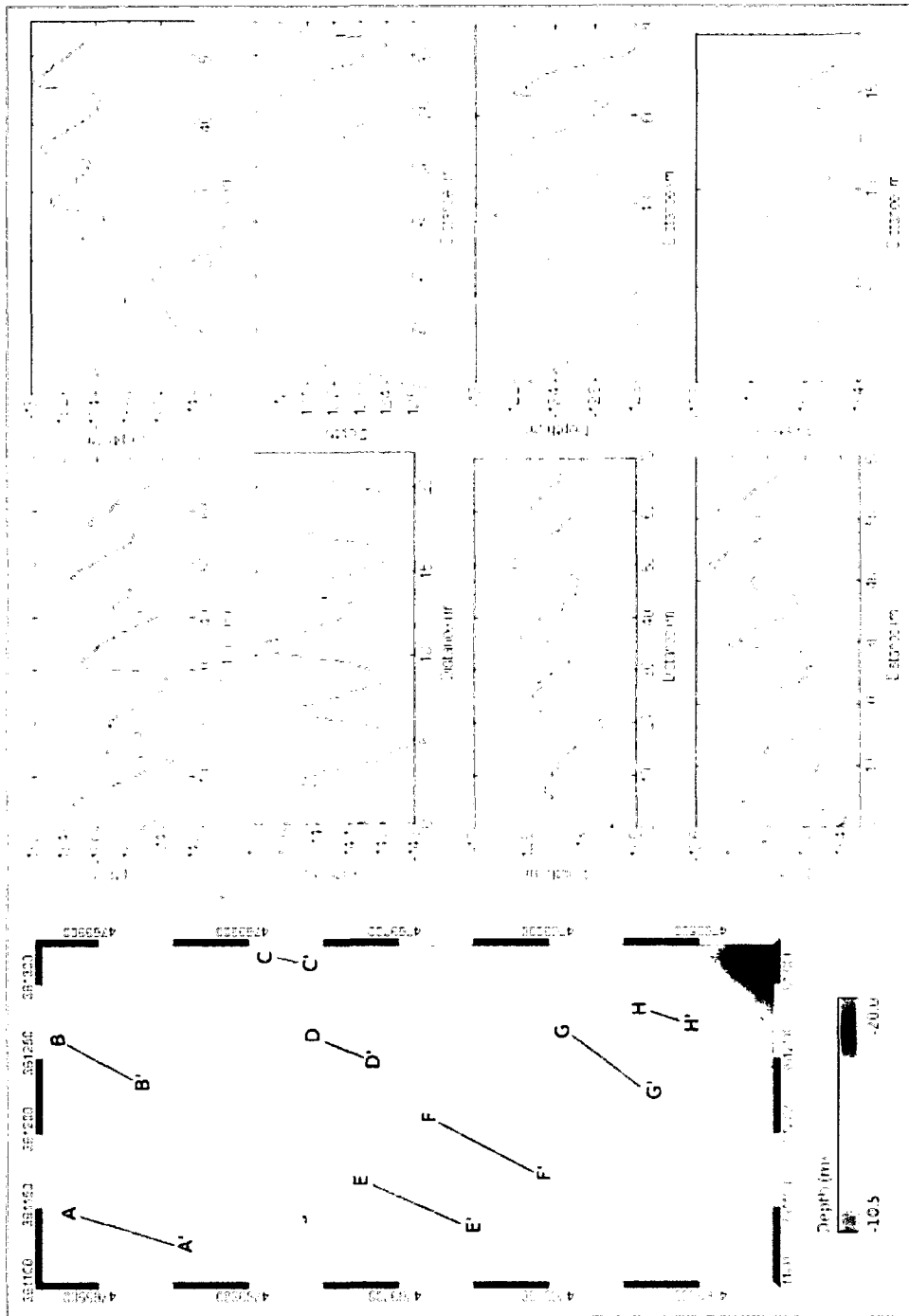


Figure 5-7. Multibeam echosounder (MBES) bathymetry from 2007 with bed elevation profiles. Note that vertical exaggeration is different for each profile. Bathymetry is from the 8 June 2007 (1400 UTC) survey.

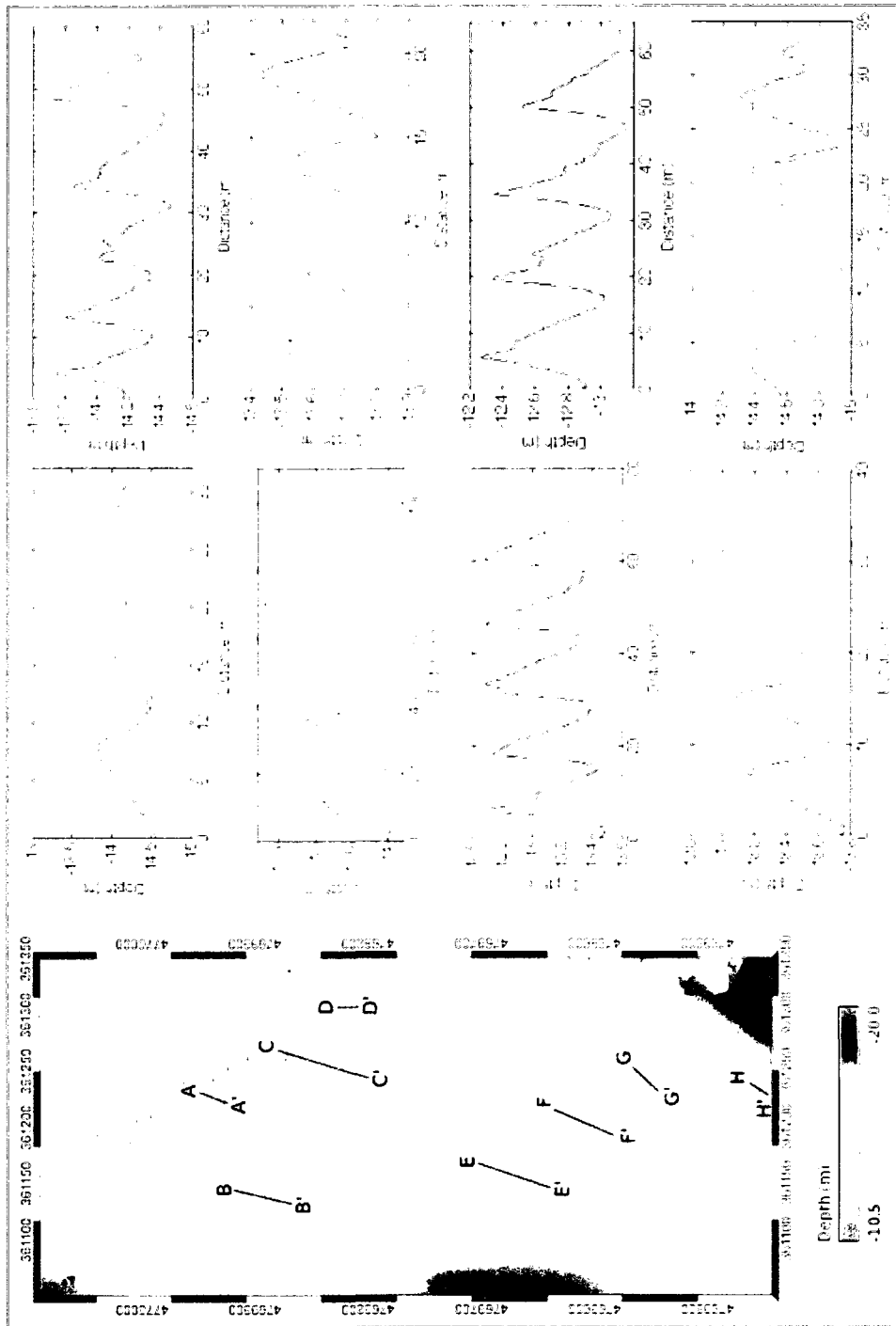


Figure 5-8. Multibeam echosounder (MBES) bathymetry from 2008 with bed elevation profiles. Note that vertical exaggeration is different for each profile. Bathymetry is from the 3 July 2008 (1420 UTC) survey.

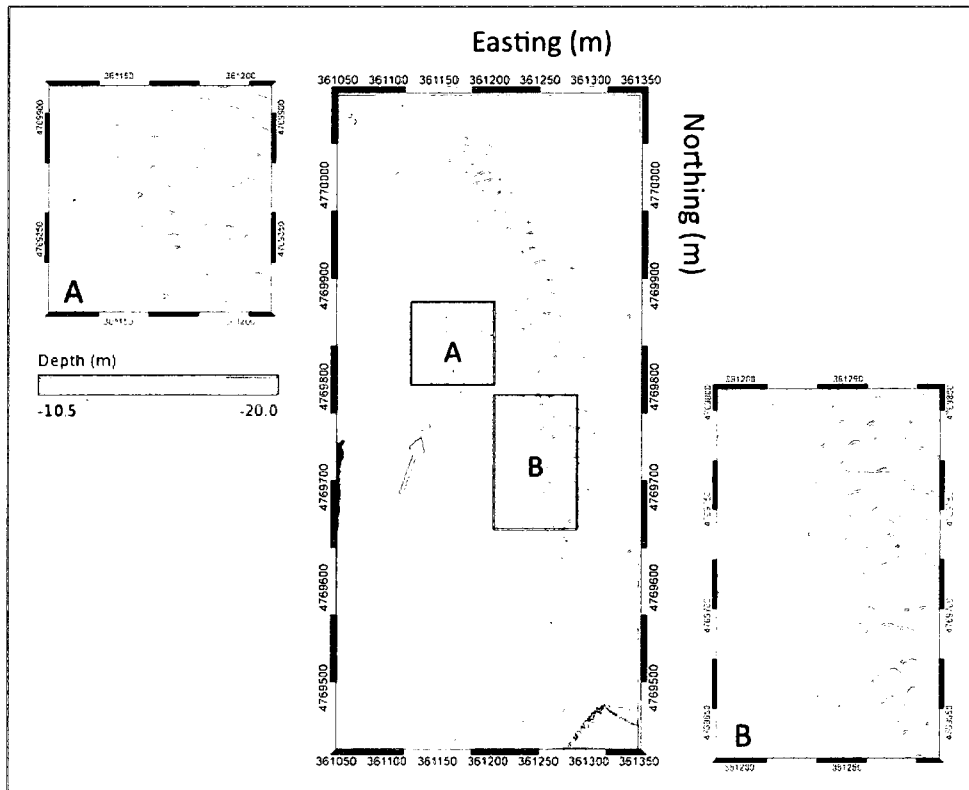


Figure 5-9. Close-up views of multibeam echosounder (MBES) bathymetry from 2008. Image A shows detail of complex bedforms in northwest quadrant of dune field, including ladderbacks and cusped bedforms. Image B shows detail of dune-crest bifurcations. Arrow indicates location of large (10 m by 12 m) target.

This area of complex bedforms is located to the north and east of a large (10 m by 12 m) target that appears to be a bedrock outcrop (Fig. 5-9).

The flood-ebb asymmetry of medium and large dunes within the interior of the study area is dramatically different from 2007 to 2008. The dunes in 2007 were uniformly flood-oriented across the bedform field (e.g., cross sections A, B, D, E, F and G in Figure 5-7). Dunes in 2008 in the western sector of the bedform field were moderately flood-oriented (e.g., cross sections B, E and F in Figure 5-8), whereas dunes in the eastern sector of the bedform field were moderately to strongly ebb-oriented (e.g. cross sections A, C and G in Figure 5-8). Dune crests of opposite asymmetry often join

together at a dune bifurcation (Fig. 5-9). Overall flood-oriented asymmetry was stronger in 2007 than in 2008. The orientation of medium and large dunes within the interior of the study area remained the same over 6-hr, 24-hr and multi-day periods observed in 2007 and 2008; ebb-oriented dunes remain ebb-oriented, and vice versa, upon the reversal of the tide.

The orientation of small dunes within the eastern periphery of the bedform field differed from 2007 to 2008. Small dunes were weakly flood-oriented in 2007 (cross sections C and H in Figure 5-7) and moderately to weakly ebb-oriented in 2008 (cross sections D and H in Figure 5-8). However, further inspection of bathymetry from the 2007 surveys indicates that the small-dune morphology was variable over time-scales longer than 24 hr (see cross section C from Figure 6-9).

5.3 Ridge Maps and Dune Migration

5.3.1 BISHNU Results

Very good agreement was observed between the BISHNU ridge-map output and the bathymetric surfaces. Figure 5-10 shows the BISHNU output for the MBES survey conducted on 8 June 2007 (1400 UTC), and Figure 5-11 shows the BISHNU output for the MBES survey conducted on 3 July 2008 (1420 UTC). The BISHNU input parameters used to obtain the results in this study (see Section 3.5 for further explanation) were a smoothing kernel size of 10 pixels (2.5 m) that was iterated a total of five times over the image, and a vicinity radius of 8 pixels (2.0 m). As shown in Figure 5-10 and Figure 5-11, the BISHNU ridge map successfully delineated dune crests visible on the bathymetric surface, regardless of wavelength; BISHNU delineated the crests of medium

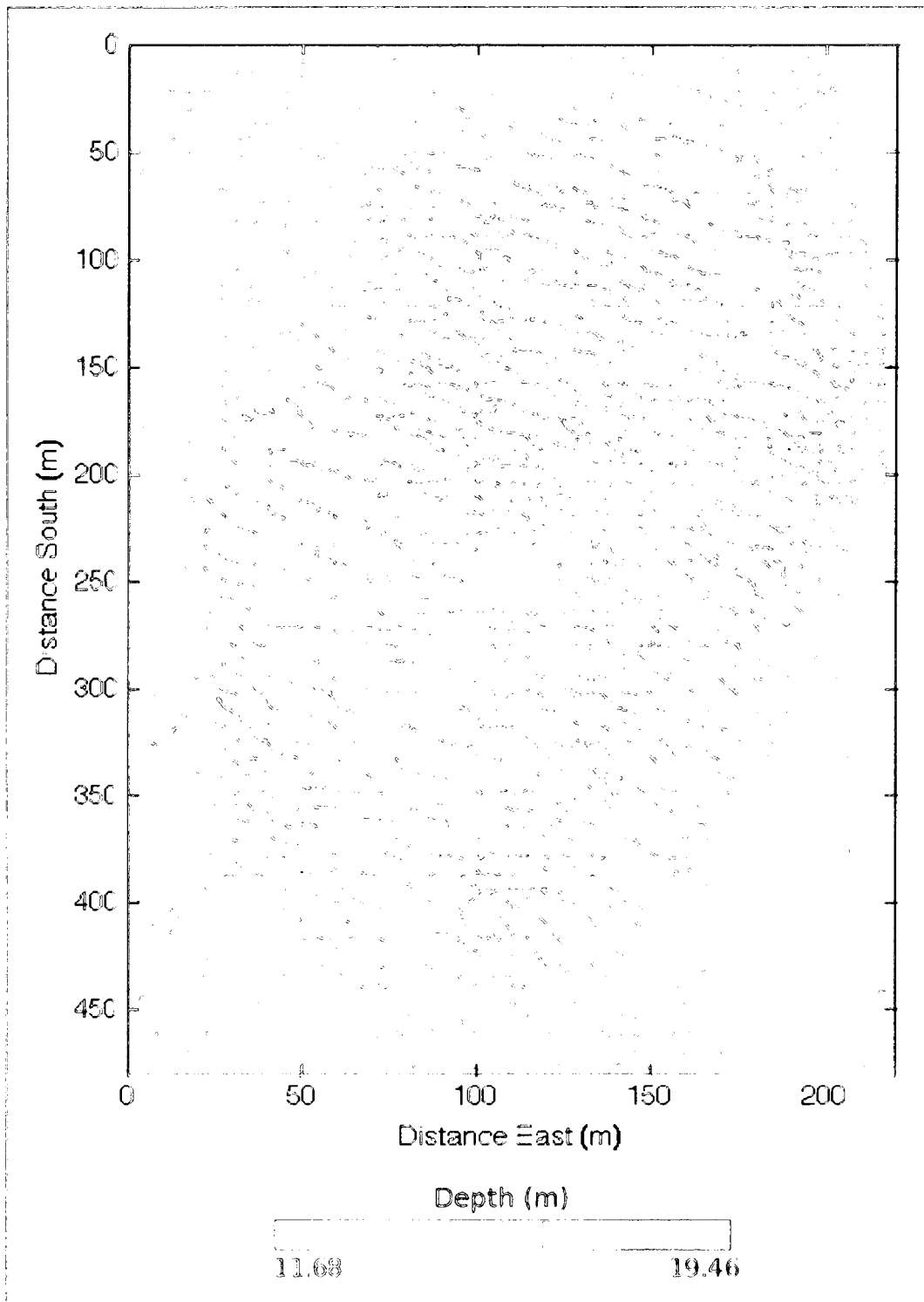


Figure 5-10. BISHNU results for 8 June 2007 (1400 UTC) survey superimposed on bathymetry. Depth range is approximately 10 m to 20.5 m (MLLW). Horizontal line is an artifact from the BISHNU algorithm, and has no significant impact on subsequent spatial cross-correlation.

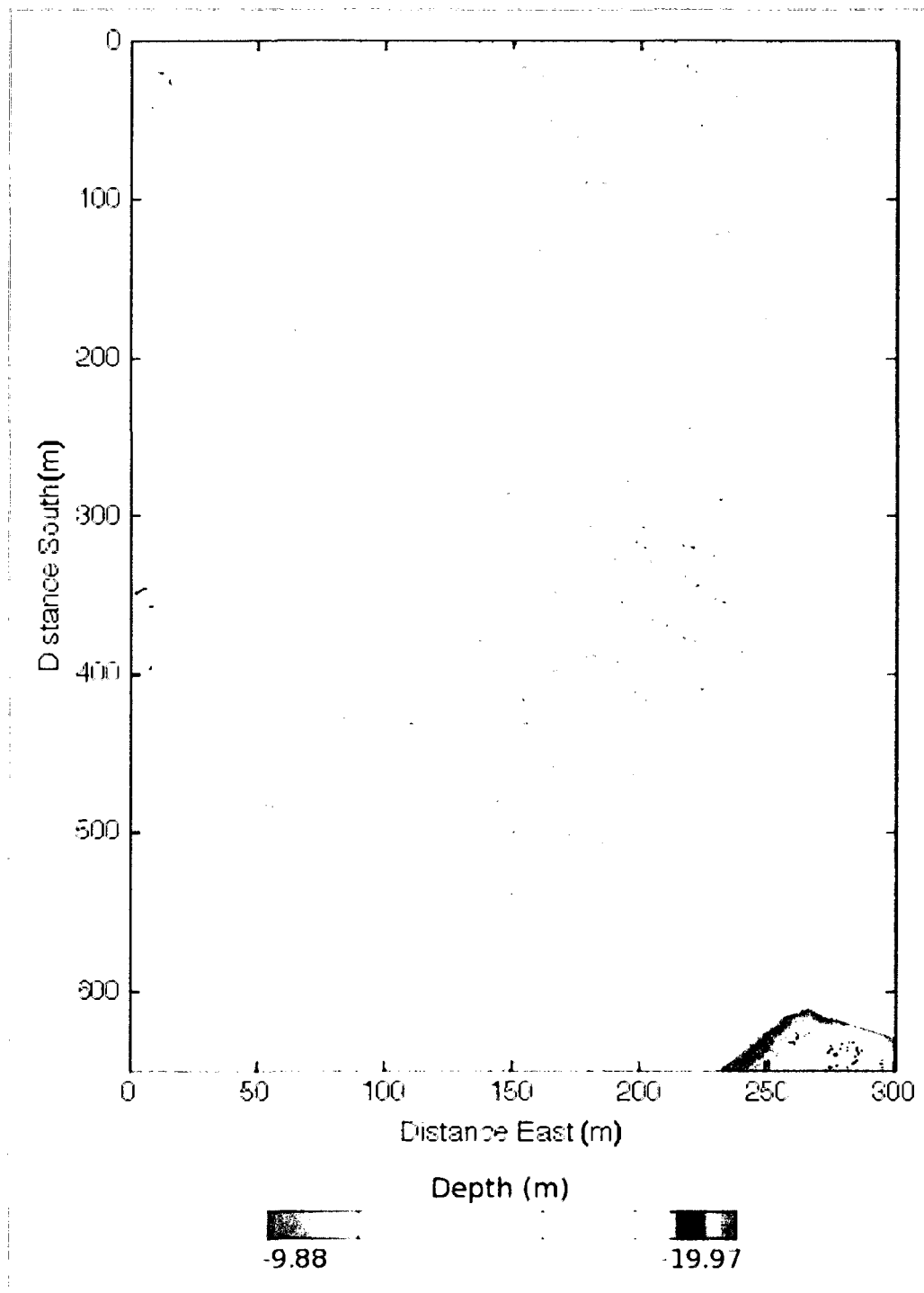


Figure 5-11. BISHNU results for 3 July 2008 (1420 UTC) survey superimposed on bathymetry. Depth range is approximately 10 m to 20.5 m (MLLW).

to large (8 m to 12 m wavelength) and small (3 m to 5 m wavelength) dunes alike. In the regions outside of the dune field, BISHNU correctly identified other small targets as ridges, particularly within areas of coarser-textured seafloor east and west of the dune field (see, e.g., Figure 5-1 for textural data from these areas).

5.3.2 Spatial Cross-Correlation Results

Estimates of dune migration were obtained through normalized, two-dimensional spatial cross-correlation of the BISHNU ridge maps (Duffy and Hughes-Clarke, 2005). An example of the full vector-field output from the cross-correlation algorithm (performed for spatial variables $f(x,y) = 3 \text{ m by } 3 \text{ m}$ and $g(x,y) = 6.5 \text{ m by } 6.5 \text{ m}$) is presented in Figure 5-12. The dune migration results are shown in Figure 5-13 (6-hr period on 8 June 2007); Figure 5-14 (6-hr period on 14 June 2007); Figure 5-15 (1-day period from 14 June 2007 to 15 June 2007); Figure 5-16 (7-day period from 8 June 2007 to 15 June 2007) and Figure 5-17 (6-day period from 3 July 2008 to 9 July 2008). To facilitate interpretation, the vectors represent spatially-averaged individual vectors, where each displayed migration vector depicts the average dune migration magnitude and direction over a 20 m by 20 m area.

It is evident from the preceding figures that dunes within the study area are actively migrating over time-scales as short as 6 hr. However, the overall trend of dune migration on such short time-scales is highly spatially variable (Fig. 5-13, Fig. 5-14). A more coherent pattern of dune migration begins to develop on time-scales of 1 day or longer (e.g. Fig. 5-15, Fig. 5-16, Fig. 5-17). It is worth noting again that the results have been spatially averaged, so that each migration vector represents the average magnitude and direction of dune migration over a specified area, rather than the “instantaneous”

magnitude and direction of dune migration of a unit width of dune crest. Overall trends of dune migration in the study area can be discerned from the histograms of “instantaneous” magnitude and direction presented in Figure 5-18, thus providing further context for the spatially-averaged vector field output.

The results indicate that dunes are actively migrating on time-scales of 6 hr. The dune-migration vectors observed over the period 1400 to 2000 UTC on 8 June 2007 (Fig. 5-13), on a rising tide under neap tidal conditions, are highly spatially variable, although the overall trend of dune migration is flood-oriented. The histograms in Figure 5-18 indicate that dune migration is predominantly directed to the northwest as indicated by a direction peak at 330° , although a low, broad peak from 0° to 180° indicates some movement in directions ranging from north to south. Magnitude of dune migration observed over this period is predominantly in the range of 0.2 to 0.6 m (Fig. 5-18). The migration vector field for the period 1330 to 1930 UTC on 14 June 2007, on a falling tide under spring tidal conditions, is also highly spatially variable (Fig. 5-14). Histograms of dune migration and direction for this period indicate that dune migration is primarily directed to the southeast and northwest, as indicated by direction peaks at 150° and 320° , respectively (Fig. 5-18). Magnitudes of dune migration observed over this period are predominantly 0.2 to 0.4 m, which is slightly less than the range observed over the 6-hour period on 8 June 2007.

The vector field from a 24-hr period observed from 14 June 2007 (1330 UTC) to 15 June 2007 (1400 UTC) under spring tidal conditions characterizes a more coherent pattern of bedform migration (Fig. 5-15). Dunes in the eastern sector of the bedform field clearly migrate in a net ebb (south to southeast) direction, while dune migration in

the western sector of the bedform field remains spatially variable. A histogram of dune migration direction (Fig. 5-18) indicates one peak centered on 330° and another low, broad peak centered on 180° . The broad peak at 180° likely corresponds to the ebb-migrational dunes in the eastern sector of the bedform field, whereas the peak at 330° indicates a flood component of dune migration directed to the northwest within the western margin of the bedform field. Magnitudes of dune migration observed over the 24-hr period from 14 June 2007 to 15 June 2007 are predominantly in the range of 0.2 to 1.0 m (Fig. 5-18).

A coherent pattern of bedform migration is strongly apparent over the 7-day period observed from 8 June 2007 (2000 UTC) to 15 June 2007 (1400 UTC) (Fig. 5-16). Dunes in the eastern sector of the bedform field migrate in a net ebb (south to west-southwest) direction, whereas dunes in the western sector of the bedform field migrate in a net flood (northwest to northeast) direction. This reciprocal pattern of bedform migration in the east vs. west sectors is apparent from the histogram of dune-migration direction in Figure 5-18, which contains migration peaks centered on 0° (flood) and $\sim 200^\circ$ (ebb). Note the low, broad ebb peak that indicates that ebb migration directions ranged from southeast to southwest (Fig. 5-18). The magnitude of dune migration observed over this period reached nearly 2.0 m (Fig. 5-18).

The reciprocal pattern of dune migration is absent over the 6-day period observed from 3 July 2008 (1420 UTC) to 9 July 2008 (1630 UTC) (Fig. 5-17). Over this period, there was a net ebb (south-southwest) migration of dunes in the eastern sector of the bedform field, although migration directions were somewhat variable, particularly along the eastern periphery of the dune field. Dunes in the western sector of the bedform field

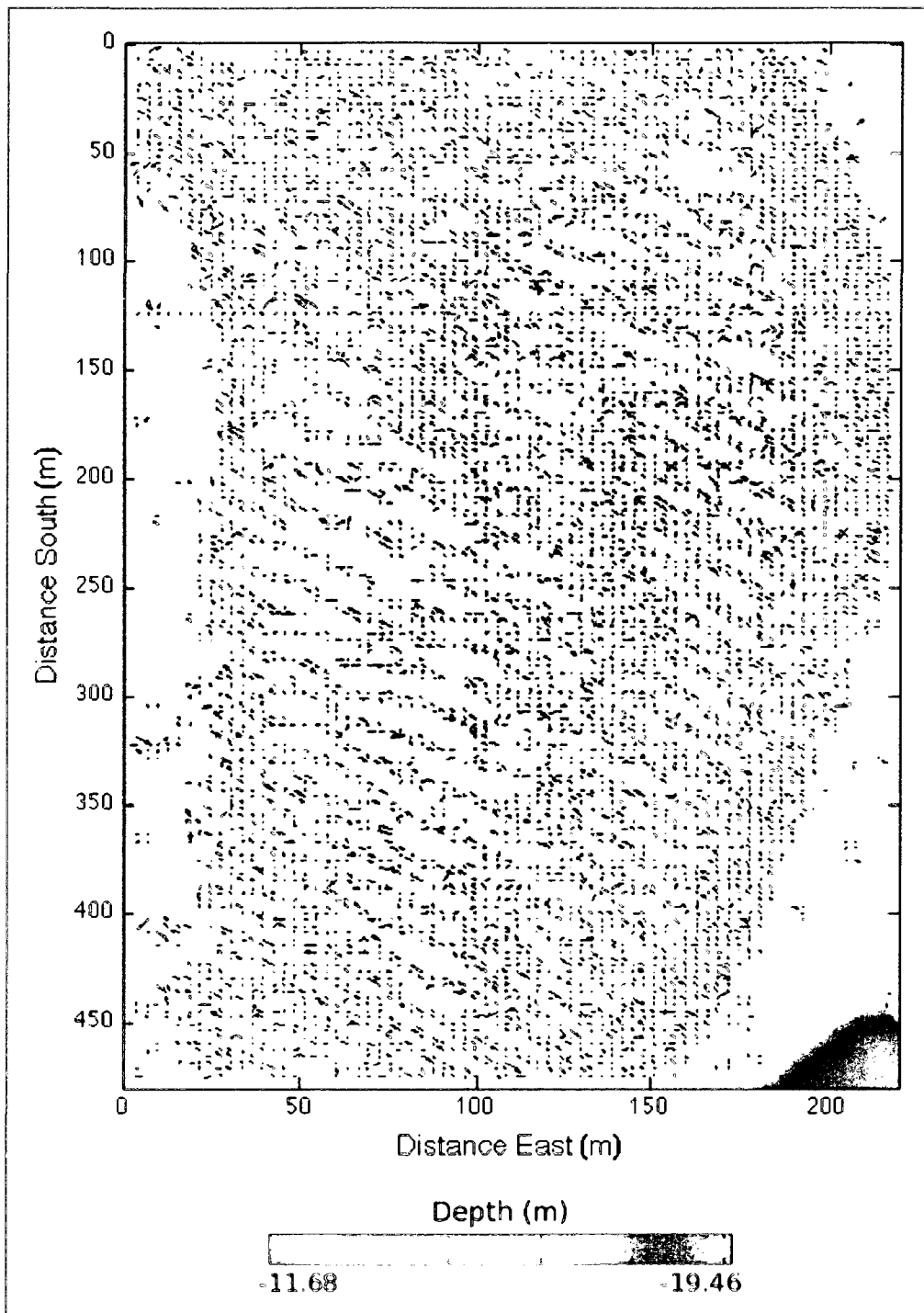


Figure 5-12. Vector field output from cross-correlation algorithm depicting dune migration over a 6-hr period from 8 June 2007 (1400 UTC) to 8 June 2007 (2000 UTC). Input parameters for spatial cross-correlation routine are window size of 3 m by 3 m and search area of 6.5 m by 6.5 m. Background image is bathymetry from MBES survey conducted on 8 June 2007 (1400 UTC).

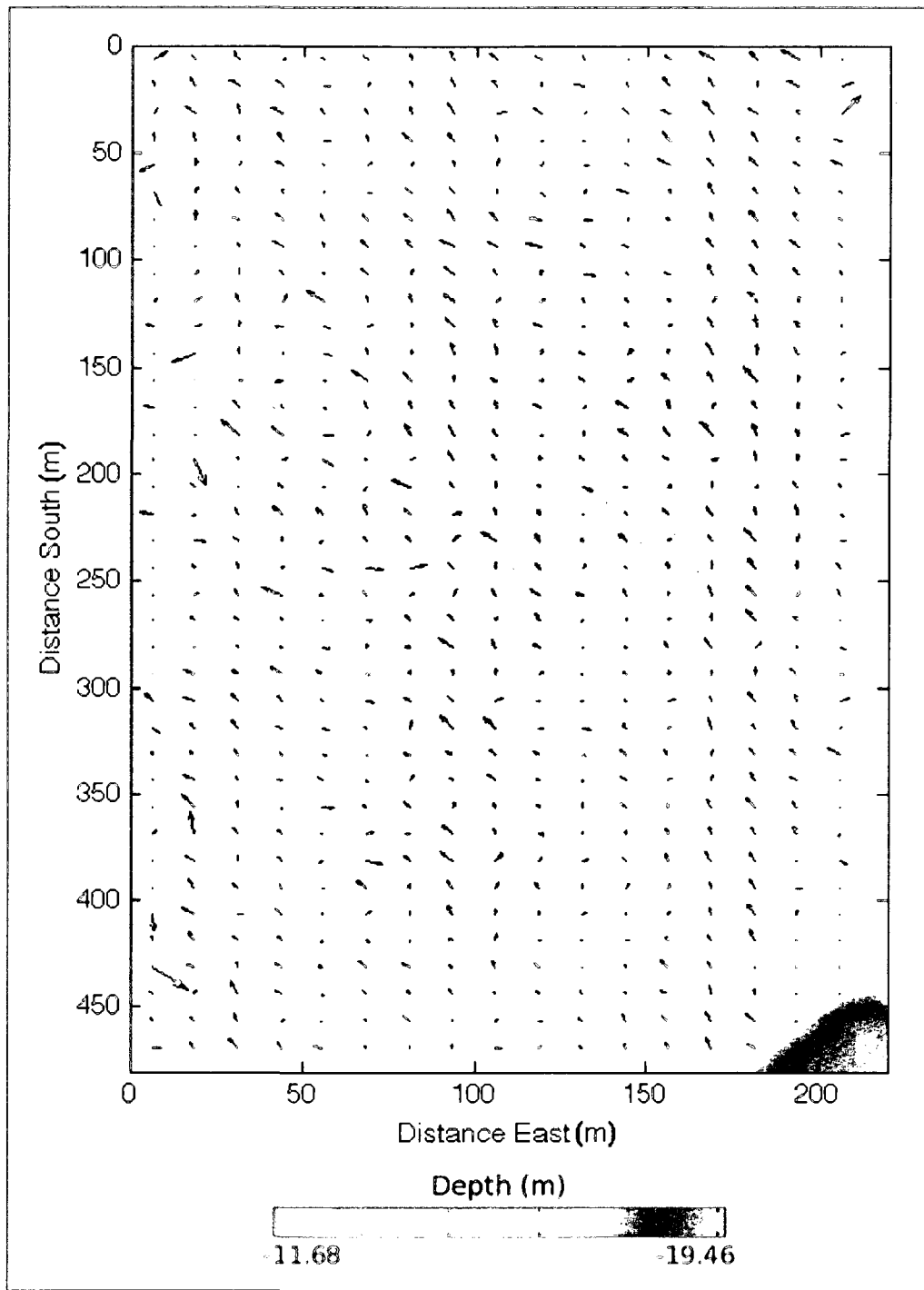


Figure 5-13. Spatially averaged dune-migration vectors over a 6-hr period from 8 June 2007 (1400 UTC) to 8 June 2007 (2000 UTC). Each vector represents the average migration magnitude and direction over a 25 m by 25 m region. Background image is bathymetry from MBES survey conducted on 8 June 2007 (1400 UTC).

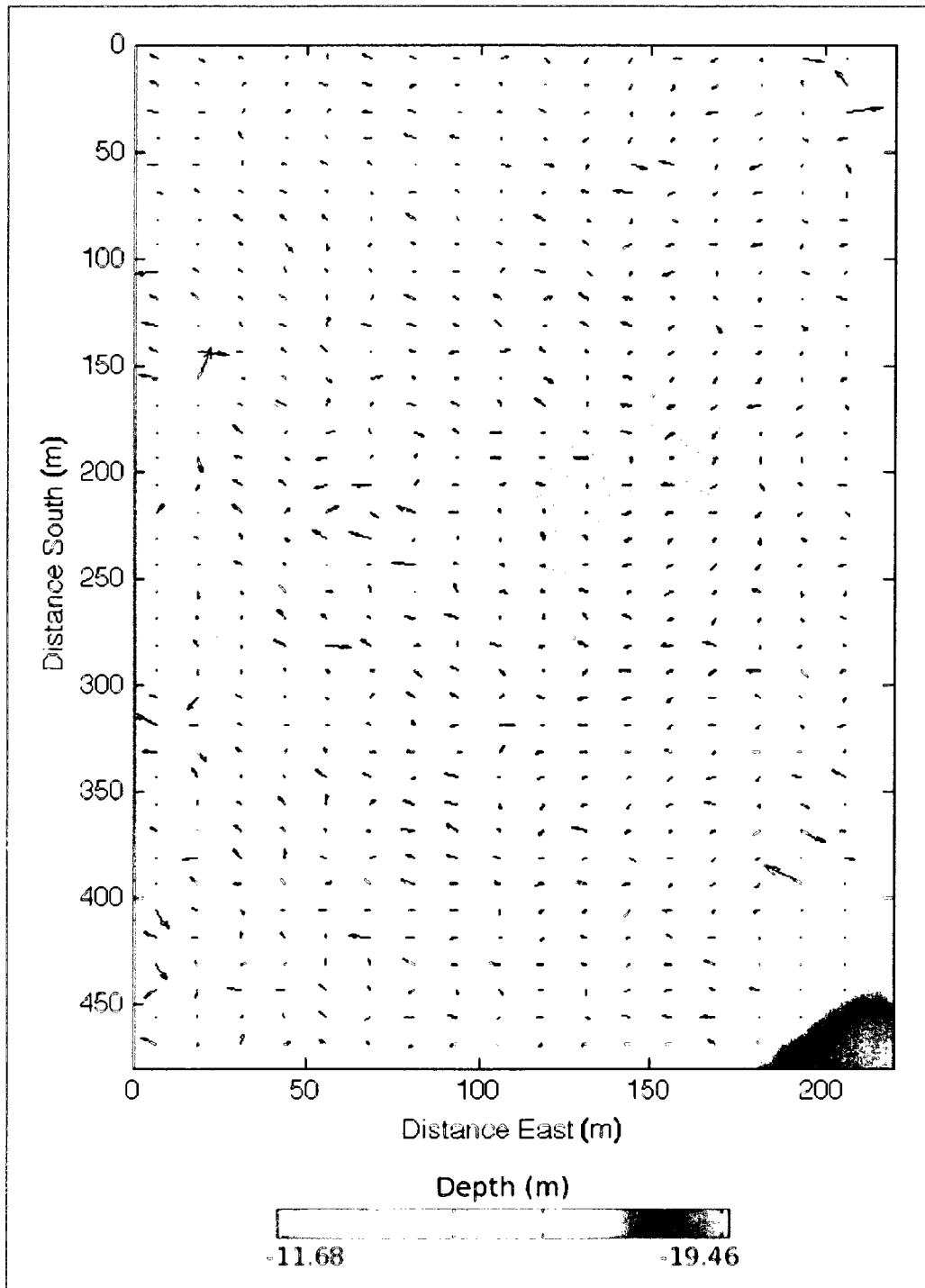


Figure 5-14. Spatially averaged dune-migration vectors over a 6-hr period from 14 June 2007 (1330 UTC) to 14 June 2007 (1930 UTC). Each vector represents the average migration magnitude and direction over a 25 m by 25 m region. Background image is bathymetry from MBES survey conducted on 14 June 2007 (1330 UTC).

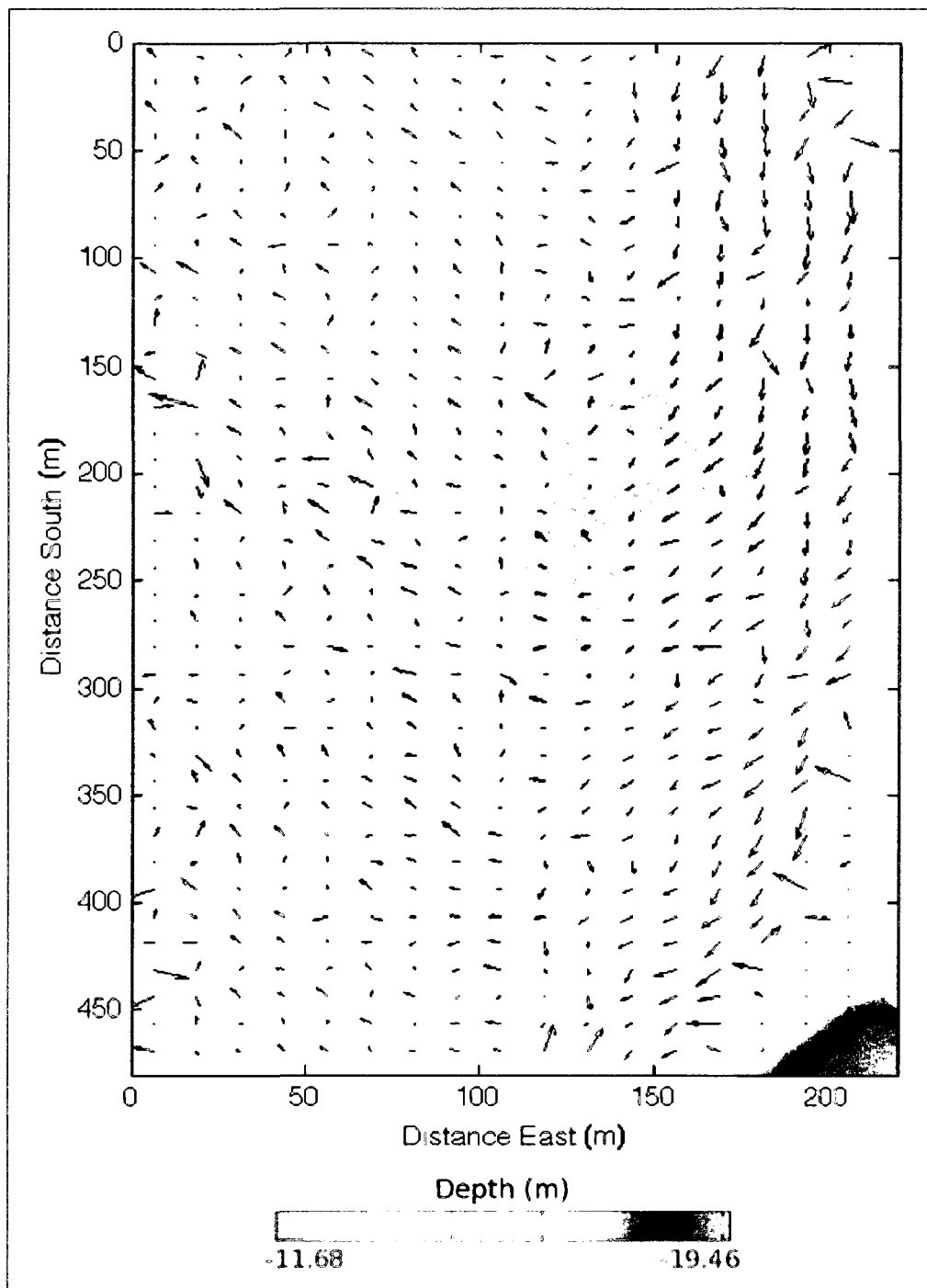


Figure 5-15. Spatially averaged dune-migration vectors over a 1-day period from 14 June 2007 (1330 UTC) to 15 June 2007 (1400 UTC). Each vector represents the average migration magnitude and direction over a 25 m by 25 m region. Background image is bathymetry from MBES survey conducted on 14 June 2007 (1330 UTC).

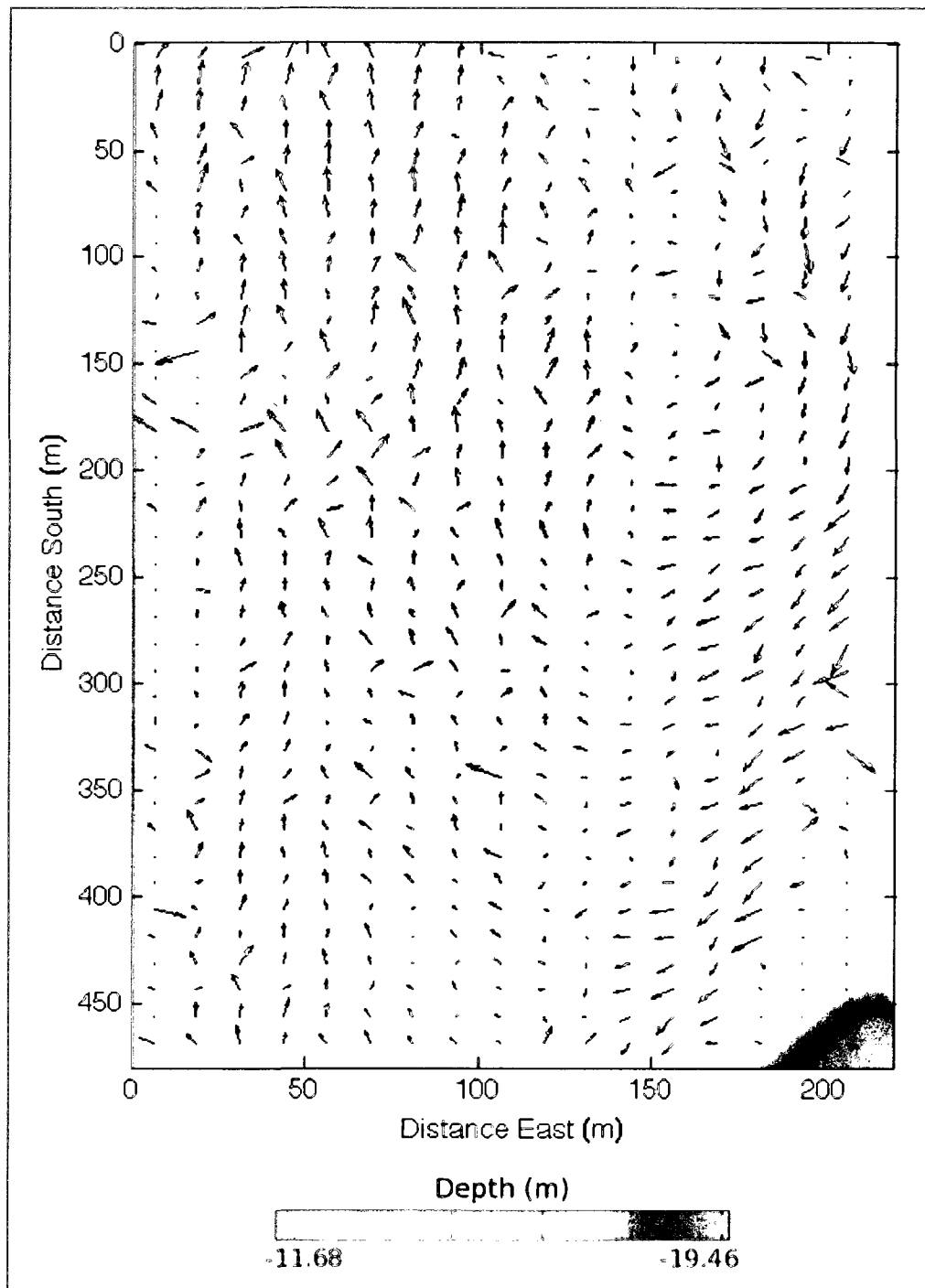


Figure 5-16. Spatially averaged dune-migration vectors over a 7-day period from 8 June 2007 (1400 UTC) to 15 June 2007 (1400 UTC). Each vector represents the average migration magnitude and direction over a 25 m by 25 m region. Background image is bathymetry from MBES survey conducted on 8 June 2007 (1400 UTC).

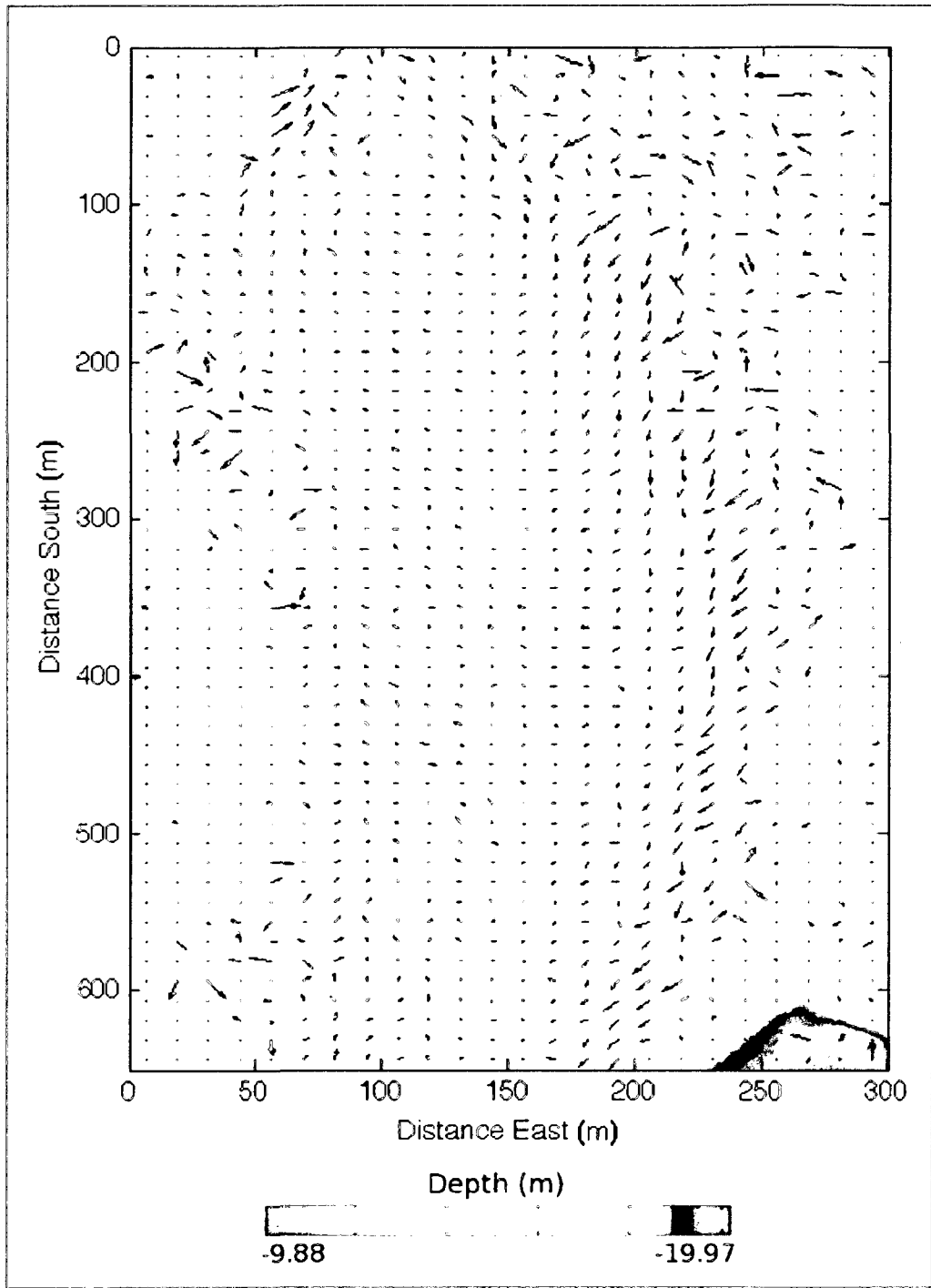


Figure 5-17. Spatially averaged dune-migration vectors over a 6-day period from 3 July 2008 (1420 UTC) to 9 July 2008 (1630 UTC). Each vector represents the average migration magnitude and direction over a 25 m by 25 m region. Background image is bathymetry from MBES survey conducted on 3 July 2008 (1420 UTC).

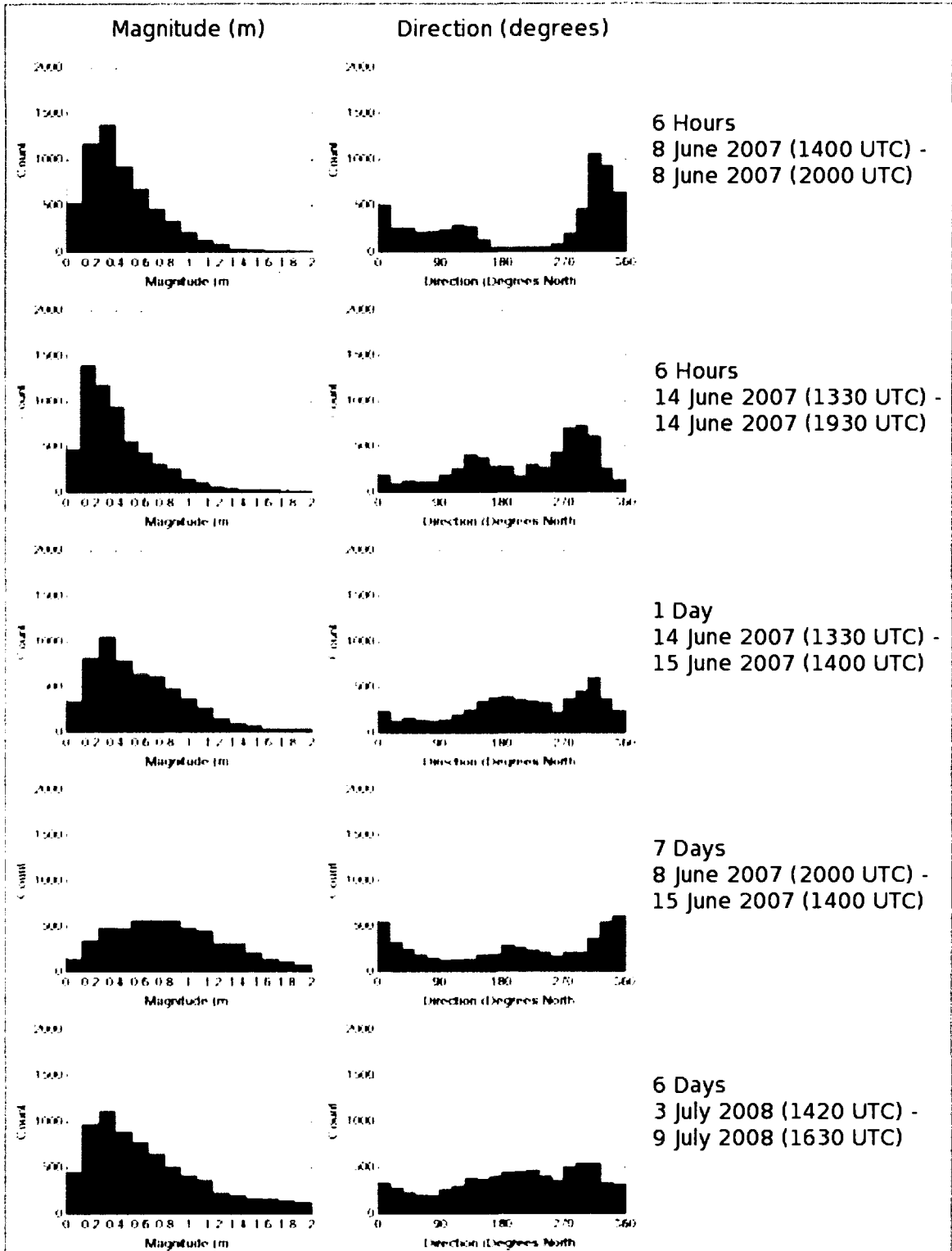


Figure 5-18. Histograms of dune migration magnitude (in meters) and direction (in degrees) over 6-hr, 1-day and 7-day observation periods (2007) and 6-day observation period (2008).

were significantly less dynamic over this period. The histogram of dune migration over this time period (Fig. 5-18) contains a low, broad peak centered on 180° that contains the ebb-migrating dunes in the eastern sector of the dune field. A second peak centered on 300° indicates bedform migration in this direction as well, perhaps in the southwest quadrant of the dune field (Fig. 5-17). The maximum magnitude of dune migration observed during this period was 2.0 m, although more typical values of dune migration were much less, ranging from 0.2 to 1.0 m.

Figure 5-17 indicates some net movement within bathymetric lows located east and west of the dune field, although the migration vectors are suspect. This effect is not seen in areas of smoother seafloor topography, such as the shoals in the far left of Figure 5-17. This suggests that the suspect vectors are noise that resulted from the cross-correlation of ridges identified in rough seafloor terrain, and that the ridges are not bedforms.

5.4 Current Observations

Current observations from the ADCP and MAVS current meters were obtained from 2 to 5 July 2008 during spring tidal conditions. On 5 July 2008 at 19:12:00 GMT the ADCP record abruptly terminated. Although the MAVS record ran until 16 July 2008, the record has been truncated to the ADCP observation period for direct comparison. The time-series of ADCP and MAVS current speeds and directions are shown in Figure 5-19. A plot of ADCP current speeds and directions for the entire recorded depth (1.03 to 8.83 m above bottom) is presented in Figure 5-20.

Peak current velocities at 1 m above bottom are 73 cm/s at the ADCP station and 49 cm/s at the MAVS station. Both locations show a strong flood/ebb inequality. The

ADCP station (located in the eastern sector of the bedform field) is ebb-dominated, with maximum flood and ebb current velocities of 54 cm/s and 73 cm/s, respectively. The MAVS station, located in the western sector of the bedform field, is flood-dominated, with a maximum flood-current velocity of 49 cm/s and very weak (<20 cm/s) ebb-current velocities, although ebb currents briefly spike to ~40 cm/s at the onset of ebb tide. The ADCP record shows a semi-diurnal inequality of the ebb current, in which each 24-hr period contains one stronger and one weaker maximum ebb current.

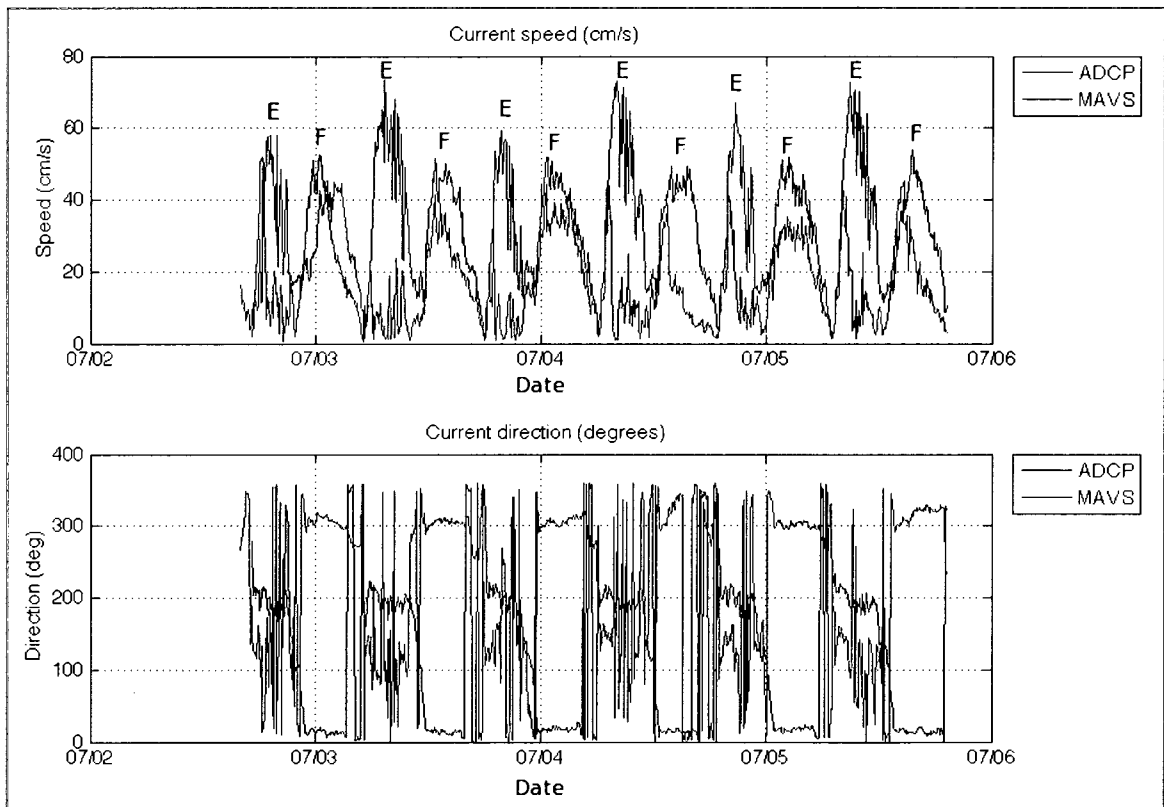


Figure 5-19. Time-series of ADCP and MAVS current speed (in cm/s) and direction (in degrees). Ebb and flood currents ('E' and 'F', respectively) are labeled in the plot of current speed at top. At the ADCP station flood currents are north-flowing ($\sim 0^\circ$) and ebb currents are south-flowing ($\sim 200^\circ$). At MAVS station flood currents are northwest-flowing ($\sim 300^\circ$) and ebb currents are highly variable. ADCP currents were observed at a 20-cm bin centered on 1.03 m above bottom. MAVS currents were observed at a single point 1.00 m above bottom.

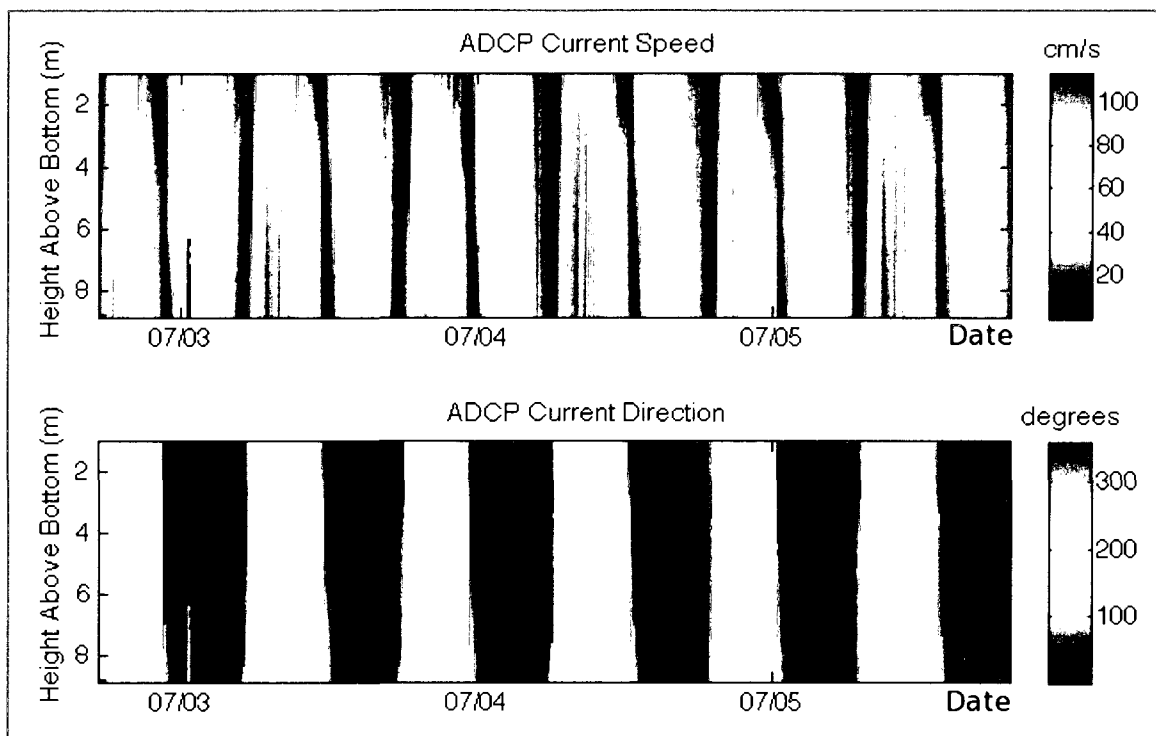


Figure 5-20. Time-series of ADCP current speed (in cm/s) and direction (in degrees) for all bins, corresponding to 1.03 to 8.83 m above bottom. Flood currents are north-flowing (dark blue/red in bottom image) and ebb currents are south-flowing (green).

The time-series of ADCP current profiles (Fig. 5-20) shows an increase in current speed with height above bottom. Current speeds between 4 m and 9 m above bottom routinely exceed 100 cm/s during the flood tide. Speed asymmetry of the currents is strongly apparent in Figure 5-20, which shows ebb currents that frequently exceeded speeds of ~ 0.8 cm/s (represented in Figure 5-20 as red hues) whereas flood currents were significantly weaker. A diurnal inequality of the ebb currents is also apparent from Figure 5-20, as each 24-hour period contains one stronger ebb current and one weaker ebb current.

5.5 Bed Shear Stress

Bed shear stress was calculated according to the log-fit (LF) method of Sherwood et al. (2006) and a drag coefficient (DC) method (Wright, 1995; Soulsby, 1997), which calculates total bed shear stress based on a reference current speed and a z_0 value that characterizes the bed roughness. Because the LF method requires a profile of observed current velocities within the log layer, it was applied to the ADCP data only. The LF method was not applied to the MAVS data because it measures current velocity at only one point above the bottom. The log layer at the ADCP site extended to a height of 3.03 m above bottom, so the velocity profile from 1.03 to 3.03 m above bottom was chosen for the log fit. The DC method was applied to both the ADCP and MAVS data, because it requires current observations at a single elevation above the bottom. Total bed shear stress evaluated using the LF and DC methods is denoted as $\tau_{b,lf}$ and $\tau_{b,dc}$, respectively.

A series of residual plots (Fig. 5-21) were created to test the goodness-of-fit of the LF and DC methods applied to the ADCP data. To create the residual plots, model velocity was computed for each method by applying estimates of z_0 and u_* into Equation 3.5. Residual plots were created by subtracting the model velocities $U(z)_{lf}$ and $U(z)_{dc}$ from the observed velocity $U(z)$. It is apparent from Figure 5-21 that the LF method yields the best fit to the observed current profiles; the residual barely exceeds 0.06 cm/s. The DC method also yields a very good fit; it is within 0.05 cm/s most of the time, except during a few periods around slack water. However, the poor fit around slack water is fine, considering that the bed shear stress is typically small or negligible during these conditions.

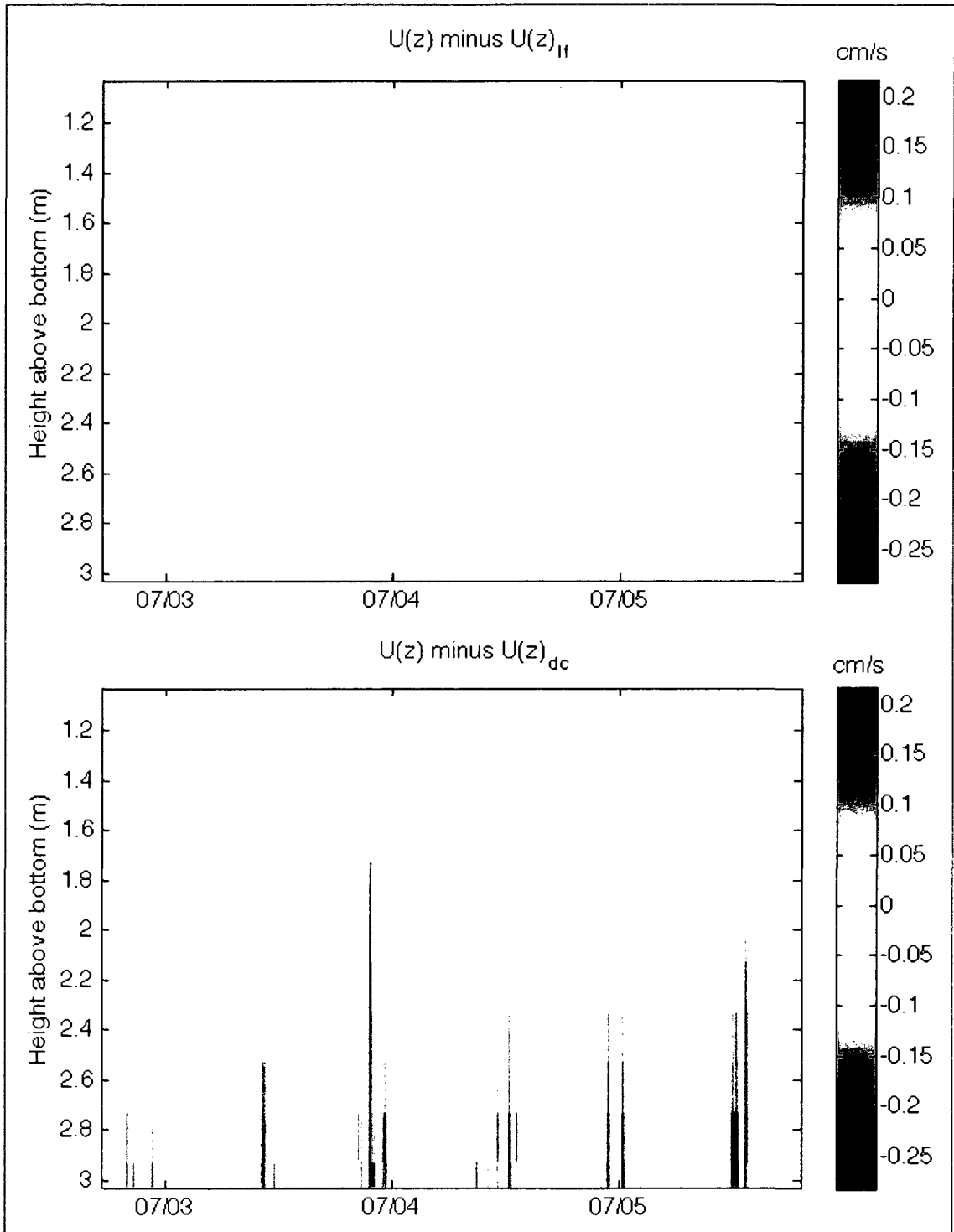


Figure 5-21. Time-series of observed velocity minus modeled velocity from log fit (LF) (Top) and drag coefficient (DC) (Bottom) methods. Modeled velocities were computed from the Von Karman-Prandtl equation using estimates of z_0 and u_* from the LF method (Top) and DC method (Bottom).

Total bed shear stress ($\tau_{b,lf}$) estimates for the ADCP station over the period 3 to 5 July 2008, computed using the LF method, are given in Figure 5-22. The LF method calculates u_* directly from a least-squares fit to the observed current profiles, and u_* was subsequently converted to total bed shear stress ($\tau_{b,lf}$) and the Shields parameter ($\theta_{b,lf}$) using Equation 3.7 and Equation 3.2. The LF method also computes an error (r^2) value based on the u_* estimate. The u_* estimates are reasonable except during near-slack conditions, as the observed current-speed profile does not conform to the law of the wall during this time period. Critical values for the initiation of sediment motion are plotted (in magenta) in the $\tau_{b,lf}$ and $\theta_{b,lf}$ sub-plots of Figure 5-22, although they are far exceeded by the total bed shear stress.

Partitioned bed shear stress results for the ADCP and MAVS sites are given in Figure 5-23. The partitioning ratio τ_b/τ_{sf} was calculated from Equation 3-13 using values of bedform height (η) and wavelength (λ) from the ADCP ($\eta = 0.37$ m and $\lambda = 7$ m) and MAVS ($\eta = 0.7$ m and $\lambda = 14$ m) locations. The partitioning ratio was 2.97 for the ADCP site and 3.57 for the MAVS site. Estimates of total bed-shear stress τ_b from the ADCP and MAVS locations were divided by τ_b/τ_{sf} to evaluate the skin-friction shear stress τ_{sf} . It is evident from Figure 5-23 that the skin-friction shear stress τ_{sf} based on a form-related roughness length z_0 is much higher in magnitude than τ_{sf} based on a grain-related z_0 . However, even the lower estimates of τ_{sf} based on the grain-related z_0 exceed the threshold bed shear stress τ_{cr} during the observation period, thus indicating that bedload sediment transport occurred. Although τ_{sf} exceeds τ_{cr} during flood and ebb current conditions at the ADCP site, the threshold value is primarily exceeded during

flood current conditions at the MAVS site, with the exception of brief spikes of τ_{sf} at the onset of the ebb tide (Figure 5-23).

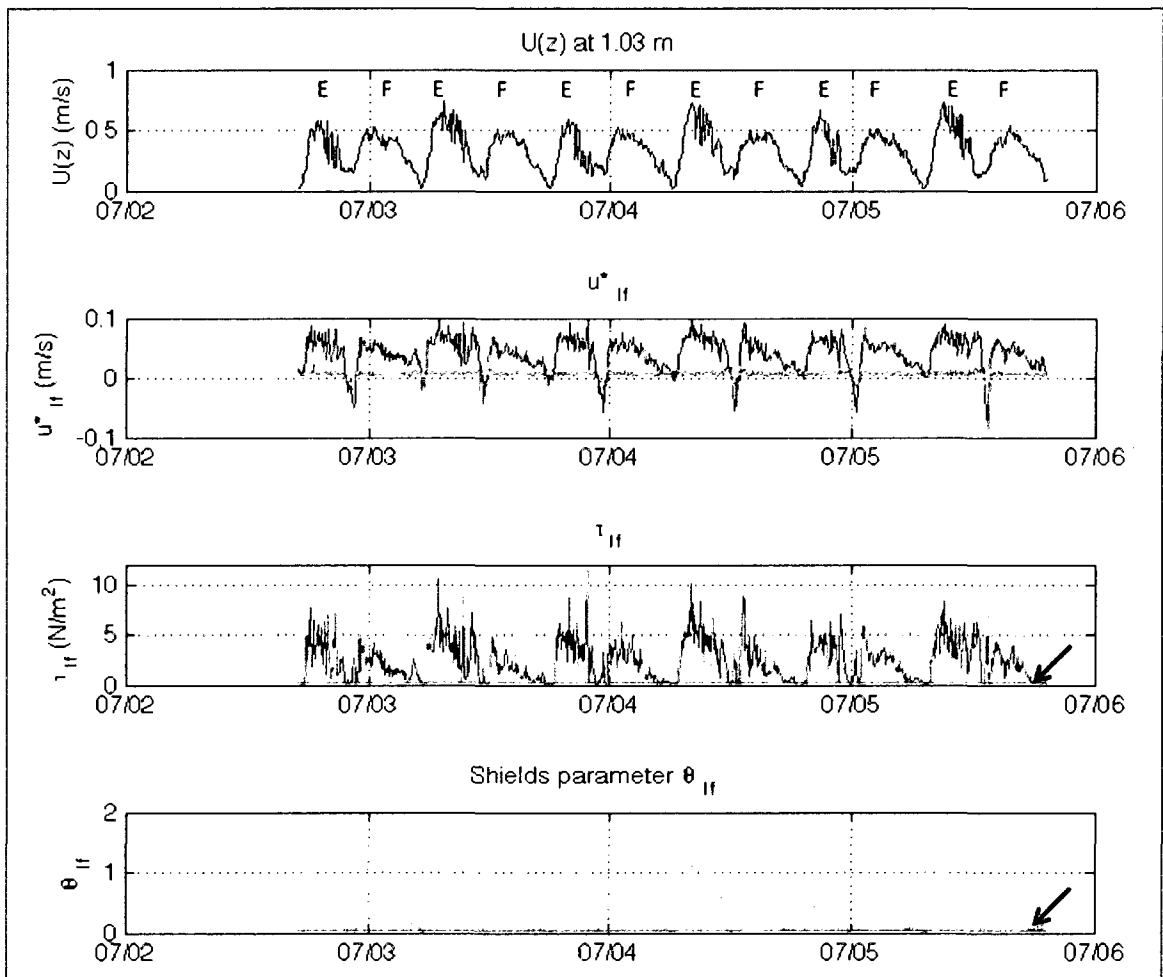


Figure 5-22. Observed current speed ($U(z)$), shear velocity (u_{lf}^*), bed shear-stress (τ_{lf}) and Shields parameter (θ_{lf}) at the ADCP site during the observation period (3 July – 6 July 2008), as computed by the log fit (LF) method of Sherwood et al. (2006). Magenta line in the u_{lf}^* plot is the error (r^2) in calculating u_{lf}^* (see p. 39). Magenta line (indicated by black arrows) in the τ_{lf} and θ_{lf} plots is the threshold value required for initiation of sediment motion. Ebb and flood currents are indicated on plot of $U(z)$ at top.

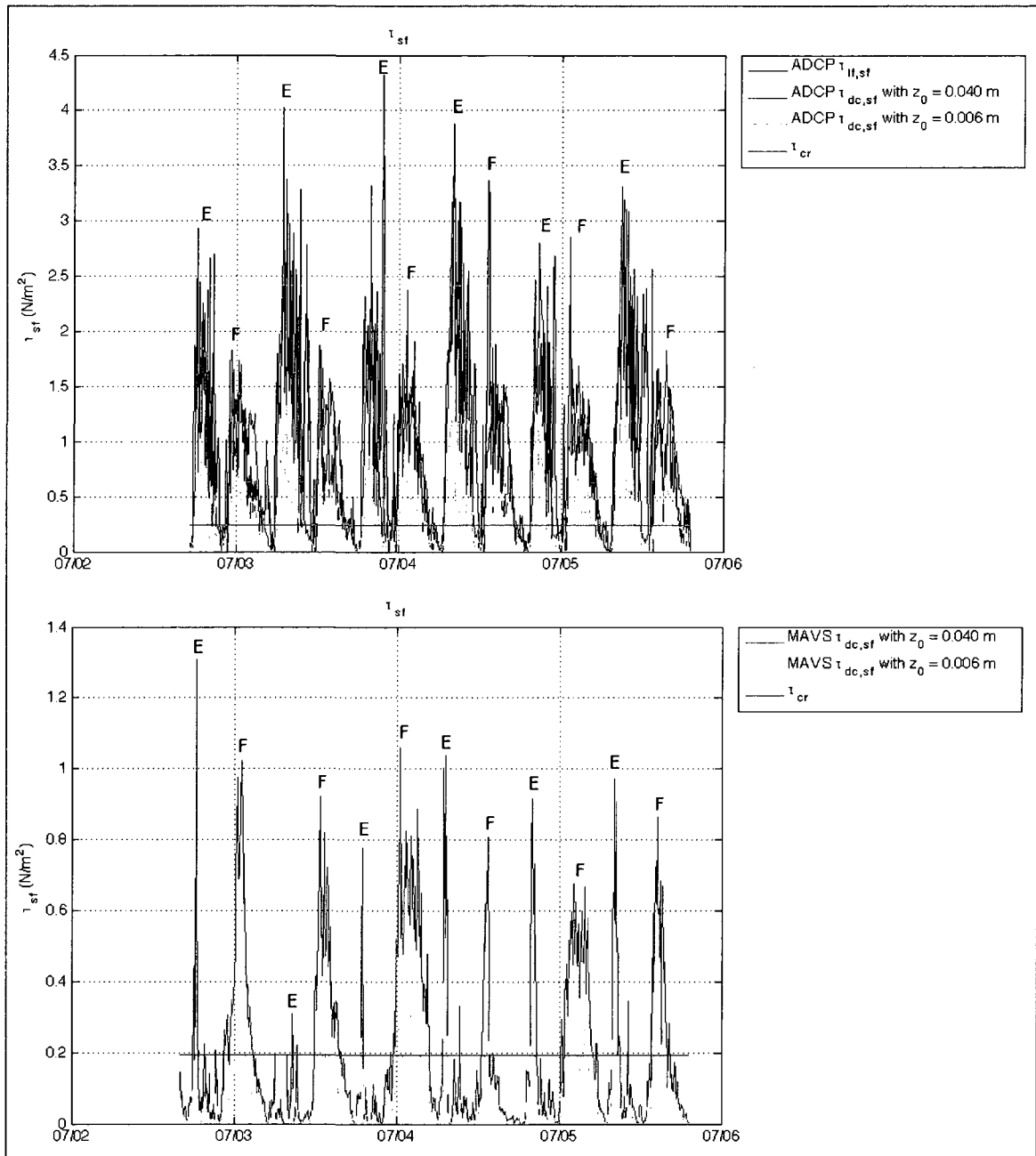


Figure 5-23. Partitioned bed shear-stress (τ_{sf}) for ADCP site (top) and MAVS site (bottom) during the observation period 3-6 July 2008. $\tau_{sf,lf}$ is the skin-friction shear-stress computed from the log fit method (ADCP only) while $\tau_{sf,dc}$ is the skin-friction shear-stress computed from the drag coefficient method (ADCP and MAVS). τ_{cr} is the threshold bed shear-stress that must be exceeded for initiation of bedload sediment transport.

CHAPTER 6

DISCUSSION

6.1 Bedform Migration in Portsmouth Harbor

The bedform migration estimates from 24-hr and multi-day periods in 2007 and 2008 indicate strong differences in sediment transport across the east-west axis of the Portsmouth Harbor dune field. Dunes within the eastern sector of the bedform field are observed to have migrated in a net ebb (southeast to southwest) direction over 24-hr and multi-day periods in 2007 and 2008 (Fig. 5-15, Fig. 5-16, Fig. 5-17). Dune migration in the western sector of the bedform field appears to have been temporally variable. Over a 24-hr period in 2007 there is no strong pattern of dune migration in this area, although migration appears to have been directed generally to the northwest (Fig. 5-15, Fig. 5-18). A strong coherent pattern of dune migration is apparent in the western sector of the bedform field over a 7-day period in 2007, when dune migration was oriented in a net flood (northwest to northeast) direction (Fig. 5-16). Conversely, over a 6-day period in 2008 there was relatively little migration of dunes in the western sector of the bedform field (Fig. 5-17).

This strong east-west difference in bedform migration is reflected in the morphology observed from a timeline of MBES bathymetric surveys of the dune field extending back to November 2000. Surveys were conducted by the NOAA Ship *Whiting* in November 2000 with a Reson 8101 MBES (Fig. 6-1); by the University of New

Hampshire vessel R/V *Coastal Surveyor* in June 2001 using a Kongsberg EM3000D (Fig. 6-2); by Science Applications International Corporation (SAIC) in November 2001 with a dual-head Reson 8125 (Fig. 6-3); and by the R/V *Coastal Surveyor* in June 2004 using a Kongsberg EM3002 (Fig. 6-4). MBES bathymetry acquired by the R/V *Coastal Surveyor* in June 2007 and July 2008 (Dual-head Kongsberg EM3002D) are presented for comparison in Figure 6-5 and Figure 6-6.

With the exception of the bathymetry from June 2007, all profiles indicate a pattern of east-west differences in bedform morphology, whereby dunes in the eastern sector of the bedform field tend to be ebb-oriented (southward-migrating) to symmetrical and dunes in the western sector of the bedform field are flood-oriented (northward-migrating). Figure 6-7 shows a series of bed elevation profiles from the time-series of bathymetry, where Profile A is from the eastern sector of the dune field, and Profile B is from the western sector of the dune field. Bedforms from Profile A are weakly to moderately ebb-oriented (although some symmetrical bedforms exist) for all surveys except the June 2007 Kongsberg EM3002D survey, which is strongly flood-oriented. However, it should be noted that apparent symmetry of bedforms in Profile A may be caused by the fact that not all transects were taken at a direction perfectly normal to the dune crests. Bedforms from Profile B are strongly flood-oriented for all surveys. The east-west differences in dune asymmetry discussed here were briefly noted, but not analyzed, in a seafloor-habitat characterization study in Portsmouth Harbor (Cutter, 2005).

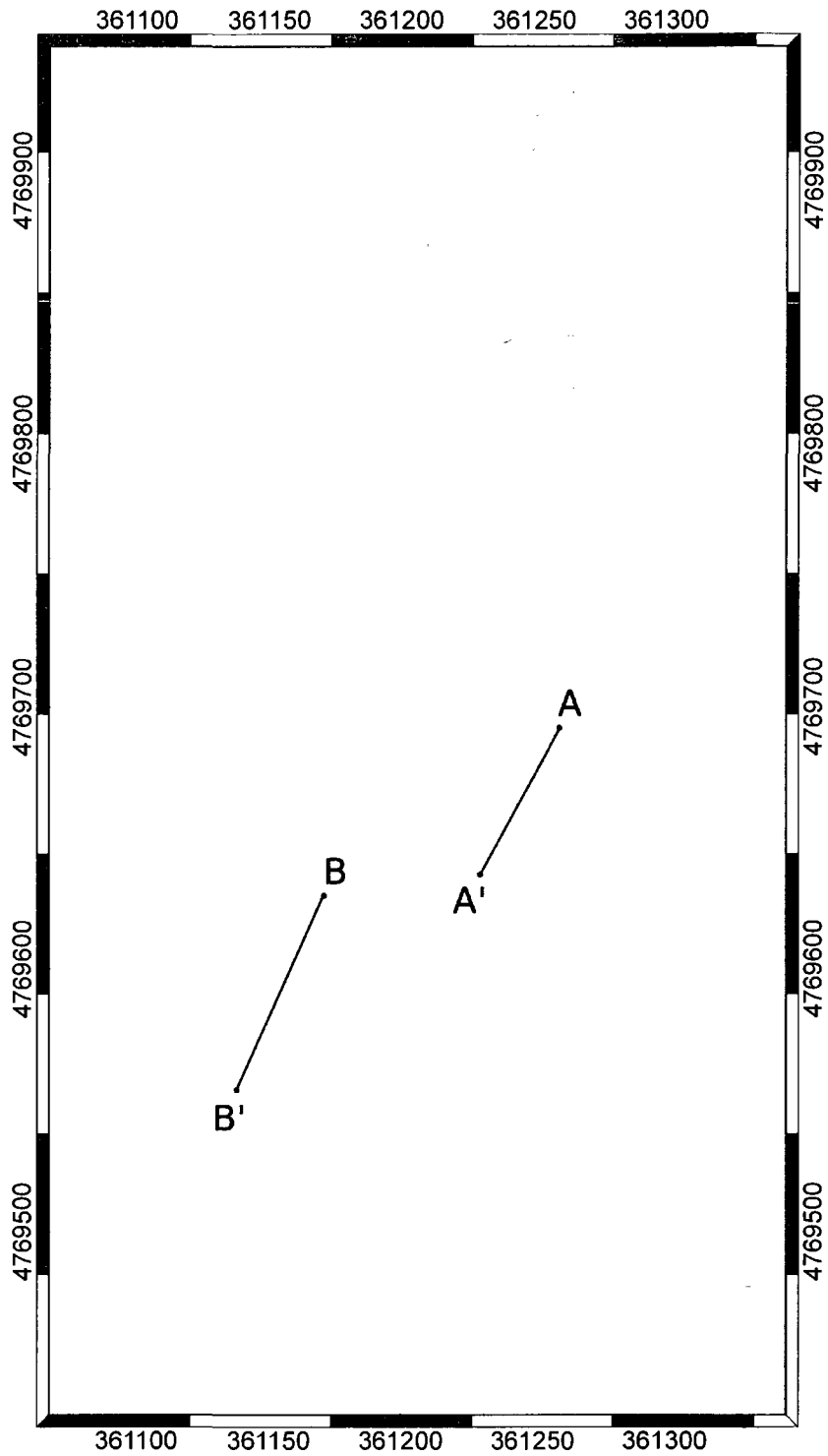


Figure 6-1. Reson 8101 bathymetry (0.5 m grid resolution) acquired by the NOAA Ship *Whiting* in November 2000. Cross sections A-A' and B-B' are presented in Figure 6-7. Grid is projected in UTM coordinates (Zone 19 N).

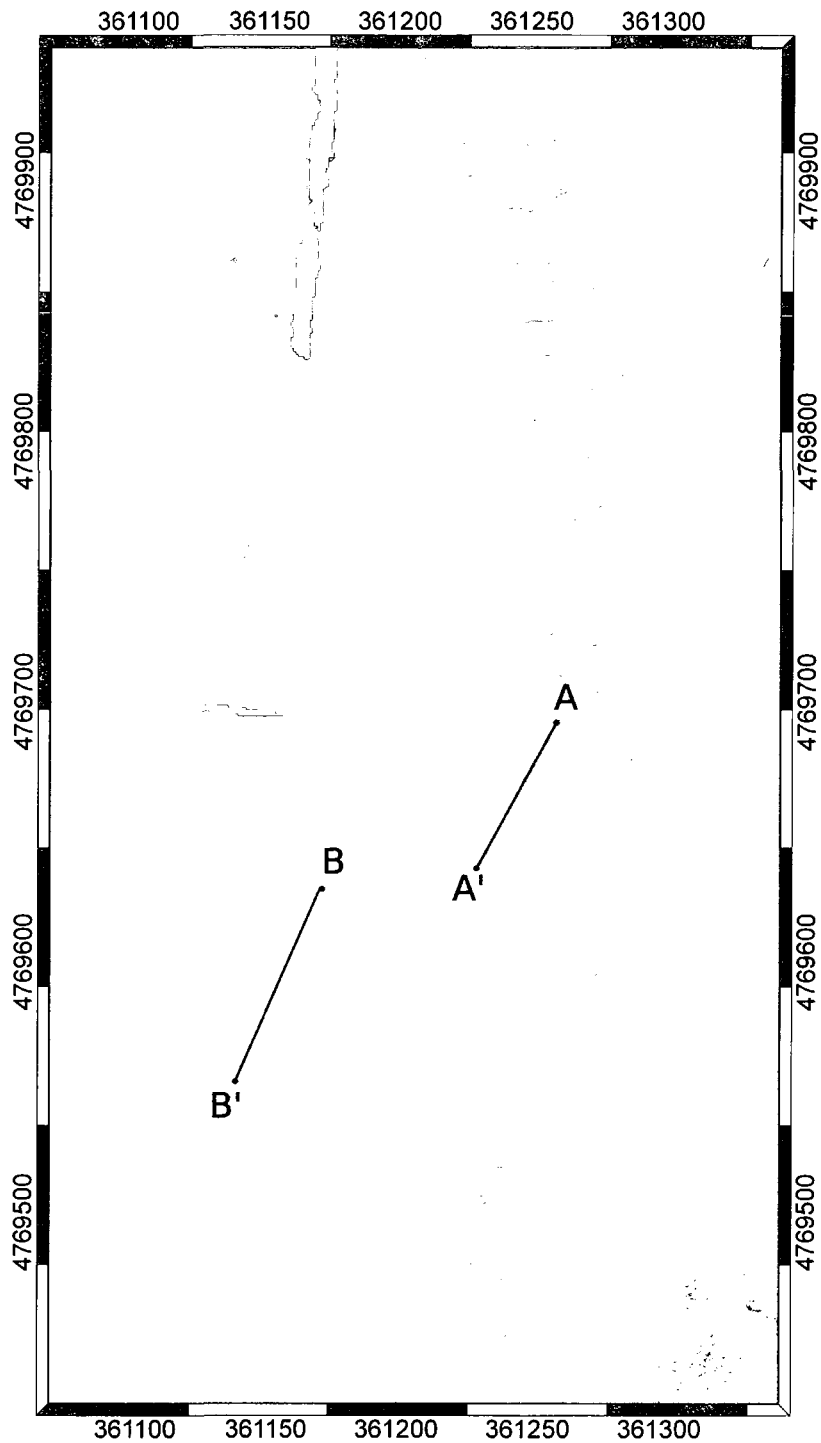


Figure 6-2. Kongsberg EM3000D bathymetry (0.5 m grid resolution) acquired by the University of New Hampshire vessel R/V *Coastal Surveyor* in June 2001. Cross sections A-A' and B-B' are presented in Figure 6-7. Grid is projected in UTM coordinates (Zone 19 N).

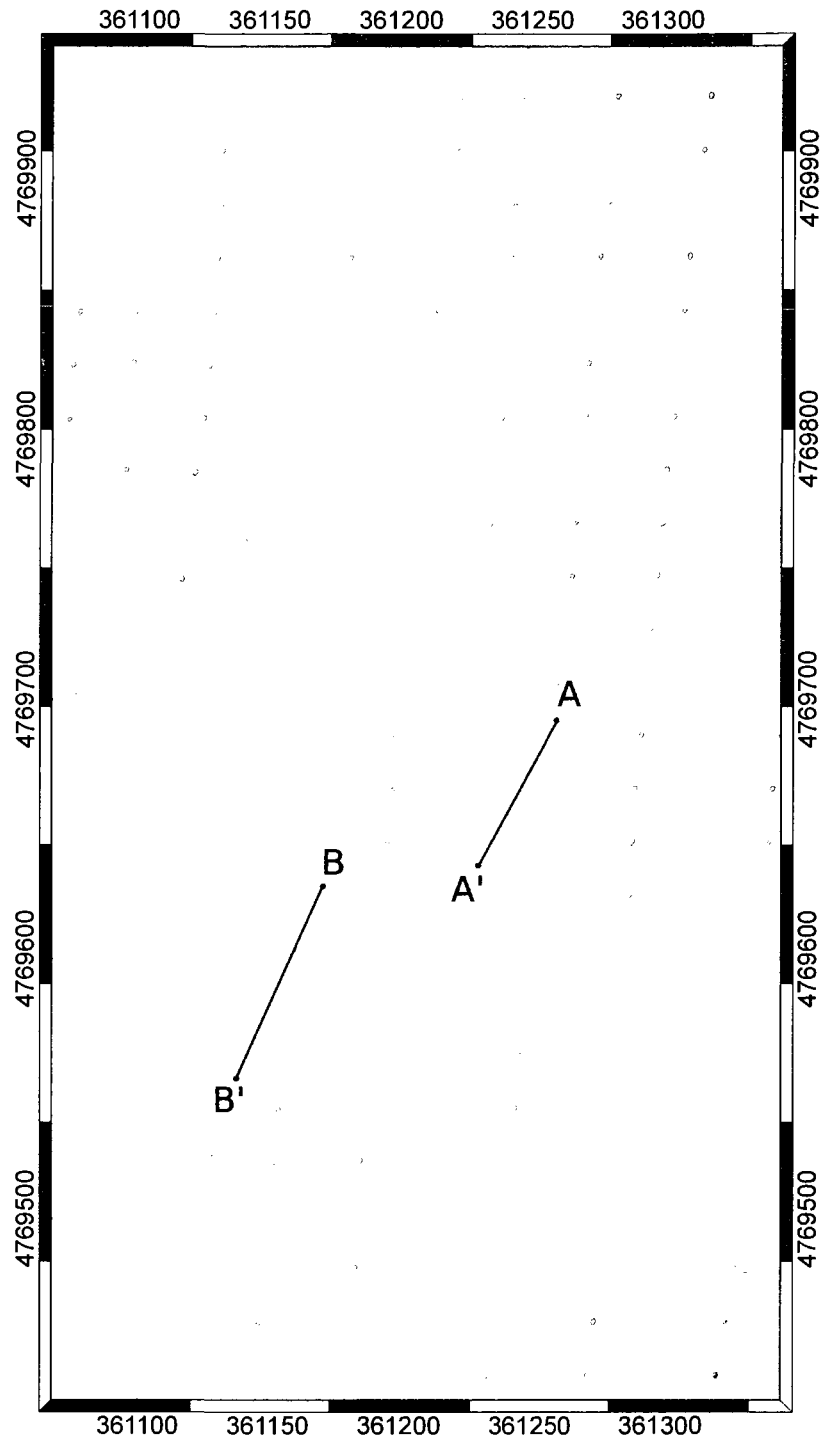


Figure 6-3. Dual-head Reson 8125 bathymetry (0.5 m grid resolution) acquired by SAIC in November 2001. Cross sections A-A' and B-B' are presented in Figure 6-7. Grid is projected in UTM coordinates (Zone 19 N).

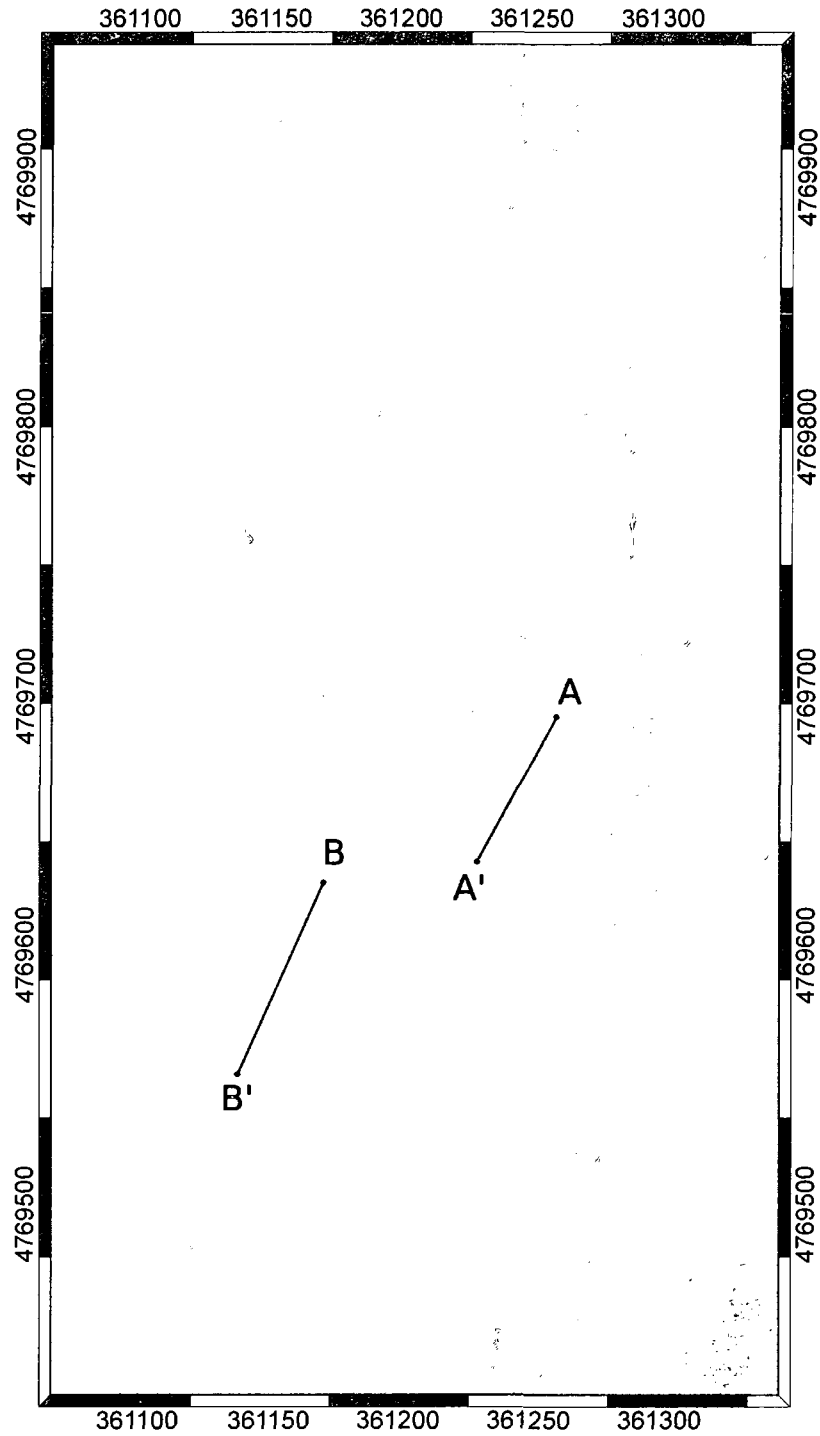


Figure 6-4. Kongsberg EM3002 bathymetry (0.5 m grid resolution) acquired by the University of New Hampshire vessel R/V *Coastal Surveyor* in June 2004. Cross sections A-A' and B-B' are presented in Figure 6-7. Grid is projected in UTM coordinates (Zone 19 N).

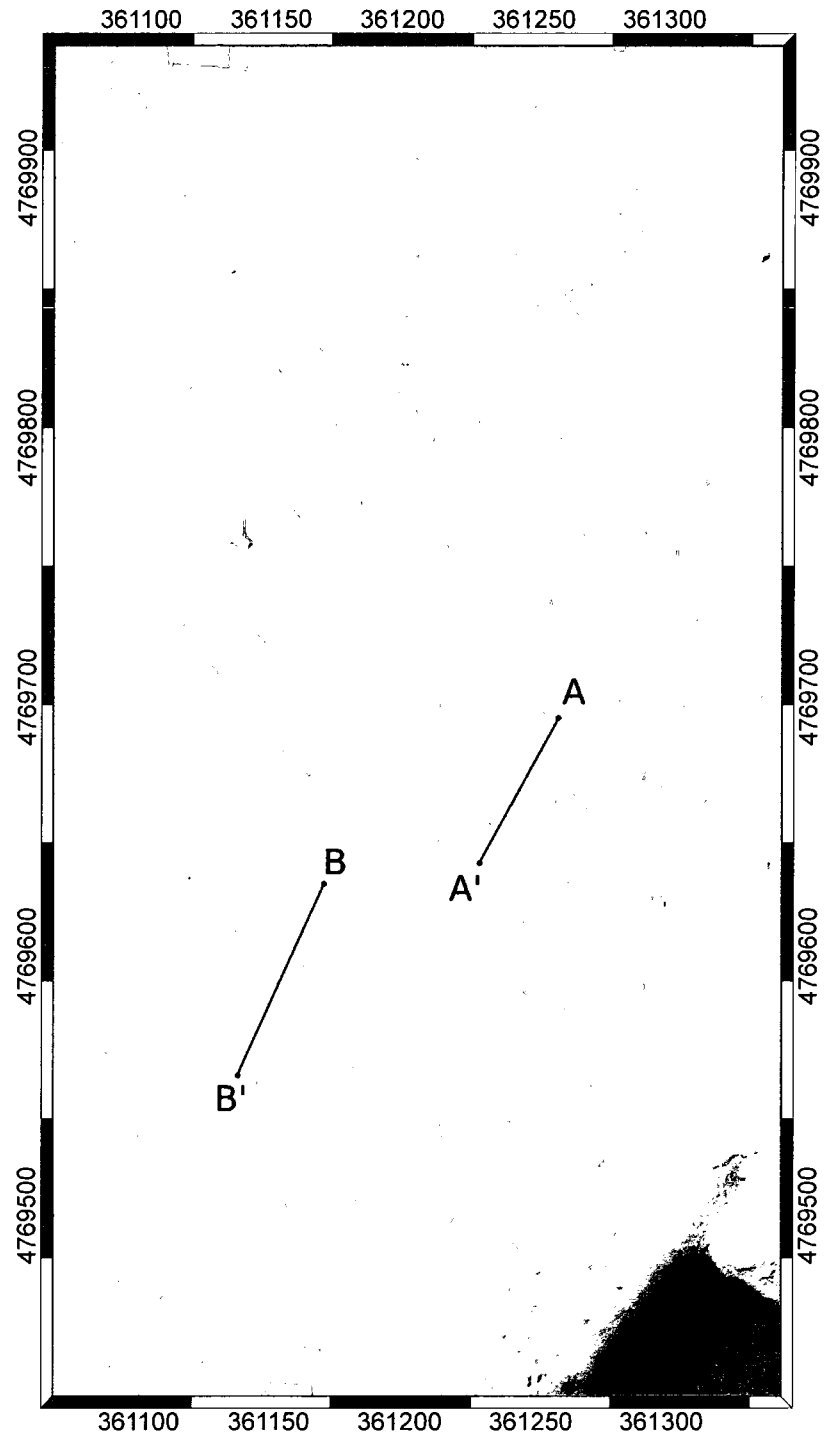


Figure 6-5. Dual-head Kongsberg EM3002D bathymetry (0.25 m grid resolution) acquired by the University of New Hampshire vessel R/V *Coastal Surveyor* in June 2007. Cross-sections A-A' and B-B' are presented in Figure 6-7. Grid is projected in UTM coordinates (Zone 19 N).

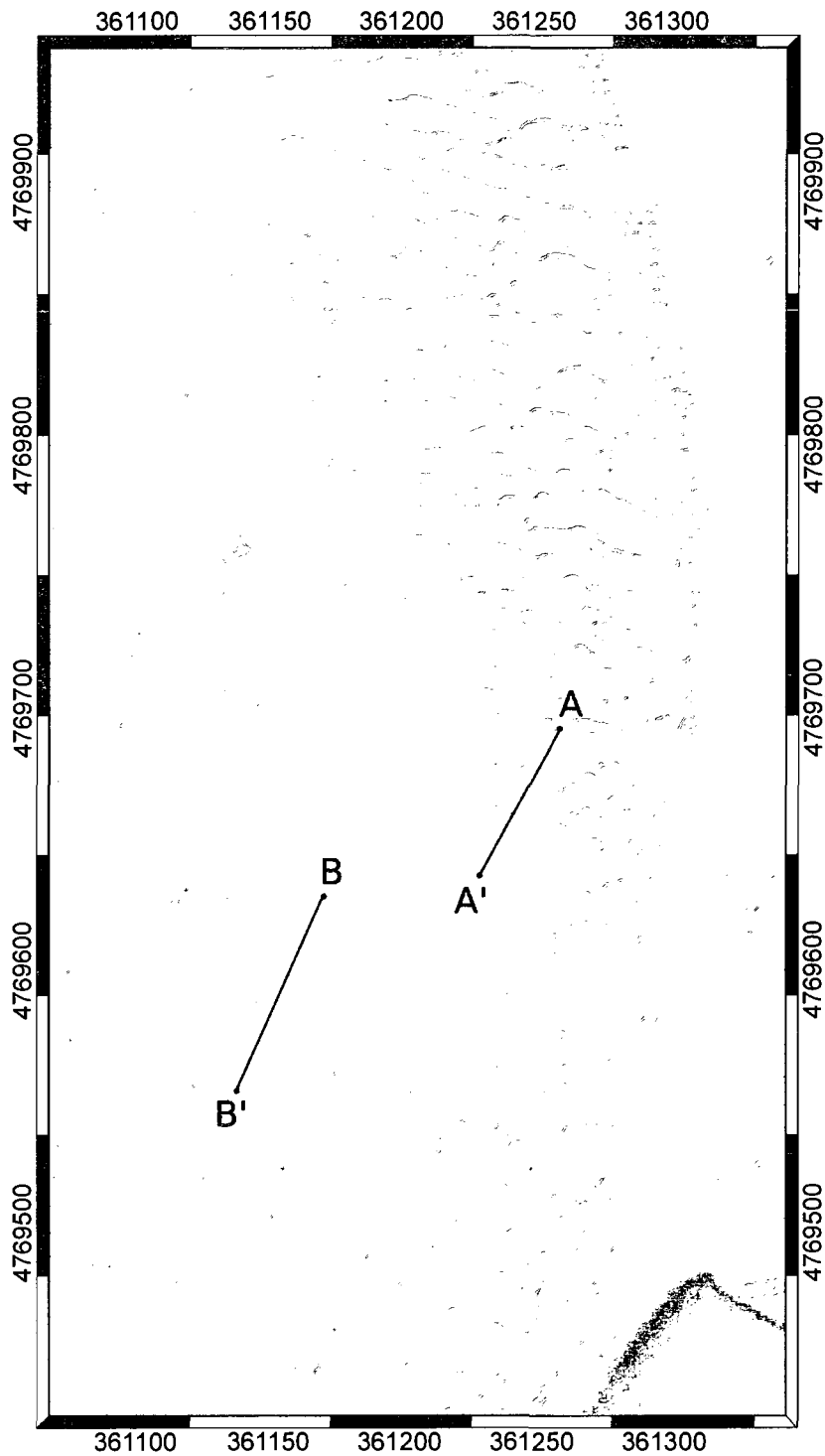


Figure 6-6. Dual-head Kongsberg EM3002D bathymetry (0.25 m grid resolution) acquired by the University of New Hampshire vessel R/V *Coastal Surveyor* in July 2008. Cross sections A-A' and B-B' are presented in Figure 6-7. Grid is projected in UTM coordinates (Zone 19 N).

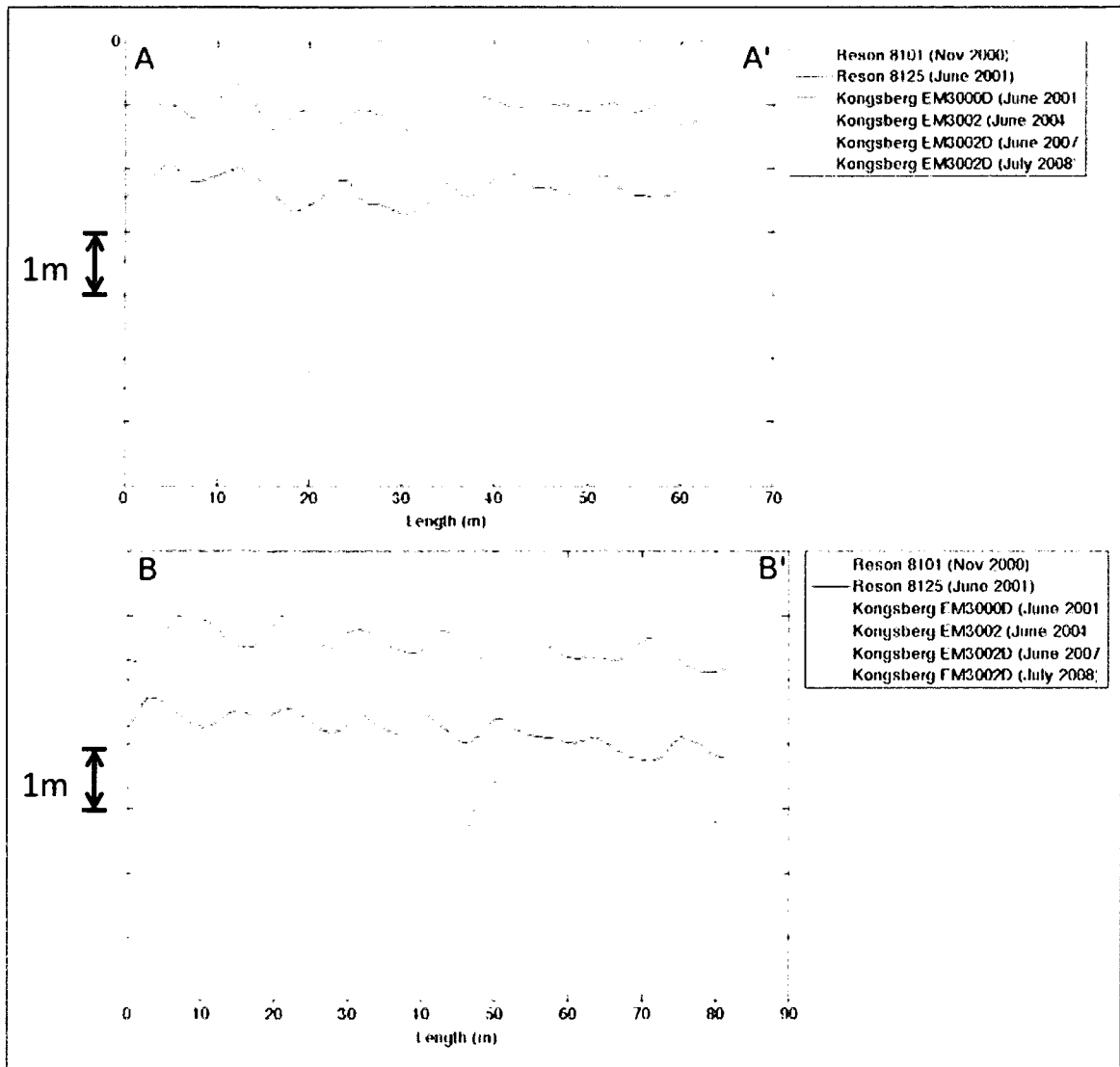


Figure 6-7. Cross-sections A (top) and B (bottom) from Figure 6-1 through Figure 6-6. North (A and B) is to the left on each graph, and South (A' and B') is to the right. Note that cross-sections have been offset for the purposes of comparison; Y axis does not represent surveyed depth, and should be used to evaluate bedform height only. In cross-section A (except that of the June 2007 EM3002D survey), bedforms are predominantly weakly to moderately ebb-oriented, although some asymmetrical bedforms exist. Cross-section A from the June 2007 EM3002D survey is strongly flood-oriented. In cross-section B, bedforms are moderately to strongly flood-oriented for all surveys.

Although bedform morphologies in the June 2007 surveys were flood-oriented across the survey area (Fig. 5-7, Fig. 6-5, Fig. 6-7), spatial cross-correlation results presented in Chapter 5 clearly indicate that the bedforms in the eastern sector of the dune field were migrating in a net ebb direction (Fig. 5-15, Fig. 5-16). Inspection of a time-series of bed-elevation profiles from the five surveys conducted in 2007 (Fig. 6-8, Fig. 6-9) suggests that the apparent ebb migration direction of the flood-oriented dunes was the result of a subtle shift in dune asymmetry. From 8 June to 15 June, dunes in the eastern sector of the bedform field (Profiles A and D of Figure 6-9) became slightly less flood-asymmetrical. By the next available survey in July of 2008, the bedforms in this area had resumed their ebb asymmetry (Fig. 5-8). It should be noted that Figures 6-8 and 6-9 also provide further evidence of strong east-west differences in dune migration during the 7-day period in 2007. Dunes in the western sector of the bedform field (profile B in Figure 6-9) had migrated in a net flood direction, whereas dunes in the eastern sector of the bedform field (profile C in Figure 6-9) had migrated in a net ebb direction.

The dominant pattern of reciprocal dune orientation corresponds with the velocity asymmetry of the observed current data. The current data were observed during spring tidal conditions from 3 to 6 June 2008, a period that was concurrent with the 2008 multibeam echosounder surveys (Fig. 5-19, Fig. 5-20). Although the current observations are assumed to be representative of normal hydrodynamic conditions in Portsmouth Harbor in the absence of wave forcing, it should be noted that the observations are quite limited, spanning only six tidal cycles, and that the current-meter stations ADCP and MAVS were located in the eastern and western sectors of the bedform field, respectively (Fig. 3-1).

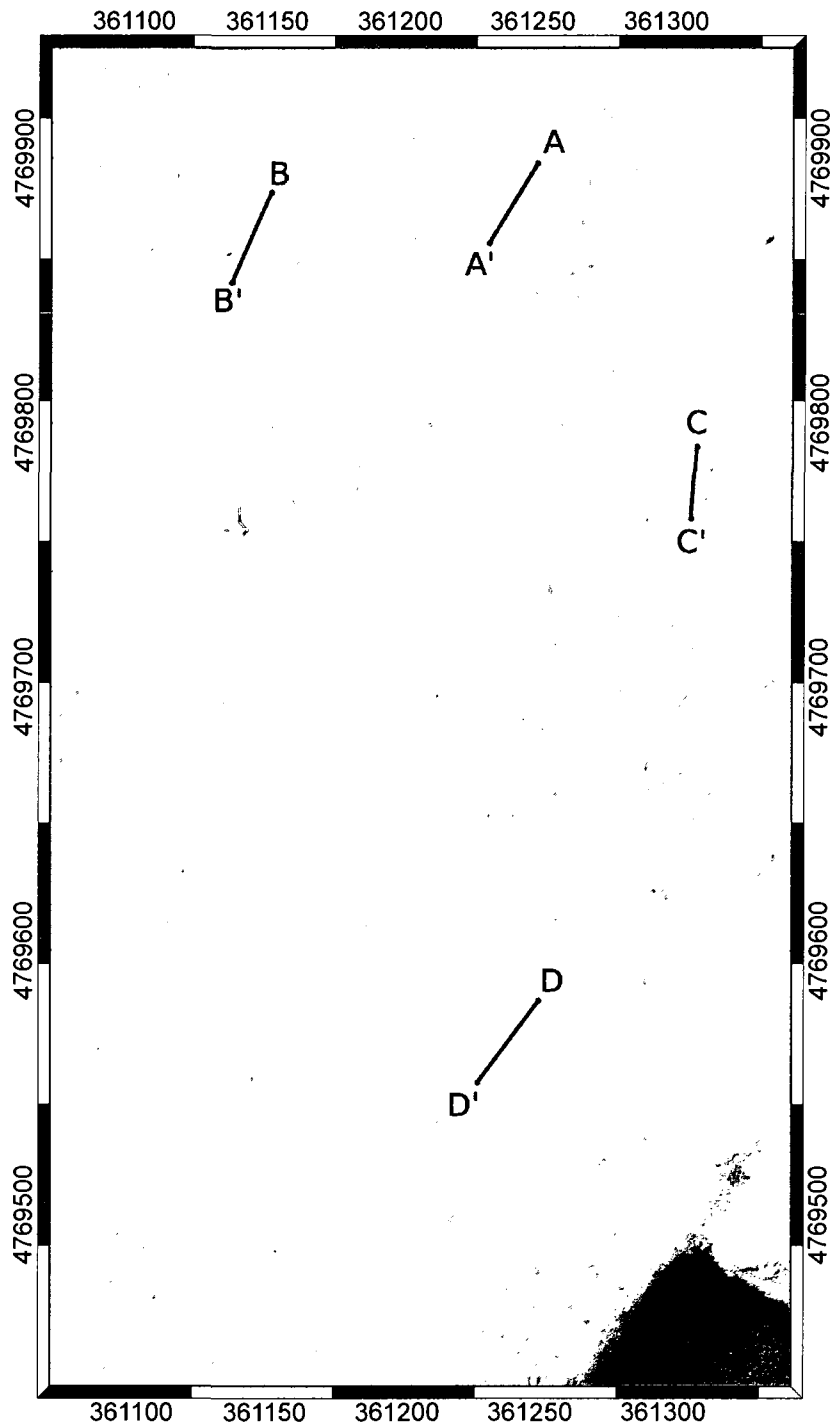


Figure 6-8. Map showing location of bed elevation profiles (Fig. 6-9) from multibeam bathymetry acquired on 8 June 2007 (1400 UTC), 8 June 2007 (2000 UTC), 14 June 2007 (1330 UTC), 14 June 2007 (1930 UTC) and 15 June 2007 (1400 UTC). Grid is projected in UTM coordinates (Zone 19 N).

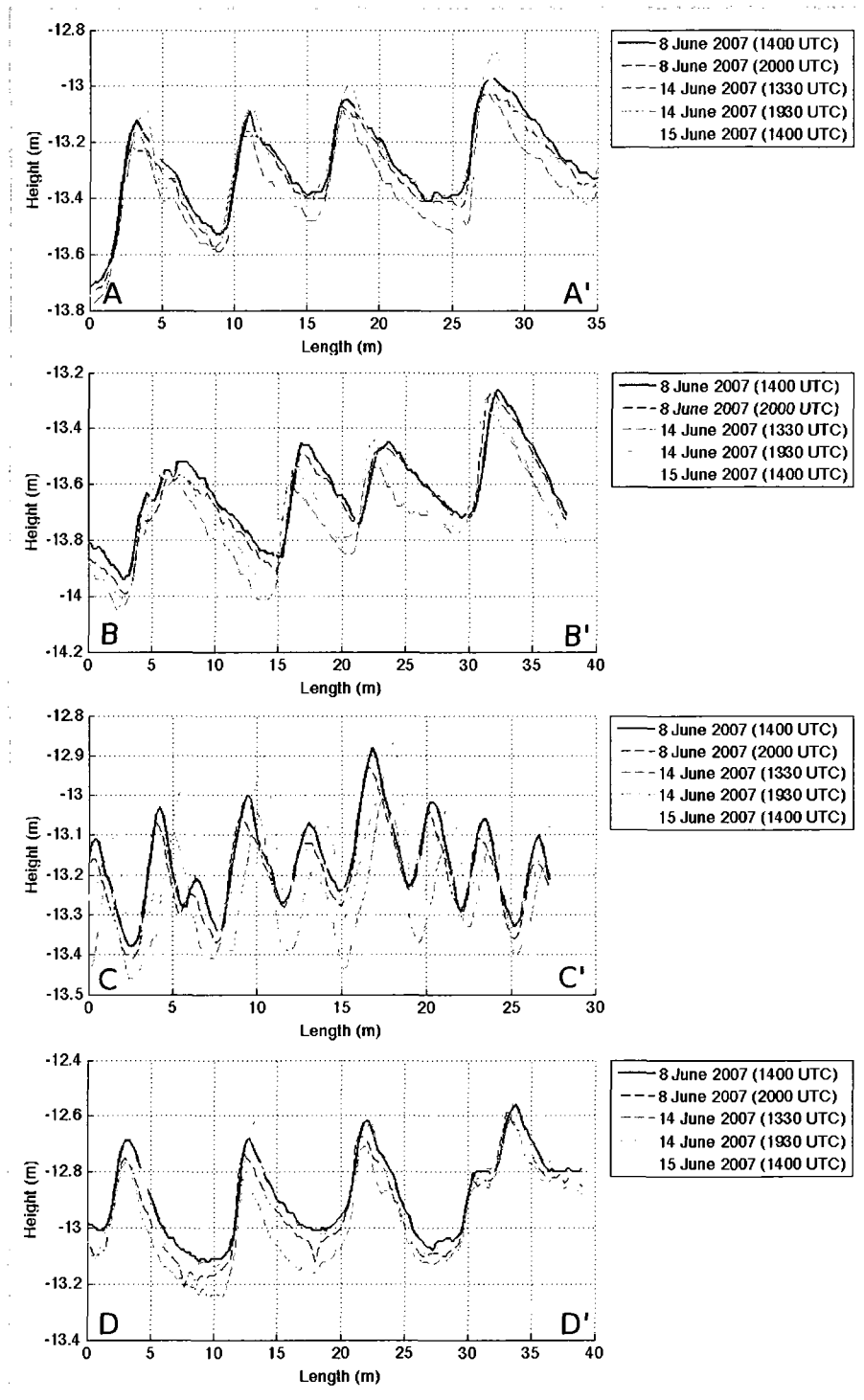


Figure 6-9. Bed elevation profiles A, B, C and D from bathymetry acquired on 8 June 2007 (1400 UTC), 8 June 2007 (2000 UTC), 14 June 2007 (1330 UTC), 14 June 2007 (1930 UTC) and 15 June 2007 (1400 UTC) (see Fig. 6-8). Bold blue and green curves indicate bed elevation profiles from first (8 June 2007, 1400 UTC) and last (15 June 2007, 1400 UTC) surveys, respectively

The current-meter data in Figure 5-19 show ebb-dominant currents at the ADCP site (1.03 m above bottom) and strongly flood-dominant currents at the MAVS site (1.00 m above bottom). Maximum flood and ebb currents at the ADCP site are 54 cm/s and 73 cm/s, respectively, while maximum flood and ebb currents at the MAVS site are 49 cm/s and <20 cm/s (with brief excursions to ~40 cm/s). Plots of partitioned bed shear stress at the ADCP and MAVS sites (Fig. 5-23) indicate that the critical bed shear stress τ_{cr} was exceeded at both locations. At the ADCP site τ_{cr} was exceeded during flood and ebb tidal conditions, although the skin-friction bed shear stress τ_{sf} was much stronger during ebb conditions (maximum 3 N/m²) than it was during flood-tidal conditions (maximum 1.5 N/m²). Conversely, at the MAVS site, τ_{cr} was commonly exceeded during flood-tidal conditions, but very rarely (and for shorter periods) during ebb-tidal conditions (Fig. 5-23).

If typical current-dominated hydrodynamic conditions such as those observed in July 2008 were responsible for initiating and sustaining the dominant pattern of dune morphology (i.e., reversal in dune asymmetry across the east-west axis of the bedform field) observed in the multibeam bathymetry from 2000, 2001, 2004 and 2008, then atypical current or wave-plus-current conditions may have been responsible for the anomalous bed morphology (i.e. strongly flood-asymmetrical dunes throughout the bedform field) observed in the bathymetry from 2007. Indeed, strongly flood-dominated current or wave-plus-current conditions would be necessary to have formed the bedform-orientation pattern observed in 2007. Such conditions could potentially be initiated by storm forcing, particularly if accompanied by a significant storm surge and/or significant wave height. The formation and endurance of relic bedform morphology produced by

such low-frequency events has been documented previously by Whitmeyer and FitzGerald (2007).

If the bedform morphologies observed in 2007 were a relic caused by a low-frequency storm event, then one would expect to find evidence of probable cause in the meteorological record. Figure 6-10 is a plot of data from the Gulf of Maine Ocean Observing System (GoMOOS) Buoy B01, which is moored at 43.1805°N, 70.4281°W along the Western Maine Shelf, approximately 26 km northeast of the Portsmouth Harbor study area (GoMOOS, 2009). Buoy B01 was the closest point of observation to the study area that also had a continuous record of meteorological and wave data for the six months preceding the 2007 MBES surveys. The GoMOOS record indicates the occurrence of a low-pressure event in the western Gulf of Maine from 16-20 April 2007. This event was accompanied by high wind speeds (maximum of 20 m/s) and a multiday period of large significant wave heights (maximum of 10 m). Although continuous meteorological and wave observations are unavailable for locations nearer to the study area, water-level observations from this period were obtained from NOAA Tide Gauge 8423898 (Fort Point, New Castle, New Hampshire) (Fig. 6-11). The water-level record at Fort Point shows a water level increase (residual) in the range of 0.5 m to 1.0 m from 16 to 20 April 2007. This increase in water level may indicate a storm surge driven by a decrease in atmospheric pressure and increase in sustained wind speed, an excess of freshwater discharge to Great Bay Estuary, or possibly both. Regardless, such conditions of increased mean current speed associated with increased water levels in the lower estuary, coupled with high wave-orbital velocities, might have sufficiently altered the background hydrodynamic conditions to induce a reconfiguration of the seabed.

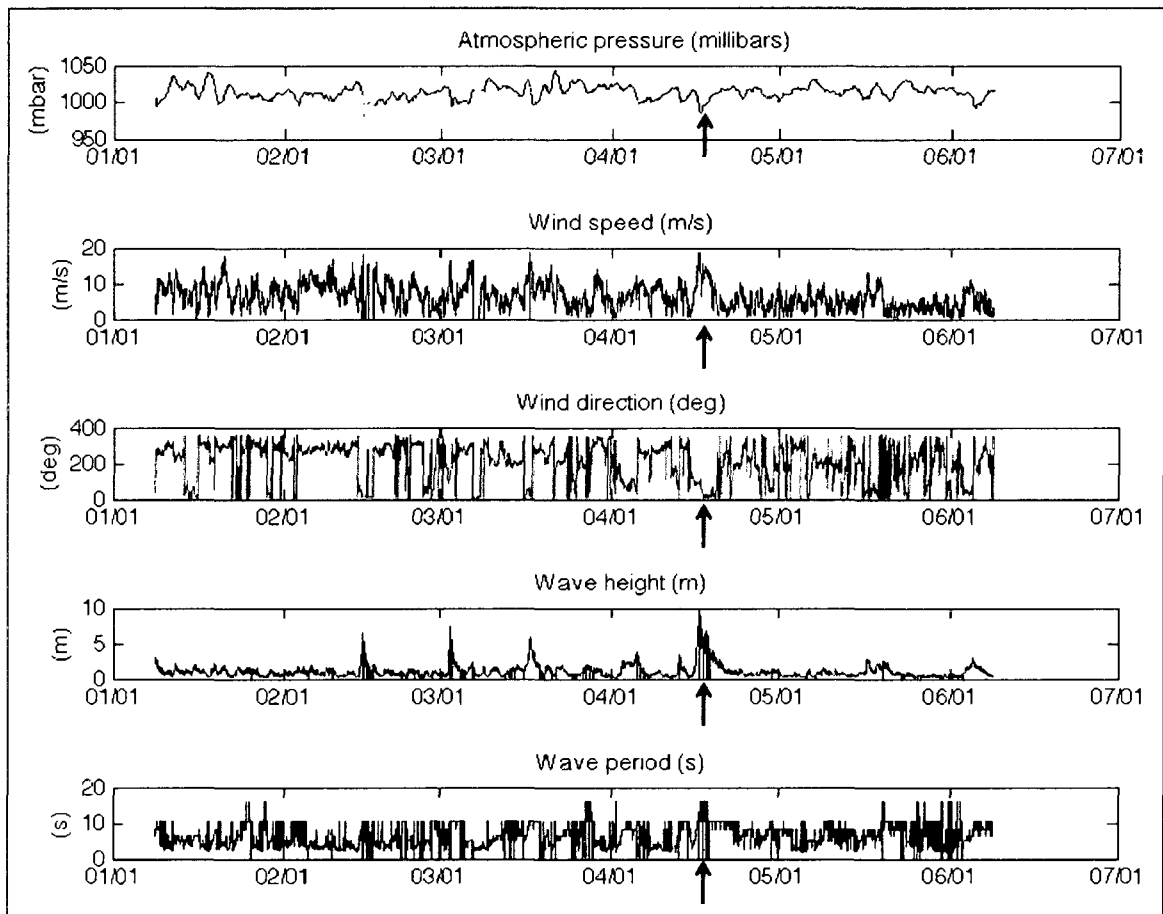


Figure 6-10. Atmospheric pressure (millibars), wind speed (m/s), wind direction (degrees), significant wave height (m) and dominant wave period (s) from GoMOOS Buoy B01, located at 43.1805°N, 70.4281°W along the Western Maine Shelf (approx. 26 km northeast of the study area). Note presence of stalled low-pressure system (indicated by red arrow) from 16-21 April 2007 causing a prolonged period of elevated wave height.

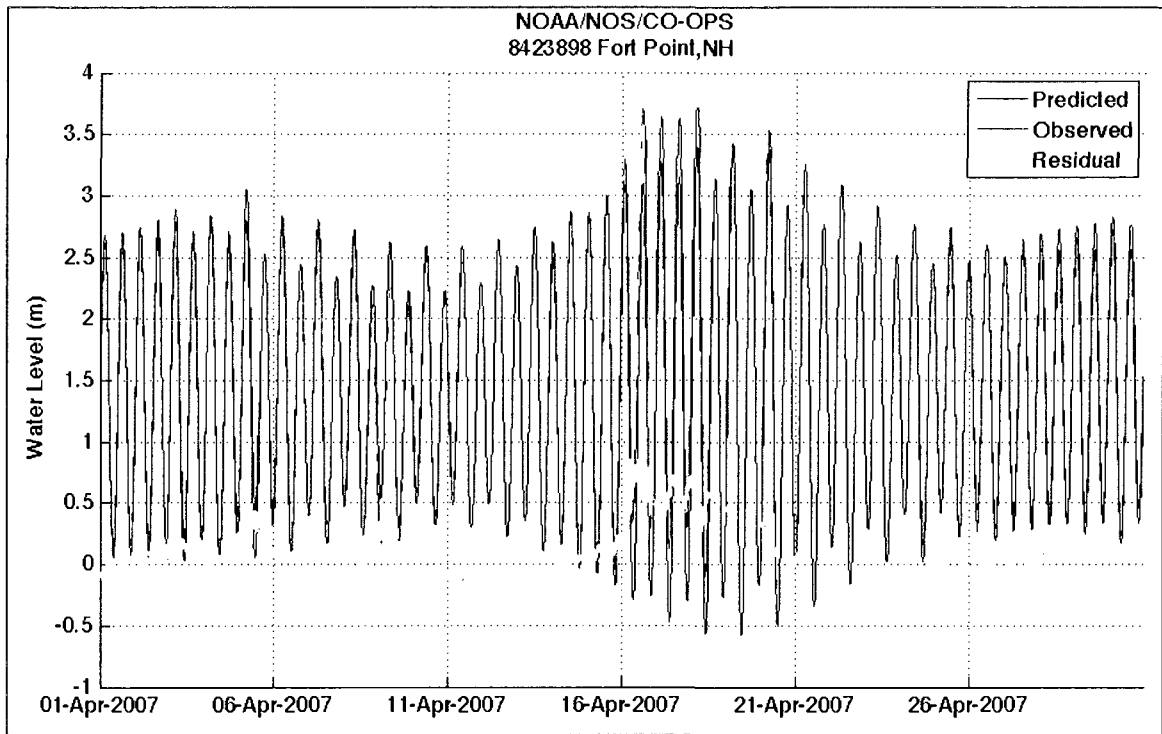


Figure 6-11. Predicted (blue) and observed (red) water level data from NOAA/NOS/CO-OPS tide gauge 8423898 (Fort Point, New Hampshire). Residual (observed-predicted) depicts the storm surge experienced during the period from 16-21 April 2007. Missing observations are dropouts in logged data from the tide gauge. Note storm surge of between 0.5 and 1 meter for several days after 16 April.

CHAPTER 7

CONCLUSIONS

Bedform migrations were detected in this study from repeat high-resolution multibeam echosounder surveys of a dune field near the entrance to Portsmouth Harbor. Surveys were conducted over periods that range from 6 hr to 7 days in June 2007 and July 2008 in order to capture the response of dune morphology to ebb-flood and neap-spring tidal cycles. Current observations were made at two locations within the study area concurrent with the July 2008 MBES survey in order to provide context for the observed patterns of bedform migration and in order to calculate bed shear stress. A targeted sediment sampling and underwater video survey was conducted in February 2007 in order to characterize seafloor sediments within the study area and to provide necessary textural information for calculations of bed shear stresses.

A new technique was developed for detecting bedform migration. This technique (BISHNU) utilizes a fingerprint-detection algorithm (Bishnu et al., 2002) to convert bathymetry to a binary map of dune crests, which are subsequently tracked using a normalized two-dimensional spatial cross-correlation technique (Duffy and Hughes-Clarke, 2005). Ridge maps are a better candidate for spatial cross-correlation than the bathymetric or maximum-slope surfaces because they provide stronger emphasis of dune crests, which are the primary features to be tracked. Results of BISHNU coupled with

the spatial cross-correlation routine yield reasonable estimates of bedform-migration magnitude and direction.

Results indicate that bedform migration magnitudes of approximately 0.2 to 0.4 m were observed over 6-hr periods during spring and neap tidal conditions. Bedform migration magnitudes of 0.2 to 1.2 m were observed over a 1-day period during spring tidal conditions, whereas migration magnitudes in excess of 2.0 m were observed during 6-day and 7-day periods. Bedform migrations observed over 6-hr periods indicate the episodic response of the seafloor to oscillatory tidal currents. Results from repeat surveys conducted over 6-hr periods on 8 June 2007 and 14 June 2007 suggest a high degree of spatial variability in dune migration across the study area (Fig. 5-13, Fig. 5-14). Conversely, bedform migration observed over 24-hr and multi-day periods show the response of the seafloor to residual currents, perhaps as the result of flood-ebb velocity asymmetry (Fig. 5-15, Fig. 5-16, Fig. 5-17). Results over multi-day periods in 2007 and 2008 indicate a coherent pattern of bedform migration within the study area characterized by strong cross-channel differences in dune migrations (Fig. 5-16, Fig. 5-17). Results over a 7-day period in 2007 indicate a reciprocal pattern of bedform migrations, whereby dunes in the eastern sector of the bedform field migrated in a net ebb (southward) direction, and dunes in the western sector of the bedform field migrated in a net flood (northward) direction (Fig. 5-16). Results over a 6-day period in 2008 indicate a net ebb (southward) migration of dunes in the eastern sector of the bedform field, but reveal only weak activity in the western sector of the bedform field (Fig. 5-17).

Acoustic current-meter observations obtained from two locations in the study area in July 2008 provide context for the observed patterns of bedform migrations. The

current-meter data show ebb-current dominance at the ADCP station in the eastern half of the bedform field and flood-current dominance at the MAVS station in the western half of the bedform field. Plots of partitioned bed shear stress indicate that the critical bed shear stress τ_{cr} was exceeded at both stations during both flood and ebb tides. At the ADCP site, τ_{cr} was exceeded during both flood and ebb tidal conditions, though the skin-friction shear stress τ_{sf} was much higher in magnitude during ebb tidal conditions. τ_{cr} at the MAVS site was commonly exceeded during flood tidal conditions but only rarely during ebb tidal conditions, indicating that bedload transport was primarily to the north at this location. The magnitude of τ_{sf} at the ADCP site was highest in magnitude during ebb tidal conditions, indicating that bedload transport was primarily to the south.

The observed east-west differences in bedform migration are reinforced by a time-series of multibeam bathymetry extending back to November 2000. With the exception of surveys conducted in June 2007, all surveys show a pattern of dune morphologies that were ebb-oriented (southward-migrating) in the eastern sector of the dune field, and flood-oriented (northward-migrating) in the western sector of the dune field. Dune morphologies during surveys conducted in June 2007 were strongly flood-asymmetrical across the study area. The bed morphologies observed in June 2007 may be relict morphologies created during a stalled low-pressure system in the Gulf of Maine during mid-April. Observations from GoMOOS Buoy B01 located 26 km northeast of the study area measured significant wave heights that topped 10 m during this period, whereas NOAA Tide Gauge 8423898 (Fort Point, NH) indicated a water level surge of 0.5 to 1.0 m in Portsmouth Harbor. Wave- and residual current- reinforced hydrodynamics during this period may have created this relict bed morphology, which

seems to have been in the process of being reworked during the June 2007 observation period. By July 2008, the reciprocal pattern of bedform asymmetry had resumed.

The results of this study could be enhanced by the acquisition and analysis of high-resolution *in situ* observations of instantaneous and mean current speeds and bed shear stresses below 1.0 m above the seabed, which are necessary to more accurately assess bedload transport in the study area, although reasonable estimates thereof are provided by this study. A further improvement on this work would be simultaneous high-frequency observations of bed dynamics and bed shear stress via bottom tripods, which would be necessary to assess the instantaneous response of the seabed to tidal and wave-reinforced tidal conditions. A worthwhile extension of this study would be to continue extending the timeline of high-resolution multibeam bathymetry within the study area in order to monitor long-term changes in bedform morphologies.

LIST OF REFERENCES

LIST OF REFERENCES

- Ashley, G.M., 1990. Classification of large-scale subaqueous bedforms; a new look at an old problem. *Journal of Sedimentary Research* 60: 161-172.
- Barnhardt, W.A., Belknap, D.F., Kelley, J.T., 1997. Stratigraphic evolution of the inner continental shelf in response to late Quaternary relative sea-level change, northwestern Gulf of Maine. *GSA Bulletin* 109(5): 612-630.
- Belknap, D.F., Andersen, B.G., Anderson, R.S., Anderson, W.A., Harold W. Borns, J., Jacobson, G.L., Kelley, J.T., Shipp, R.C., Smith, D.C., Robert Stuckenrath, J., Thompson, W.B., Tyler, D.A., 1987. Late Quaternary sea-level changes in Maine. In: Nummedal, D., Pilkey, O.H., Howard, J.D. (Editors), *Sea-level Fluctuation and Coastal Evolution*. Society of Economic Paleontologists and Mineralogists, Tulsa, Oklahoma, pp. 71-85.
- Belknap, D.F., Kelley, J.T., Gontz, A.M., 2002. Evolution of the glaciated shelf and coastline of the Northern Gulf of Maine, USA. *Journal of Coastal Research* (Special Issue 36): 37-55.
- Bennett, S.J., Best, J.L., 1995. Mean flow and turbulence structure over fixed, two-dimensional dunes: implications for sediment transport and bedform stability. *Sedimentology* 42: 491-513.
- Besio, G., Blondeaux, P., Brocchini, M., Vittori, G., 2004. On the modeling of sand wave migration. *Journal of Geophysical Research* 109 (C04018): 13.
- Besio, G., Blondeaux, P., Fristina, P., 2003. A note on tidally generated sand waves. *Journal of Fluid Mechanics* 485: 171-190.
- Best, J.L., 2005. The fluid dynamics of river dunes: A review and some future research directions. *Journal of Geophysical Research* 110 (F04S02).
- Bilgili, A., Swift, M.R., Celikkol, B., 1996. Shoal formation in the Piscataqua River, New Hampshire. *Estuaries* 19 (3): 518-525.
- Bishnu, A., Bhowmick, P., Dey, J., Bhattacharya, B.B., Kundu, M.K., Murthy, C.A., Acharya, T., 2002. Combinatorial classification of pixels for ridge extraction in a gray-scale fingerprint image, 3rd Indian Conference on Computer Vision, Graphics and Image Processing, Ahmedabad, India, pp. 451-456.

- Blott, S.J. Pye, K., 2001. GRADISTAT: A grain size distribution and statistics package for the analysis of unconsolidated sediments. *Earth Surface Processes and Landforms* 26: 1237-1248.
- Bokuniewicz, H.J., Gordon, R.B. Kastens, K.A., 1977. Form and migration of sand waves in a large estuary, Long Island Sound. *Marine Geology* 24: 185-199.
- Buijsman, M.C. Ridderinkhof, H., 2008. Long-term evolution of sand waves in the Marsdiep inlet. I: High-resolution observations. *Continental Shelf Research* 28: 1190-1201.
- Cutter, G.R., Jr., 2005. Seafloor Habitat Characterization, Classification, and Maps for the Loewr Piscataqua River Estuary, Ph.D. Dissertation, University of New Hampshire, Durham, 307 pp.
- Daniell, J.J., Harris, P.T., Hughes, M.G., Hemer, M. Heap, A., 2008. The potential impact of bedform migration on seagrass communities in Torres Strait, northern Australia. *Continental Shelf Research* 28: 2188-2202.
- Duffy, G.P. Hughes-Clarke, J.E., 2004. Monitoring change between time-lapsed surveys using spatial cross correlation, Canadian Hydrographic Conference, Ottawa, Canada.
- Duffy, G.P. Hughes-Clarke, J.E., 2005. Application of spatial cross correlation to detection of migration of submarine sand dunes. *Journal of Geophysical Research* 110 (F04S12).
- Dyer, K.R., 1980. Velocity profiles over a rippled bed and the threshold of movement of sand. *Estuarine and Coastal Marine Science* 10: 181-199.
- Ernstsen, V.B., Noormets, R., Hebbeln, D., Bartholoma, A. Flemming, B.W., 2006a. Precision of high-resolution multibeam echo sounding coupled with high-accuracy positioning in a shallow water coastal environment. *Geo-Marine Letters* 26: 141-149.
- Ernstsen, V.B., Noormets, R., Winter, C. Hebbeln, D., 2005. Development of subaqueous barchanoid-shaped dunes due to lateral grain size variability in a tidal inlet channel of the Danish Wadden Sea. *Journal of Geophysical Research* 110 (F04S08).
- Ernstsen, V.B., Noormets, R., Winter, C., Hebbeln, D., Bartholoma, A., Flemming, B.W. Bartholdy, J., 2006b. Quantification of dune dynamics during a tidal cycle in an inlet channel of the Danish Wadden Sea. *Geo-Marine Letters* 26: 151-163.

- FitzGerald, D.M., Buynevich, I.V., Fenster, M.S. McKinlay, P.A., 2000. Sand dynamics at the mouth of a rock-bound, tide-dominated estuary. *Sedimentary Geology* 131: 25-49.
- GoMOOS, 2009. Gulf of Maine Ocean Observing System, Portland, ME. <http://www.gomoos.org>.
- Gostnell, C., 2005. Efficacy of an interferometric sonar for hydrographic surveying: Do interferometers warrant an in-depth examination? *The Hydrographic Journal* 118: 17-24.
- Harris, C.K., 2003. Form drag and skin friction. Virginia Institute of Marine Science, The College of William and Mary, Gloucester Point, VA, 5 pp.
- Horne, G.S. Patton, P.C., 1989. Bedload-sediment transport through the Connecticut River estuary. *Geological Society of America Bulletin* 101: 805-819.
- Huff, L.C., 2001. Extending the timeline through data mining, 2nd International Conference on High-Resolution Surveys in Shallow Water, Portsmouth, NH, 24-27 September.
- Hulscher, S.J.M.H., 1996. Tidal-induced large-scale regular bed form patterns in a three-dimensional shallow water model. *Journal of Geophysical Research* 101(C9): 20,727-20,744.
- Huntley, D.A., 1988. A modified inertial dissipation method for estimating seabed stresses at low Reynolds numbers, with application to wave/current boundary layer measurements. *Journal of Physical Oceanography* 18(339-346).
- International Hydrographic Organization, 2008. IHO Standards for Hydrographic Surveys, Special Publication 44, 5th Edition, Monaco. 36 pp.
- Knaapen, M.A.F., van Bergen Henegouw, C.N. Hu, Y.Y., 2005. Quantifying bedform migration using multi-beam sonar. *Geo-Marine Letters* 25: 306-314.
- Kostaschuk, R. Best, J., 2005. Response of sand dunes to variations in tidal flow: Fraser Estuary, Canada. *Journal of Geophysical Research* 110 (F04S04): 10.
- Lesser, G.R., Roelvink, J.A., van Kester, J.A.T.M. Stelling, G.S., 2004. Development and validation of a three-dimensional morphological model. *Coastal Engineering* 51 (8-9): 883-915.
- Lindenbergh, R., Wust, H. Menting, P., 2007. Predicting sand wave dynamics. *International Hydrographic Review* 8 (2): 25-36.

- Mayer, L.A., Raymond, R., Glang, G., Richardson, M.D., Traykovski, P. Trembanis, A.C., 2007. High-resolution mapping of mines and ripples at the Martha's Vineyard Coastal Observatory. *IEEE Journal of Oceanic Engineering* 32 (1): 133-149.
- McLean, S.R., Wolfe, S.R. Nelson, J.M., 1999. Predicting boundary shear stress and sediment transport over bed forms. *Journal of Hydraulic Engineering* 125 (7): 725-736.
- Middleton, G.V. Southard, J.B., 1984. *Mechanics of Sediment Movement*, Society of Economic Paleontologists and Mineralogists, Short Course, No. 2., Providence, Rhode Island.
- Morelissen, R., Hulscher, S.J.M.H., Knaapen, M.A.F., Nemeth, A.A. Bijker, R., 2003. Mathematical modeling of sand wave migration and the interaction with pipelines. *Coastal Engineering* 48 (3): 197-209.
- Nemeth, A.A., Hulscher, S.J.M.H. de Vriend, H.J., 2002. Modelling sand wave migration in shallow shelf seas. *Continental Shelf Research* 22: 2795-2806.
- Nittrouer, J.A., Allison, M.A. Campanella, R., 2008. Bedform transport rates for the lowermost Mississippi River. *Journal of Geophysical Research* 113 (F03004).
- National Oceanic and Atmospheric Administration, 2007. C-MIST Cumulative Data Analysis Report (PIR0701), NOAA Center for Operational Oceanographic Products and Services, Silver Spring, MD. <https://cmist.noaa.gov>.
- National Oceanic and Atmospheric Administration, 2009. NOAA Tides and Currents: Center for Operational Oceanographic Products and Services. <http://tidesandcurrents.noaa.gov>.
- Reichard, R.P. Celikkol, B., 1978. Application of a finite element hydrodynamic model to the Great Bay Estuary system, New Hampshire, USA. In: Nihoul, J.C.J. (Ed.), *Hydrodynamics of Estuaries and Fjords*. Elsevier, Amsterdam, pp. 349-372.
- Sanford, L.P., 1991. Tidal resuspension of sediments in northern Chesapeake Bay. *Marine Geology* 97: 87-103.
- Sanford, L.P., 1994. Wave-forced resuspension of upper Chesapeake Bay muds. *Estuaries* 17(18): 148-165.
- Sherwood, C.R., Lacy, J.R. Voulgaris, G., 2006. Shear velocity estimates on the inner shelf off Grays Harbor, Washington, USA. *Continental Shelf Research* 26: 1995-2018.

- Short, F.T., 1992. The Estuarine Hydrosystem. In: Short, F.T. (Ed.), The Ecology of the Great Bay Estuary, New Hampshire and Maine: An Estuarine Profile and Bibliography. NOAA Coastal Ocean Program, Durham, New Hampshire, pp. 31-38.
- Smith, J.D. McLean, S.R., 1977. Spatially averaged flow over a wavy surface. *Journal of Geophysical Research* 82 (12): 1735-1746.
- Soulsby, R.L., 1997. Dynamics of marine sands: A manual for practical applications. Thomas Telford, London, 249 pp.
- Swenson, E., Brown, W.S. Trask, R.P., 1977. Great Bay Estuarine Field Program 1975 Data Report, Part 1: Currents and Sea Levels, University of New Hampshire, Durham, NH. 109 pp.
- Terwindt, J.H.J., 1971. Sand waves in the Southern Bight of the North Sea. *Marine Geology* 10: 51-67.
- van Dijk, T.A.G.P. Egberts, P.J.P., 2008. The variability of sand wave migration in the North Sea, *Marine and River Dune Dynamics*, Leeds, U.K., pp. 63-67.
- van Dijk, T.A.G.P. Kleinhans, M.G., 2005. Processes controlling the dynamics of compound sand waves in the North Sea, Netherlands. *Journal of Geophysical Research* 110 (F04S10).
- Ward, L.G., 1992. Estuarine Geomorphology. In: Short, F.T. (Editor), The Ecology of the Great Bay Estuary, New Hampshire and Maine: An Estuarine Profile and Bibliography. NOAA - Coastal Ocean Program, Durham, New Hampshire, pp. 39-43.
- Ward, L.G., 1995. Sedimentology of the Lower Great Bay/Piscataqua River Estuary, University of New Hampshire CMB/JEL Contribution Series Number 314, Department of the Navy, San Diego, California. 102 pp.
- Ward, L.G., 2008. Assessment of Sand Resources and the Geological Environment of the New Hampshire Inner Continental Shelf. Final Report for the Cooperative Agreement (0104CA34383) between the University of New Hampshire and the U.S. Department of the Interior, Minerals Management Service., Herndon, VA. 59 pp.
- Ward, L.G. Bub, F.L., 2005. Temporal variability in salinity, temperature and suspended sediments in a Gulf of Maine estuary (Great Bay Estuary, New Hampshire). In: FitzGerald, D.M. Knight, J. (Editors), *High Resolution Morphodynamics and Sedimentary Evolution of Estuaries*. Springer, Dordrecht, The Netherlands, pp. 115-142.

- Whitmeyer, S.J. FitzGerald, D.M., 2008. Episodic dynamics of a sand wave field. *Marine Geology* 252: 24-37.
- Wolfson, M.L., Naar, D.F., Howd, P.A., Locker, S.D., Donahue, B.T., Friedrichs, C.T., Trembanis, A.C., Richardson, M.D. Wever, T.F., 2007. Multibeam observations of mine burial near Clearwater, FL, including comparisons to predictions of wave-induced burial. *IEEE Journal of Oceanic Engineering* 32 (1): 103-118.
- Wright, L.D., 1995. *Morphodynamics of Inner Continental Shelves*. Marine Science Series. CRC Press, Boca Raton, FL, 241 pp.